Final Technical Report

Enhanced Geothermal Systems –

Concept Testing and Development at the Raft

River Geothermal Field, Idaho

Authors: Jacob Bradford, Joseph Moore

University of Utah
Energy & Geoscience Institute
423 Wakara Way, suite 300
Salt Lake City, UT 84105

NOTE:

Research analyses at the Raft River are summarized in this thesis.

During the period of no-cost extension, until June 2019, monitoring of injection, temperature, pressures and flow rates continued.

The final figures and results are attached in the Addendum at the end of this document.

THE APPLICATION OF HYDRAULIC AND THERMAL

STIMULATION TECHNIQUES TO CREATE

ENHANCED GEOTHERMAL SYSTEMS

by

Jacob Thornley Bradford

A dissertation submitted to the faculty of
The University of Utah
in partial fulfillment of the requirements for the degree of

Doctor of Philosophy

Department of Chemical Engineering

The University of Utah

December 2016

The University of Utah Graduate School

STATEMENT OF DISSERTATION APPROVAL

The dissertation of   **Jacob Bradford**

has been approved by the following supervisory committee members:

John McLennan	, Chair	**7/15/2016** Date Approved
Joseph Moore	, Member	**7/15/2016** Date Approved
Robert Podgorney	, Member	**date approved** Date Approved
Milind Deo	, Member	**date approved** Date Approved
Jules Magda	, Member	**7/15/2016** Date Approved

and by   **Milind Deo**   , Chair/Dean of

the Department/College/School of   **Chemical Engineering**

and by David B. Kieda, Dean of The Graduate School.

ABSTRACT

Geothermal energy production requires temperature at depth, a working fluid to transport heat to the surface, and a network of fluid pathways connecting injection and production wells. These requirements constrain the availability of geothermal energy resources. Enhanced Geothermal System (EGS) development expands geothermal resource availability by artificially generating networks of fluid pathways in the reservoir. This is accomplished through hydraulic and thermal stimulation of the geothermal reservoir.

Hydraulic and thermal techniques were applied at the Raft River geothermal field as part of a Department of Energy (DOE) EGS development project. The test well RRG-9 ST1 was hydraulically stimulated three times between February 2012 and April 2014. Since June, 2013 continuous injection of sub-reservoir temperature plant water has been used to thermally stimulate the well. The stimulation program has resulted in a large increase in the injectivity of the well, an increase from less than 20 gpm in June 2013 to nearly 1,000 gpm in April 2016. Wellbore imaging and temperature analysis identified a northeast striking fracture zone intersecting the well between 5,640 and 5,660 ft. measured depth (MD) has nominally accepted all of the injected fluid. Microseismic activity, related to stimulation program and plant activity was used to track possible fluid pathways within the reservoir. The microseismic data indicates that the injected fluid moves primarily to the northeast through the Narrows Zone, a northeast striking fault structure that bisects the

field. Tracers injected into RRG-9 ST1 and recovered at the production wells RRG-2 and RRG-4, located to the northeast of RRG-9 ST1, support this theory. It is hypothesized that water injected into RRG-9 ST1 moves through the intersecting fracture zone which connects into the Narrows Zone, and then moves along the Narrows Zone to the northeast. This conceptual model was numerical simulated using FALCON a finite element reservoir simulation code developed by Idaho National Laboratory. The modeling suggests that both thermal and hydraulic fracturing mechanisms played an important role in improving the injectivity at RRG-9 ST1. The stimulation program at Raft River has successfully demonstrated the effectiveness of hydraulic and thermal stimulation techniques. RRG-9 ST1 is now in commercial use.

Dedicated to my wife Natalie Bradford.

Table of Contents

LIST OF TABLES

LIST OF FIGURES

ACKNOWLEDGMENTS

INTRODUCTION

Successful geothermal energy production requires high temperatures near the surface, a fluid to transport the heat to the surface, and fluid pathways within the reservoir that allow the fluid to be injected, heated, and recovered. Locations containing all three criteria are relatively rare. Enhanced Geothermal Systems (EGS) utilize thermal and hydraulic stimulation techniques to generate fluid pathways that may not originally be present in the geothermal reservoir.

1.1 Enhanced Geothermal Systems

Hydraulic and thermal fracturing is the primary method by which effective fluid pathways are generated in EGS. Hydraulic fracturing is a well-established protocol in the petroleum industry and is credited with greatly improving resource recovery [1]. Hydraulic stimulation techniques generate fractures in the direction parallel to the axis of greatest in-situ stress and normal to the least principal stress [2]. However, this is not always ideal when attempting to connect geothermal production or injection wells to an existing fracture network, especially if those zones are not located in a path accessible to a fracture growing parallel to the axis of greatest in-situ stress. Thermal stimulation techniques can generate fractures in directions other than perpendicular to the axis of the least principle stress [3],

[4], [5]. Long term injection of sub-reservoir temperature water causes the rock mass to cool and contract, leading to fracture creation or the expansion of existing fractures [6], [7]. The energy resources available using EGS techniques is enormous, and virtually inexhaustible in the United States [8].

1.2 A History of Enhanced Geothermal Systems

The modern application of geothermal energy to produce electricity began at Larderello, Italy in 1904 [9]. The first successful large-scale application of geothermal energy in the United States began in the 1960's at The Geysers, just north of San Francisco. Los Alamos National Laboratory's Fenton Hill geothermal project was the origin of Enhanced Geothermal System techniques in the 1970's-1980's [10]. Following Fenton Hill other EGS projects were developed in Australia, Germany, Japan, Sweden, Switzerland, and the United Kingdom, but without significant commercial success [11]. The EGS project at Raft River has produced a commercially viable injection well using both hydraulic and thermal stimulation techniques.

1.3 Raft River Stimulation Plan

Located in Cassia County, Idaho the Raft River geothermal field is approximately 100 miles northwest of Salt Lake City on the Utah-Idaho border, Figure 1. The site was selected by the Department of Energy (DOE) to host an EGS demonstration project. The objective of this project was to hydraulically and thermally stimulate the test well RRG-9 ST1. The stimulation consisted of three hydraulic stimulations interspersed with continuous injection of sub-reservoir temperature fluid. Hydraulic stimulation 1 occurred on February 24, 2012. The second hydraulic stimulation occurred from August 23, 2013
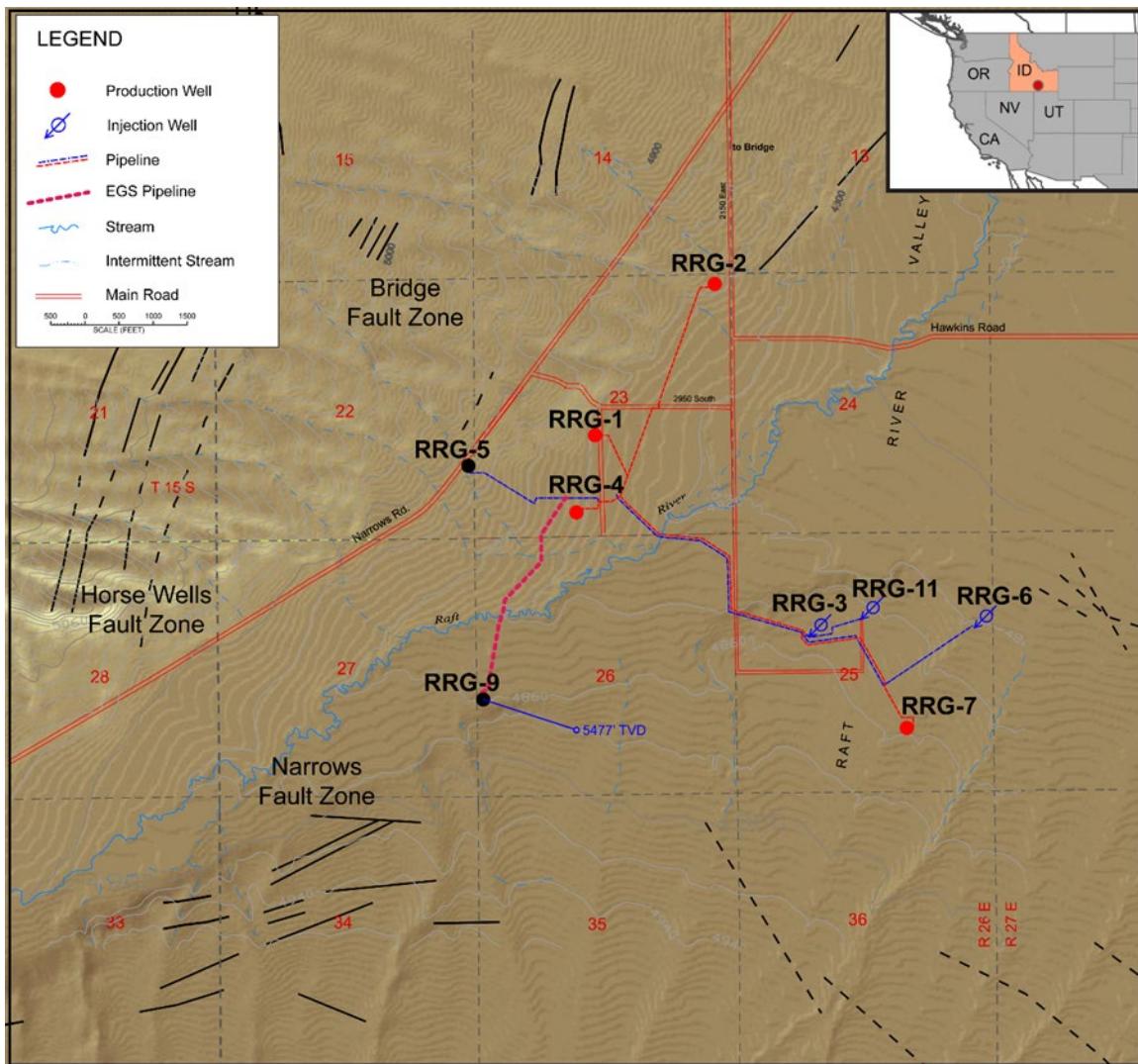
Figure 1. Raft River Geothermal Field. Injection wells and injection pipelines are shown in blue. Production wells and production pipelines are shown in red. The RRG-9 ST1 wellhead is shown in black and the 10-inch line connecting it to the power plant as a dark pink dashed line. Modified from [12].

to September 24, 2013 with injection of both plant and cold well water at increased flow rates and pressures. Hydraulic stimulation 3 occurred between April 1, 2014 and April 3, 2014 and utilized pump trucks to inject water at high rates and pressures. Near continuous injection of plant water through a 10-inch pipeline constructed between the plant and the RRG-9 ST1 wellhead began June 13, 2013. A 3-inch bypass line was constructed between the 10-inch line and the wellhead to accommodate low injection rates. Injection through the 3-inch bypass lasted from July 23, 2013 to November 25, 2014. Since February 2014 continuous injection of plant water has been through the 10-inch line. The well was shut-in from April 28, 2015 to May 26, 2015 and August 2, 2015 to August 17, 2015 to conduct pressure falloff testing. The stimulation stages are given in Table 1.

1.4 Field History

In 1971 the area was designated as a Known Geothermal Resource Area (KGRA) by the U.S. Geological Survey [13]. The field was initially developed by the Energy and

Table 1

RRG-9 ST1 Stimulation Program

Stimulation Phase	Date
Hydraulic Stimulation 1	2/24/2012
Shut-In	2/25/2012 to 6/12/2013
10-inch Line Injection	6/13/2013 to 7/22/2013
3-inch Bypass Line Injection	7/23/2013 to 8/23/2013
Hydraulic Stimulation 2	8/23/2013 to 9/24/2013
3-inch Bypass Line Injection	9/25/2013 to 3/31/2014
Hydraulic Stimulation 3	4/1/2014 to 4/3/2014
3-inch Bypass Line Injection	4/4/2014 to 11/25/2015
10-inch Line Injection	11/26/2015 to 4/27/2015
Shut-In	4/28/2015 to 5/26/2015
10-inch Line Injection	5/27/2015 to 8/1/2015
Shut-In	8/2/2015 to 8/17/2015
10-inch Line Injection	8/18/2015 to Present

Research Development Administration (ERDA), and later the Department of Energy (DOE), as a geothermal demonstration project from 1974 to 1982. From 1974 to 1980 84 exploration wells were drilled in the Raft River valley to characterize the geothermal resource [13]. Most of these wells were shallow, less than 1,000 ft. in depth, except for seven deep wells, five of which penetrated the Precambrian metamorphic basement [13]. These deep wells (RRG-1, 2, 3, 4, 5, 6, and 7) would provide the foundation for the geothermal demonstration plant in operation between 1981 and 1982 [14], [15]. In late 1979, two of these deep wells, RRG-4 and RRG-5, were hydraulically stimulated by Republic Geothermal Inc. [16]. Proppant and viscosity enhancing polymers were used in the stimulation of both wells, Table 2 [17]. As a result of this stimulation the productivity index of RRG-4 improved significantly from 0 to 0.6 gpm/psi while RRG-5 remained about the same at 2.0 gpm/psi [17]. Following the stimulation the wells were acoustically imaged,

Table 2

RRG-4 and RRG-5 Hydraulic Stimulations

Well	RRG-4	RRG-5
Date	8/20/1979	11/12/1979
Fluid	10 lb. H.P. Guar/1,000 gal 2 lb. XC Polymer/1,000 gal	30 lb. H.P. Guar/1,000 gal
Rate	2,100 gpm	2,100 gpm
Volume	331,800 gal	319,200 gal
Proppant	50,400 lb. 100 mesh 58,000 lb. 20/40 mesh proppant	84,000 lb. 100 mesh 347,000 lb. 20/40 mesh proppant
Interval	4,705-4,900 ft. (195 ft.)	4,587-4,803 ft. (216 ft.)
Fracture Height	195 ft.	135 ft.

showing that the hydraulic fracture generated in RRG-4 was nearly vertical and striking 72° East of North [18]. RRG-5's hydraulic fracture was also nearly vertical but striking 29° East of North [18]. As part of the geothermal demonstration project, a 7 MWe binary cycle geothermal power plant was constructed at the site between 1980 and 1982 [19]. The demonstration plant produced 4 MWe of electrical power [15]. Following successful demonstration of geothermal power generation, the DOE relinquished control of the site in 1982. U.S. Geothermal Inc. acquired the Raft River geothermal field in 2002. Commercial power production from the site began in 2008. A timeline of site activity prior to stimulation program is given by Figure 2.
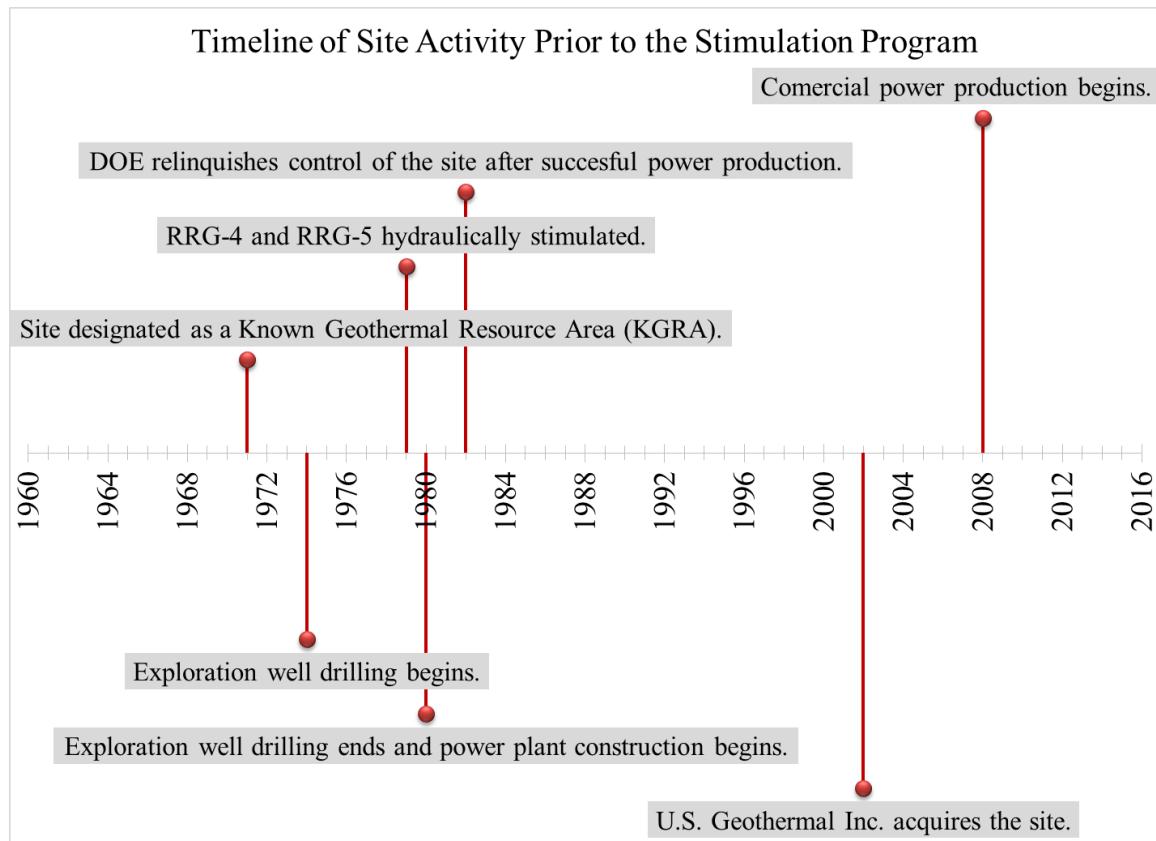
Figure 2 Timeline of site activity prior to the stimulation program.

1.5 Field Infrastructure

Currently, U.S. Geothermal operates a 13 MWe binary geothermal power plant using isopentane as the turbine working fluid. The plant is injection limited, injection rates are given in Table 3. After passing through the plant's heat exchangers, the fluid is reinjected back into the reservoir through four injection wells (RRG-3, 6, 9 ST1, and 11), Figure 3. Injection into a fifth well, RRG-5, was discontinued in September 2014. Four production wells (RRG-1, 2, 4, and 7) produce roughly 5,000 gpm of geothermal fluid from the Precambrian basement, Figure 3. Individual wells produce between 800 and 2,000 gpm; generating 1 MW of electric power per 433 gpm. The average resource temperature of the geothermal reservoir is 300 °F.

1.6 Geology

The geology of the Raft River geothermal field is complex. Quaternary and Tertiary volcanic and volcanoclastic rocks overlie Precambrian metamorphosed basement rocks. Most of the Mesozoic and all of the Paleozoic rocks are regionally missing. They have been pushed aside by regional uplifting due to an increase in thermal activity during the late Oligocene [20]. The Precambrian metamorphic basement rocks host the geothermal reservoir. Wells drilled at Raft River encountered nearly 5,000 ft. of Tertiary and Quaternary volcanic and volcaniclastic rocks comprising the Raft River and Salt Lake Formations. These formations overlie the Precambrian metamorphic basement rocks which include from top to bottom: the Quartzite of Yost, the Upper Narrows Schist, the Elba Quartzite, the Lower Narrows Schist, and the Quartz Monzonite, Figure 4. Fluid production in RRG-1, 2, and 4 is from the Elba Quartzite. RRG-7 produces from the Quartzite Monzonite. The injection wells RRG-3 and RRG-9 ST1 inject into the Precambrian

Table 3

Raft River Injection Wells

Injection Well	Injection Rates 5/15/2016 [gpm]
RRG-3	1,224
RRG-6	714
RRG-9 ST1	981
RRG-11	1,120
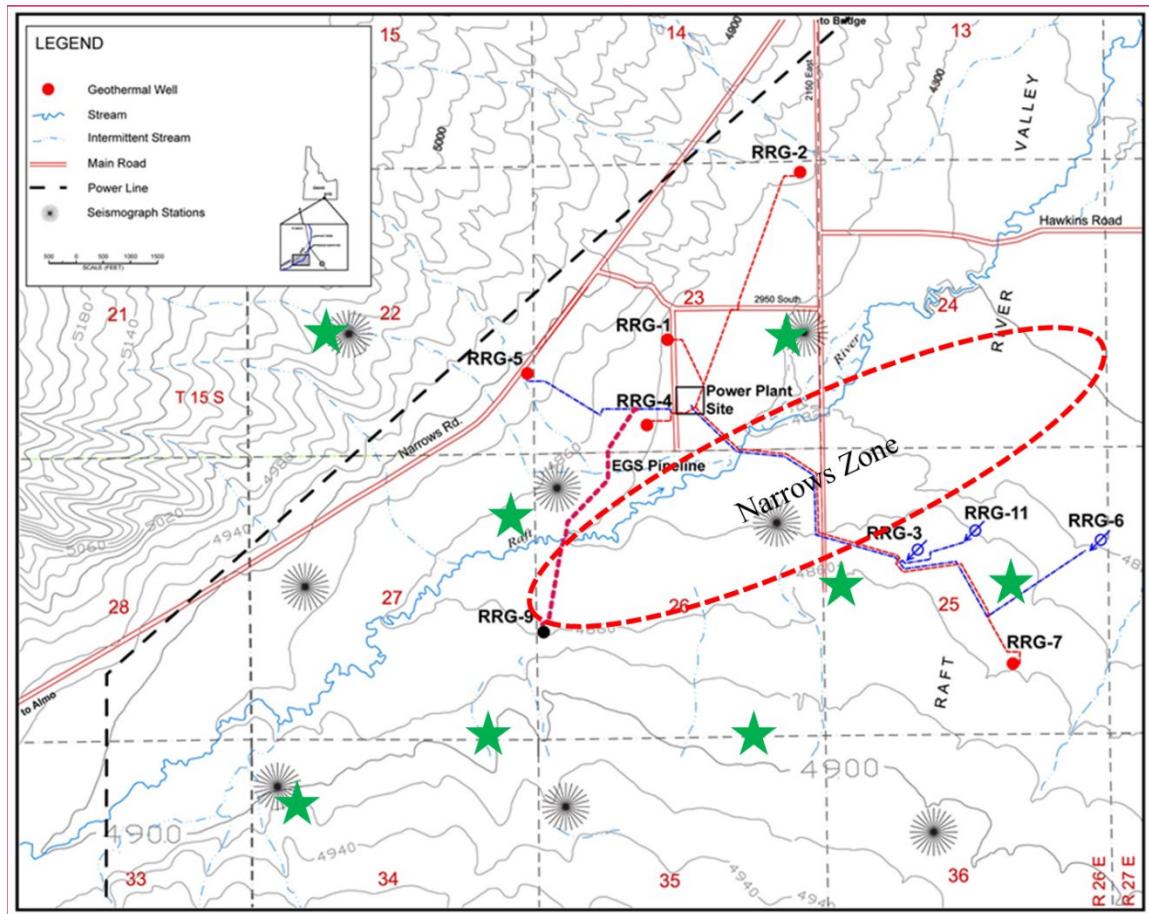
Figure 3 Raft River well locations and infrastructure. Injection wells and injection pipelines are shown in blue. Production wells and production pipelines are shown in red. The RRG-9 ST1 wellhead is shown in black and the 10-inch line connecting it to the power plant as a dark red dashed line. The previous locations of the microseismic monitoring stations are shown as black sunbursts. The current positions of the microseismic monitoring stations are shown as green stars. Modified from [12].
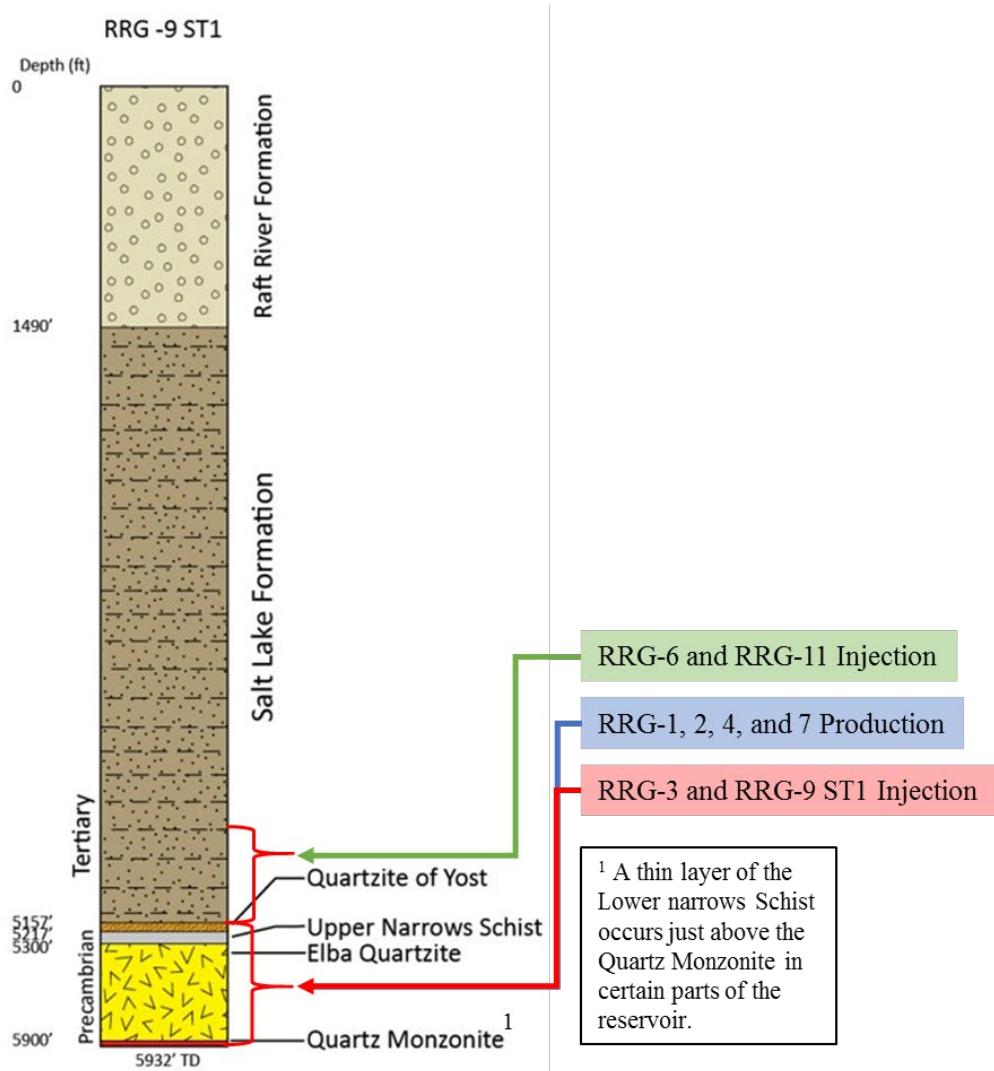
Figure 4 Raft River lithology at RRG-9 ST1. From [21].

basement while RRG-6 and RRG-11 inject into the shallower Tertiary formations. Thin sections of the Elba Quartzite from RRG-9 ST1show that the reservoir rocks have almost no matrix porosity. The low porosity of the reservoir indicates that fluid flow is predominantly through fractures and faults.

1.7 The Narrows Zone

The water chemistry at Raft River has been characterized by several studies conducted during the DOE geothermal demonstration project during the 1970's and early

1980's [14]. Additional studies were performed by U.S. Geothermal after they acquired the property in 2002, and by the Energy & Geoscience Institute (EGI) at the University of Utah in 2010 [14]. The results from these studies show that there are four distinct water types at Raft River, two deep geothermal types and two shallow ground water types. Geothermal water samples collected from wells in the northwest part of the field (RRG-1, 2, and 5) have lower salinities (reduced levels of K, Li, Ca, Cl, and Na) compared to the wells in the southeastern portion of the field (RRG-3, 6, 9, and 11) [14], Figure 5. Geothermometry indicates that both water types have the same reservoir temperatures, Figure 6. Both of these geothermal water types are produced from similar depths in the Precambrian basement. Ayling and Moore [14] suggest that the difference in chemistry reflects different fluid paths and that a fluid barrier exists between the northwest and southeast portions of the field. This barrier, referred to as the Narrow Zone, is interpreted to be a steeply dipping shear zone located in the Precambrian basement. There is no effect of the overlying rocks across this zone. The location of microseismic events can be generally correlated to the
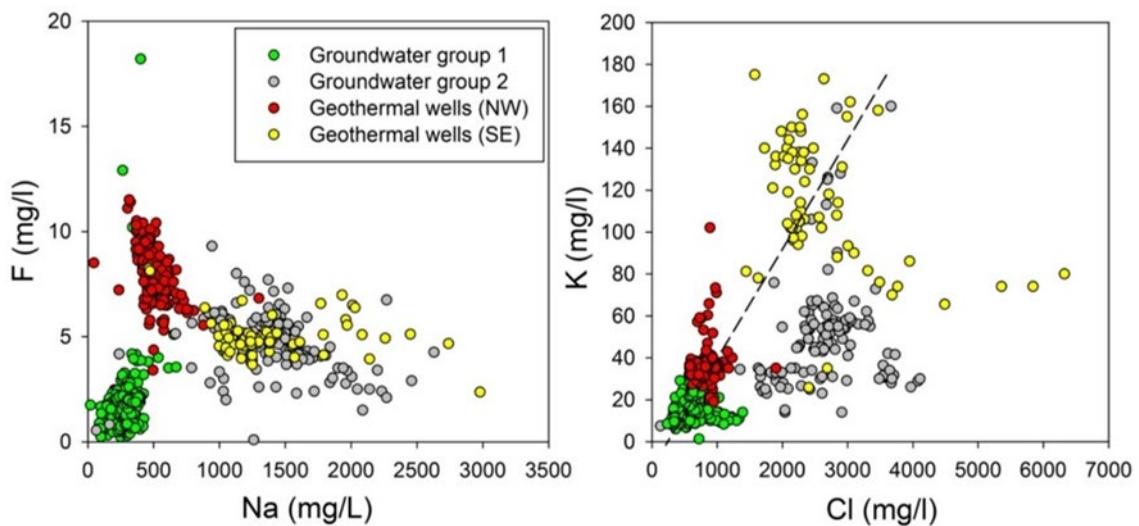
Figure 5 Raft River water chemistry.From [14].
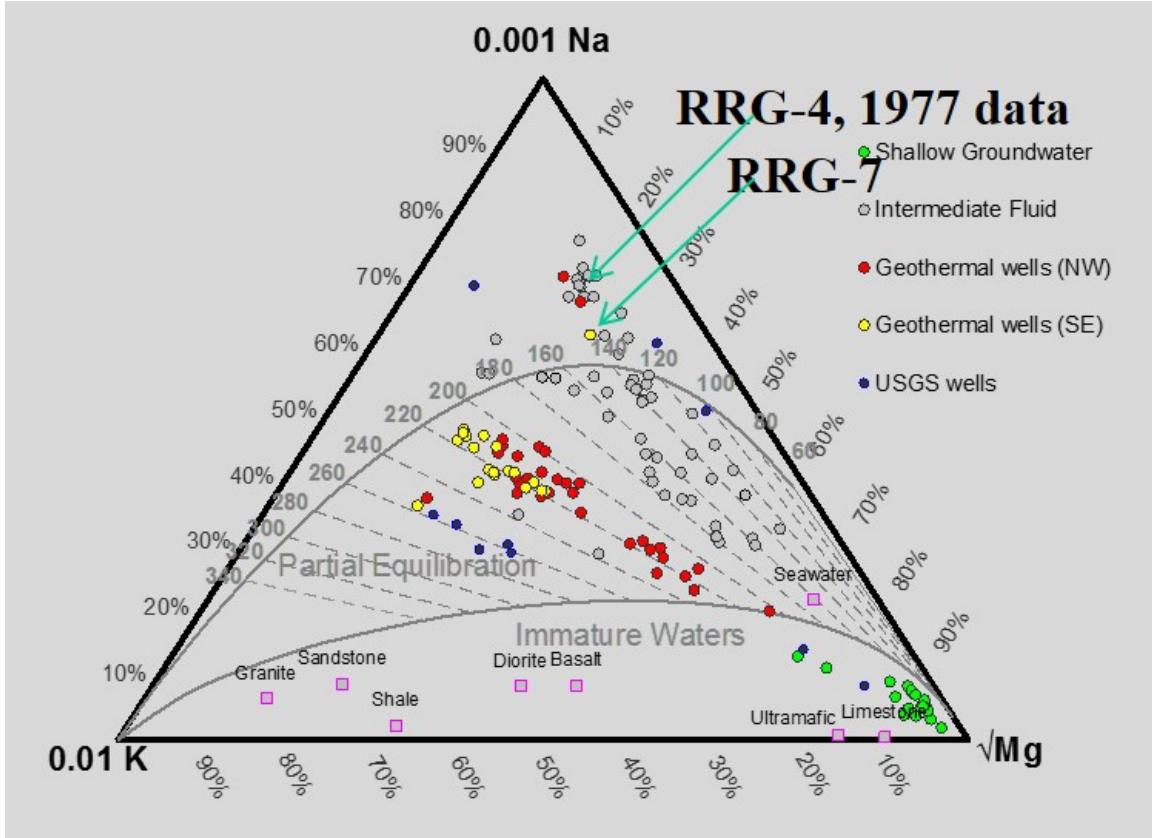
Figure 6 Raft River geothermometry. From [14].

presence of the Narrows fault zone at Raft River [22]. These data, discussed later, suggest that the Narrows Zone strikes northeast-southwest. Although this zone appears to act as a barrier to fluid flow across the fault zone there is microseismic evidence indicating that it allows fluid flow along its length to the northeast. Tracers injected into RRG-9 ST1 have been recovered at the production wells (RRG-2 and RRG-4) to the northeast. This suggests that fluid injected into the well passed through the Narrows Zone on its way to these production wells.

1.8 RRG-9 ST1

RRG-9 was originally drilled to explore the southwest extension of a high temperature fracture found in RRG-7 and the southwest extension of the Bridge fault. The

well was drilled to a depth of 6,072 ft. measured depth (MD) and penetrated the Precambrian basement at 5,286 ft. MD [21]. The well was shut in and a bridge plug was placed in the well at a depth of 2,262 ft. MD. RRG-9 was selected by the DOE as an EGS demonstration well. On December 29, 2011, preparations to make RRG-9 ready for injection were started by drilling through a bridge plug placed in the well at a depth of 2,262 ft. MD [21]. Instead of drilling through the bridge plug, encountered on January 3, 2012, the drill bit deviated from the original well course into the surrounding formation [21]. Drilling continued along this deviated course, side-tracking the well to a depth of 5,459 ft. MD by January 17, 2012. The well was logged on January 20, 2012. After logging the well was further deepened to a measured depth of 5,932 ft. RRG-9 ST1 was cased to a measured depth of 5,551 ft. leaving 381 ft. MD of open-hole below the casing shoe [21]. Drilling and completion activities were finished by February 18, 2012. RRG-9 ST1 encountered the Precambrian basement at 5,152 ft. MD and the Elba Quartzite at 5,300 ft. MD. The well penetrates through 600 ft. MD of the Elba Quartzite before entering the Lower Narrows Schist at 5,900 ft. MD. Figure 7 and Figure 8 show the spatial relationship between RRG-9 ST1 and the original RRG-9 well. A 10-inch pipeline was constructed between the plant and the wellhead to allow for continuous injection during the stimulation program. The pipeline was finished in May, 2013. When initial injection rates were lower than expected, a 3 inch bypass line was constructed in July, 2013 from the 10 inch line to the wellhead to accommodate the reduced flow.
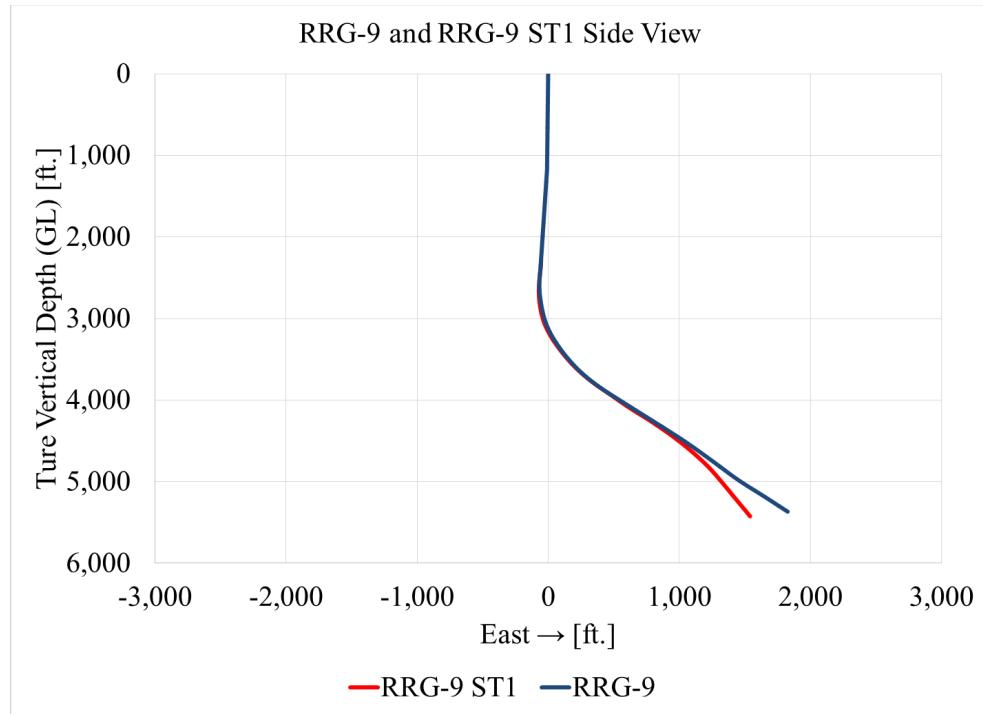
Figure 7 RRG-9 (blue) and RRG-9 ST1 (red) side view. Distance relative to ground level and the wellhead.
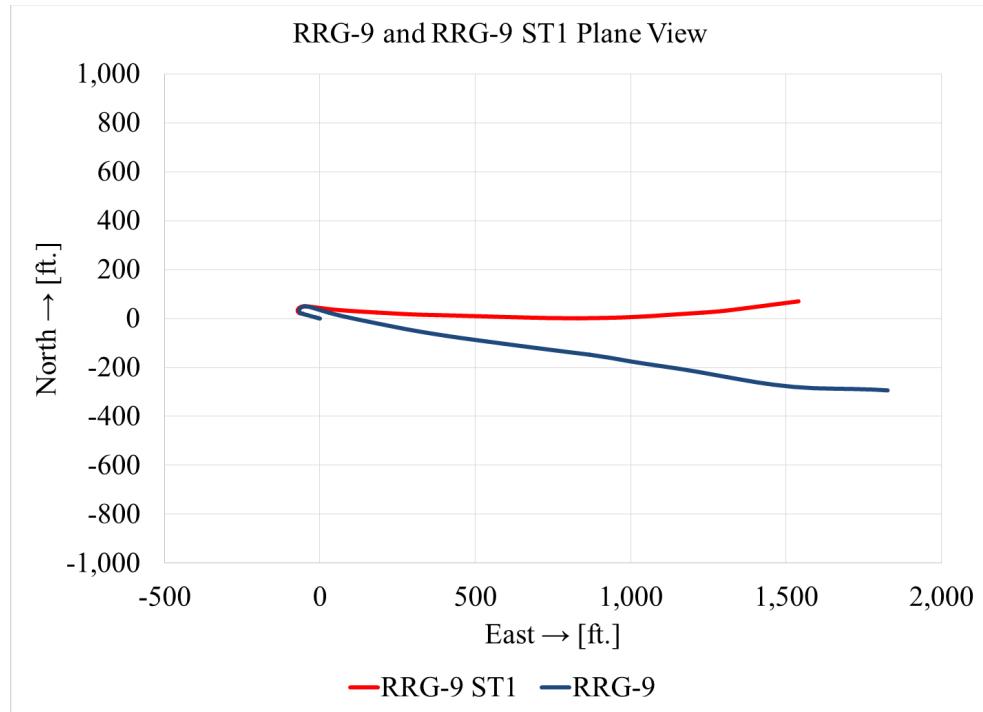
Figure 8 RRG-9 (blue) and RRG-9 ST1 (red) plane view. Distances relative to the wellhead.

FIELD DATA

The RRG-9 ST1 stimulation program consisted of three hydraulic stimulations along with nearly continuous injection of sub-reservoir temperature fluid. Injection flow rate, wellhead pressure, surface temperature, and microseismic activity have been continuously monitored. Additionally, the well has been logged and acoustically imaged.

2.1 Well Logging

A suite of wire-line logs were run by Baker Hughes from 2,320 ft. MD to a depth of 5,528 ft. MD on January 20, 2012 [21]. These logs included gamma ray, compressional wave slowness, shear wave slowness, high definition induction, and compensated z-densilog logs. From the gamma ray log the Precambrian formation tops were identified. Bulk density and neutron porosity logs show that the Precambrian basement rocks are significantly denser and have much lower porosity than the Tertiary rocks above. The Acoustic logs coupled with pressure and rate data from the first Hydraulic stimulation were used obtain an initial estimate of the horizontal stresses acting on the wellbore. A minimum horizontal stress gradient of 0.62 psi/ft. in the Elba Quartzite was inferred from the first hydraulic stimulation [23]. Additionally, the minimum horizontal stress profile obtained from the acoustic log and numerical modeling suggest that hydraulic fractures generated in the Elba Quartzite would remain in the formation and not grow into the Upper Narrows

Schist above [24].

On February 23, 2012, a borehole televiewer imaged the open-hole section of the well, 5,525 to 5,920 ft. MD. Within this open-hole section, 82 naturally occurring fractures intersected the well. The majority of these are steeply dipping at high angles and strike to the northeast, Figure 9. A major fracture zone located between 5,640 ft. MD and 5,660 ft. MD was identified. A temperature survey conducted at the same time showed that this zone was accepting fluid, indicating that the fractures were conductive. Additional monitoring via a distributed temperature sensor has shown that this zone has nominally accepted all of the injected fluid.

2.2 Stimulation Program Monitoring

Injection rate, wellhead pressure, and surface temperature have been monitored on a nearly continuous basis since June of 2013. Figure 10 shows the location of the injection rate, pressure, and temperature sensors on the 10-inch line. Pressure transducers were installed on both the 10-inch line and on the RR-9 ST1 wellhead. Additionally, a pressure sensor was placed just above the casing shoe (5,551 ft. MD) to monitor near bottom-hole pressures during the pressure fall-of testing during April and August 2015. This sensor has been operational since April 9, 2015. A temperature sensor was also placed on the 10-inch line. A Distributed Temperature Sensors (DTS) placed in the well has been used intermittently since June 2013. The DTS data suggests that nominally all of the injected fluid into RRG-9 ST1 enters the fracture zone intersecting the wellbore between 5,640 and 5,660 ft. MD. Initially, flow rates were monitored by an orifice plate meter. However, initial flow through the 10-inch line, June 13, 2013 to July 23, 2013 was not high enough to be measurable by that device. An ultrasonic flow meter was installed, July 23, 2013, on
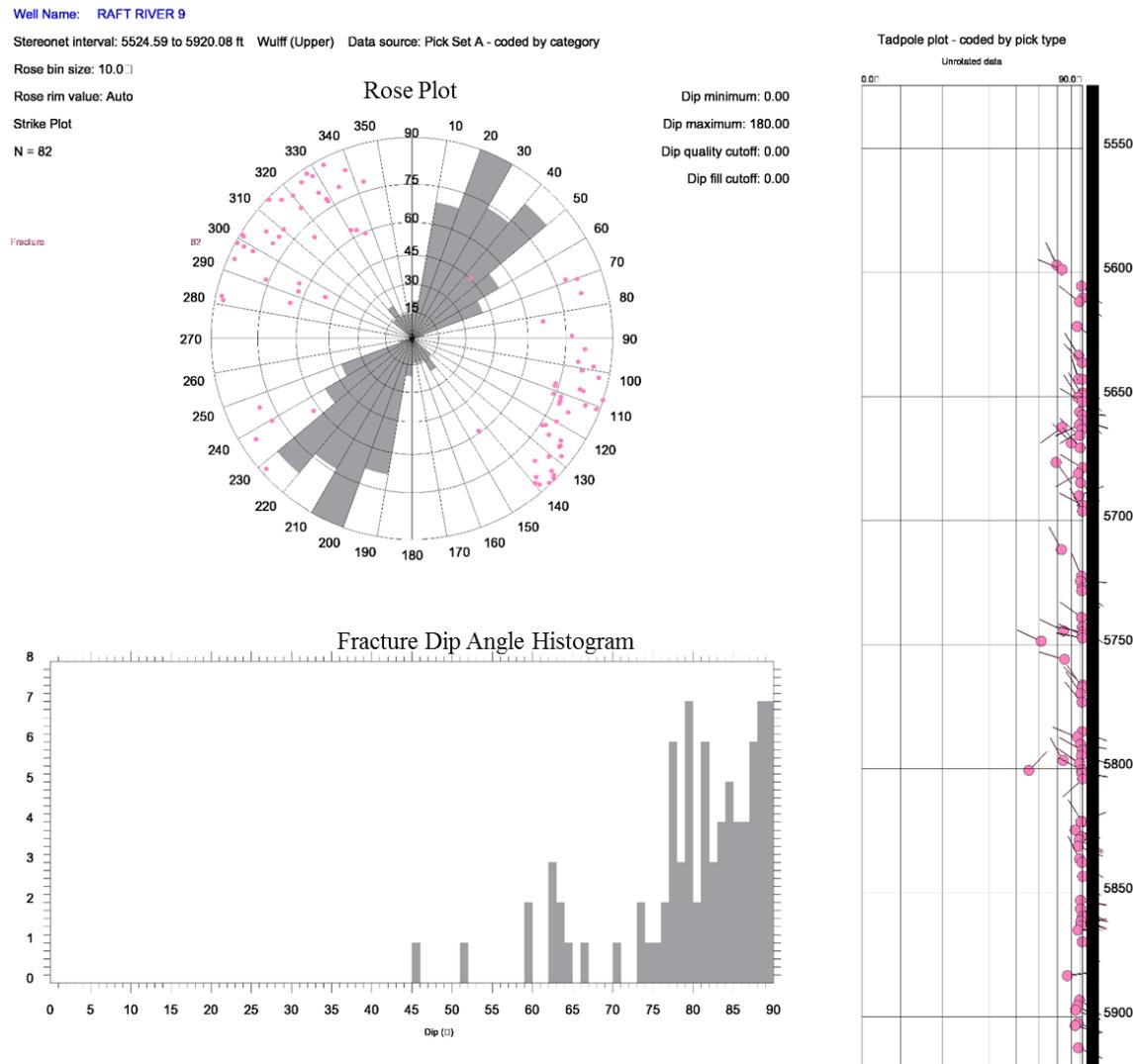
Figure 9 Statistics for fractures intersecting the wellbore between 5,525 ft. MD to 5,920 ft. MD: rose plot, fracture dip angle histogram, and tadpole plot. The rose plot shows the strike direction of the fractures. The fracture dip angle histogram shows the number of fractures that dip at a particular angle. The tadpoles show the dip angle and the dip azimuthal orientation of the intersecting fractures.
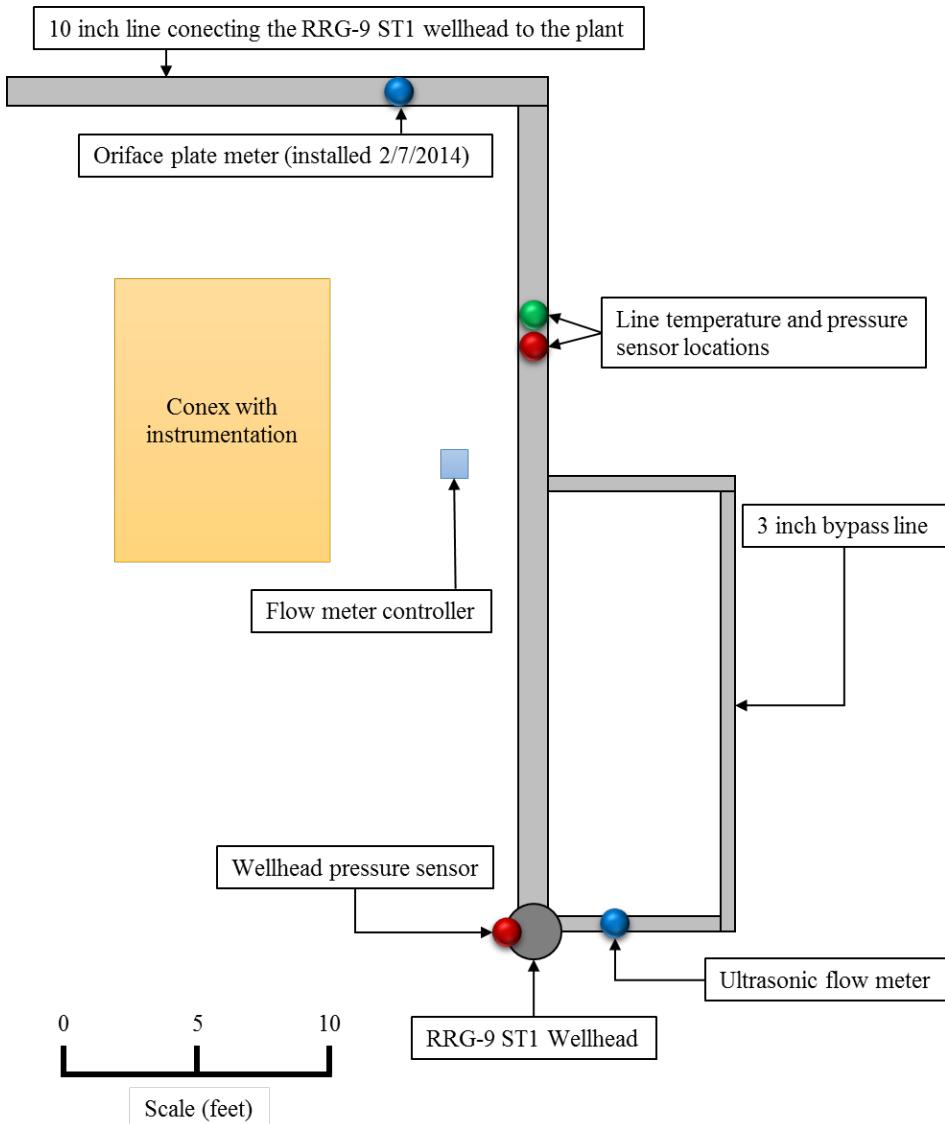
Figure 10 RRG-9 ST1 wellhead layout. The conex is a small structure that houses the instrumentation for the sensors.

the 3-inch line to correct this deficiency. On November 14, 2013 the ultrasonic flow meter stopped working properly and was replaced by an orifice plate meter on the 10-inch line, February 7, 2014. By then, flow rates through the 10-inch line were sufficient to obtain accurate readings from this device. An 8 station microseismic array was placed around RRG-9 ST1 in May 2013. Each station consists of a geophone cemented in a 300 ft. borehole. In response to microseismic activity to the northeast some microseismic stations

were repositioned in 2016, Figure 3.

2.3 Hydraulic Stimulation 1

Injection into RRG-9 ST1 began with the first hydraulic stimulation on February 24, 2012. The objective of this stimulation was to test the ability of the well to accept fluid. During the stimulation, injection rates were increased in a step wise fashion from 13 to 207 gpm in 5 steps using a pump truck, Table 4 and Figure 11. The steps lasted between 20 to 30 minutes each. The wellhead pressure increased from 147 to 778 psig. Injection was then halted for several hours due to a leak in the line. After the leak was repaired, injection resumed at a rate of 205 gpm and was increased to 779 gpm in 4 steps. Each step lasted between 20 and 30 minutes. Wellhead pressure increased from 704 to 1,139 psig. Over 55,000 gallons were injected into the well during the stimulation.

Part two of the hydraulic stimulation consisted of a step-down test, which is one of the more common methods of measuring the in-situ stress [25]. Flow rates started at 550

Table 4

Hydraulic Stimulation 1 Part 1.

Injection Stage	Average Injection Rate [gpm]	Stage Injected Volume [gal]	Average Wellhead Pressure [psi]	Stage Duration [hr:min:sec]
1	13	330	147	0:29:50
2	23	568	319	0:24:31
3	42	1,164	460	0:26:46
4	105	3,180	639	0:30:22
5	207	3,288	778	0:15:51
Injection Line Leak				
6	205	4,234	704	0:20:26
7	412	12,560	982	0:30:23
8	624	14,280	1,111	0:22:46
9	779	15,619	1,139	0:20:03
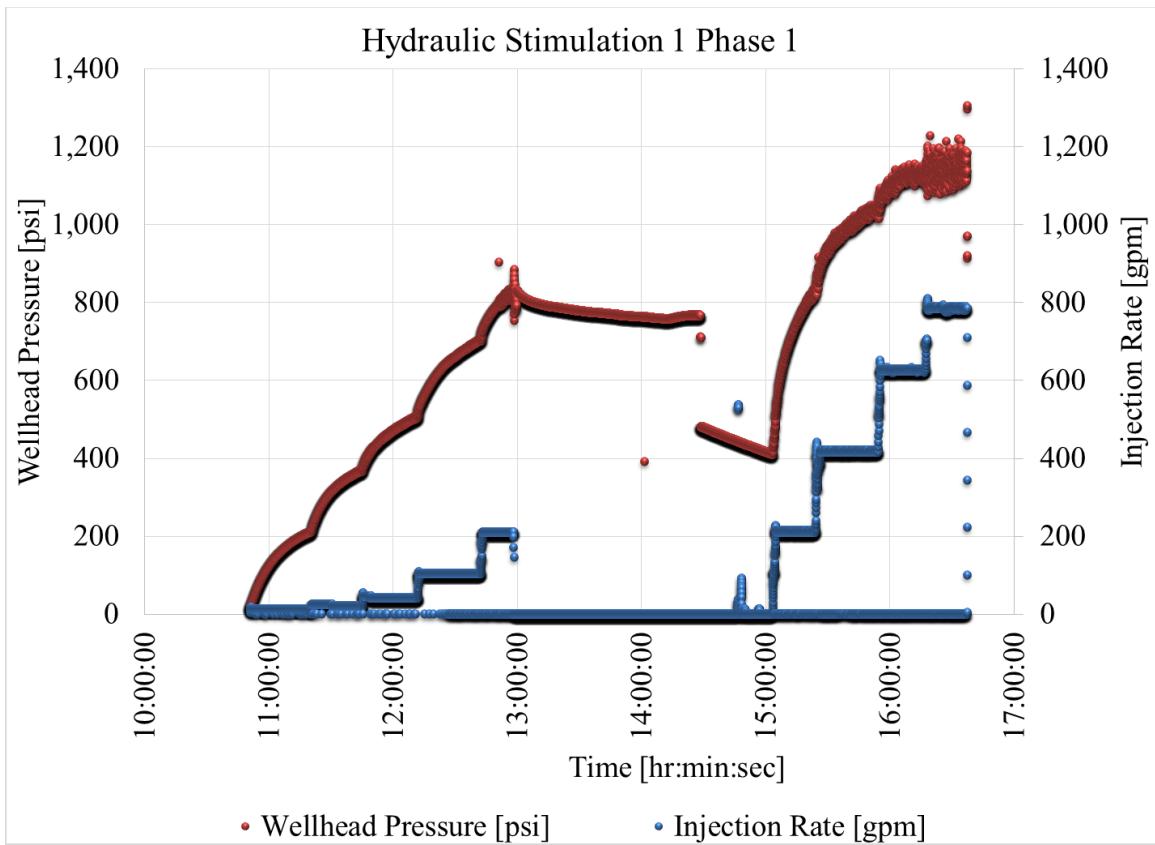
Figure 11 Hydraulic stimulation 1 part 1. Injection rates are in blue and wellhead pressures are in red. Injection rates were increased from 13 to 779 gpm at a maximum wellhead pressure of 1,139 psig.

gpm and were reduced in a step wise-manner to 12 gpm through 7 stages, Table 5 and Figure 12. Each stage lasted between 10 and 17 minutes. Wellhead pressures fell from 978 to 800 psig during this phase. Over 25,500 gallons were injected during Phase 2. Following this hydraulic stimulation, the well was shut in from February 25, 2012 to June 13, 2013. During this time period, DOE environmental reviews were completed and the 10-inch pipeline was constructed from the plant to the wellhead to facilitate continuous injection.

2.4 Hydraulic Stimulation 2

Injection through the newly installed 10-inch line began on June 13, 2013. This consisted of plant water injected into the well by an injection pump. Initial injection rates

Table 5

Hydraulic Stimulation 1 Part 2

Injection Stage	Average Injection Rate [gpm]	Stage Injected Volume [gal]	Average Wellhead Pressure [psi]	Stage Duration [hr:min:sec]
1	550	15,245	978	0:12:12
2	409	4,101	1,009	0:10:01
3	217	3,237	984	0:14:53
4	108	1,743	932	0:16:10
5	46	747	888	0:16:47
6	22	347	842	0:15:07
7	12	125	800	0:15:06
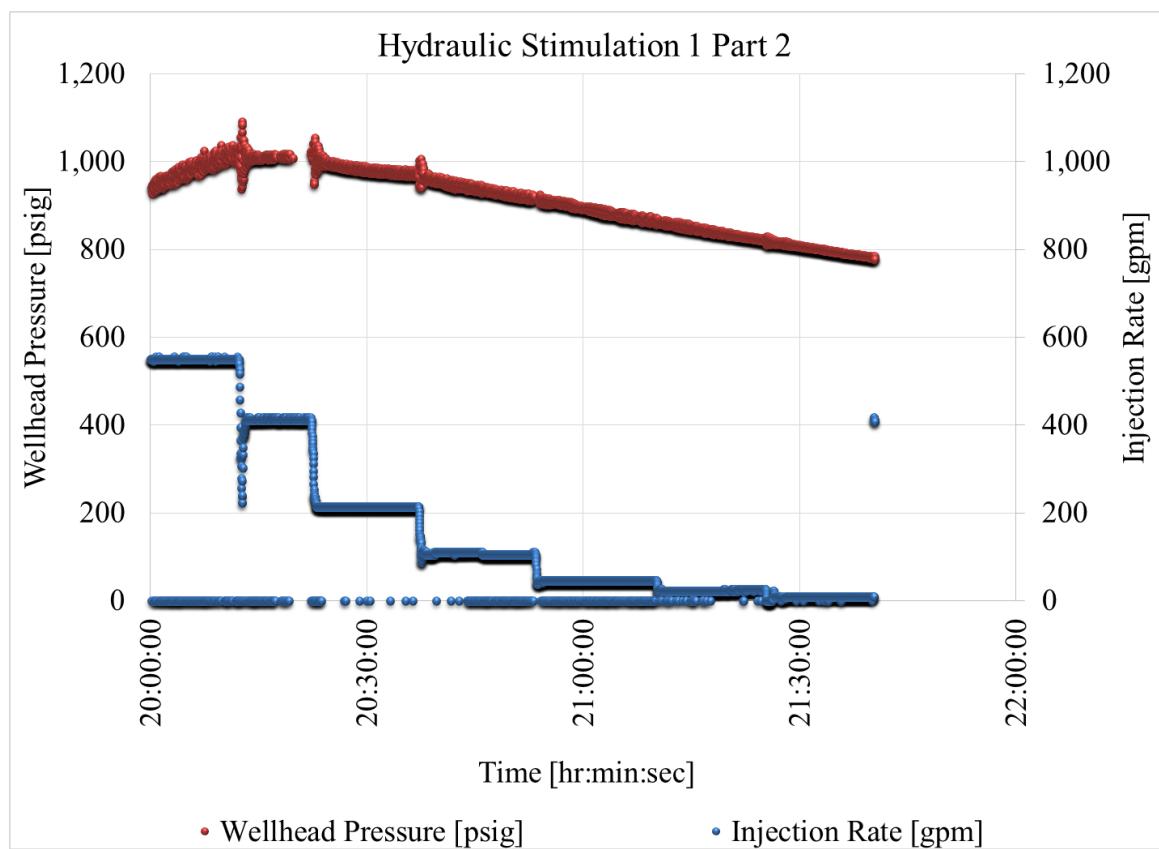
Figure 12 Hydraulic stimulation 1 part 2. Injection rates are in blue and wellhead pressure are in red. Injection rates were decreased from 550 gpm to 12 gpm.

at a wellhead pressure of 280 psig were much lower than expected (less than 40 gpm). This was likely due to the closing of the fracture opened during the first hydraulic stimulation. The average injection fluid temperature was 93 °F. Injection continued through August 23, 2013, when a second hydraulic stimulation was performed. For this second stimulation, agricultural pumps were utilized to increase injection rates and stimulate the well -in three phases, Table 6. Phase 1 of the second stimulation lasted from August 23 to August 30, 2013, during which one pump was used to increase injection rates up to 148 gpm at a wellhead pressure of 537 psig. Phase 2 began on August 31 and lasted until September 8, 2013. During this phase, an additional pump was used to further increase injection rates up to nominally 283 gpm at a wellhead pressure of nominally 862 psig. In Phase 3, injection was switched over to cold well water with injection rates up to 257 gpm at a wellhead pressure of 741 psig. Phase 3 lasted until September 24, 2013. Injection of plant water through the 10-inch line was resumed on September 25, 2013. Following this second hydraulic stimulation, injection rates increased up to124 gpm at a wellhead pressure 270 psig. Injection was maintained through March 31, 2014, Figure 13. During this time, injection improved to 141 gpm at a wellhead pressure of 276 psig.

Table 6

Hydraulic Stimulation 2

Phase	Date	Injection Source	Average Injection Rate [gpm]	Average Wellhead Pressure [psig]	Average Injection Temperature [°F]
1	8/23/2013 to 8/30/2013	Plant Water	141	541	104
2	8/31/2013 to 9/8/2013	Plant Water	262	809	115
3	9/9/2013 to 9/24/2013	Cold Well Water	210	590	66
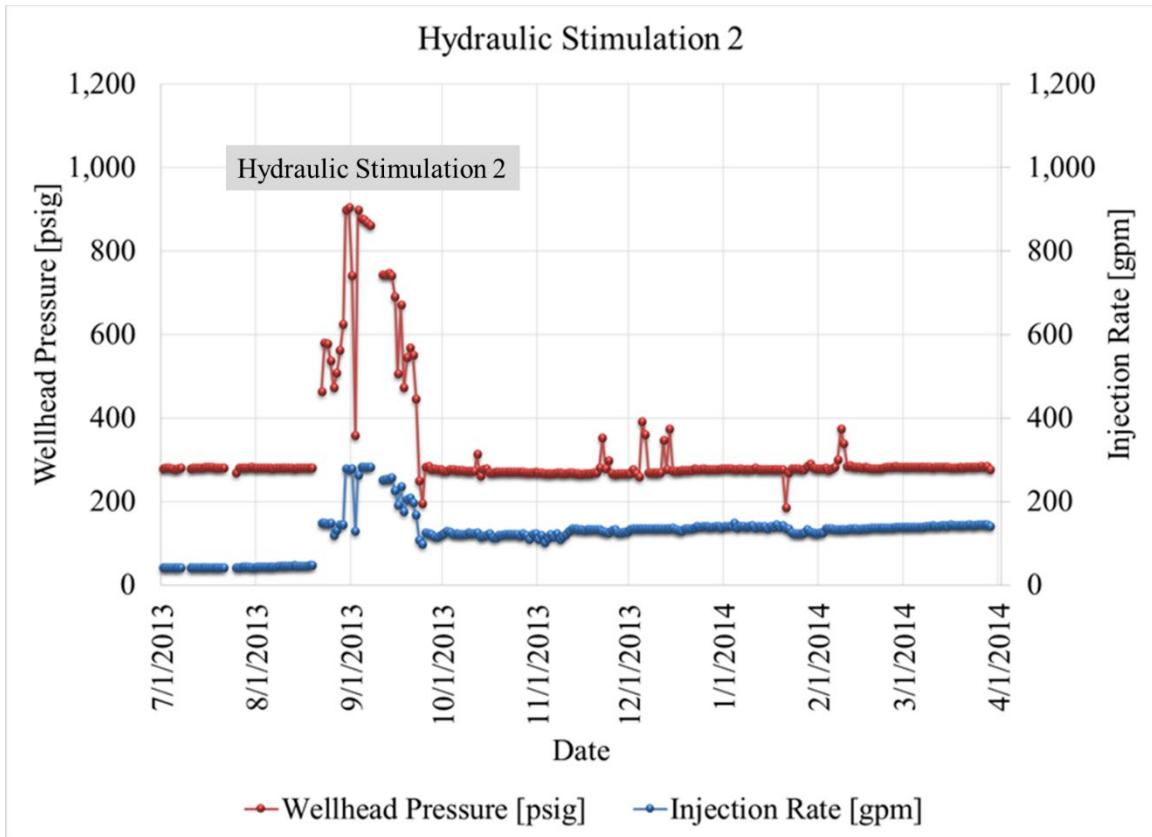
Figure 13 Hydraulic stimulation 2 Injection rates are shown in blue, and wellhead pressure are shown in red. Apart from the second hydraulic stimulation injection rates and pressures remain relatively constant during this time period.

2.5 Hydraulic Stimulation 3

A third hydraulic stimulation was conducted between April 1 and April 3, 2014, using 2 pump trucks. This stimulation was conducted in two phases. In Phase 1, a maximum flow rate of 846 gpm at a wellhead pressure of 849 psig was achieved, Table 7 and Figure 14. Pumping at this rate lasted for just under six hours. 374,355 gallons were injected in phase 1. In phase 2, injection rates were further increased to 1,207 gpm at a wellhead pressure of 924 psig by adding an additional pump truck, Table 8 and Figure 15. After a little over four hours of pumping at this rate, injection rates were reduced to 860 gpm at a wellhead pressure of 866 psig due to excessive vibration in the pumps caused by

Table 7

Hydraulic Stimulation 3 Phase 1

Stage	Average Injection Rate [gpm]	Stage Injected Volume [gal]	Average Wellhead Pressure [psi]	Stage Duration [hr:min:sec]
1	209	14,289	109	1:08:22
2	419	25,077	343	0:59:51
3	628	37,324	596	0:59:26
4	846	297,665	849	5:51:51
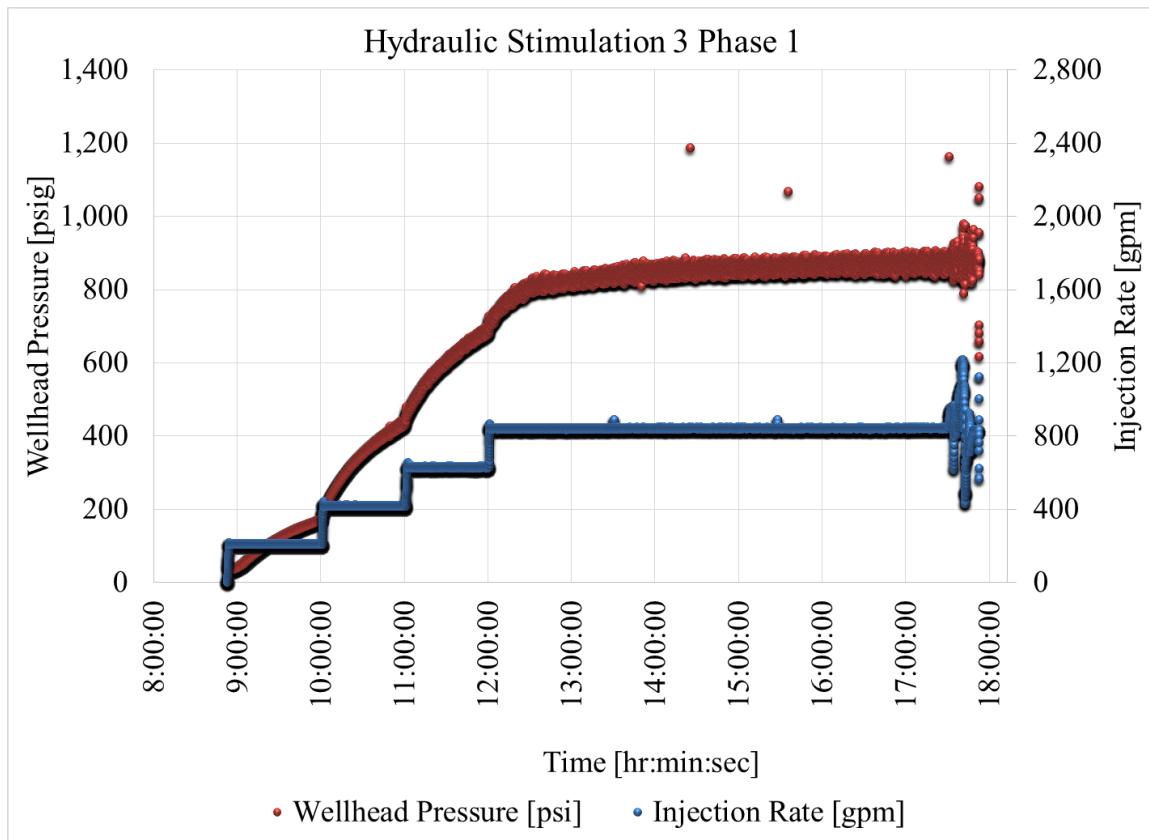
Figure 14 Hydraulic stimulation 3 phase 1. Injection rates are shown in blue and wellhead pressures are shown in red. During phase 1 an injection rates reached 846 gpm at a wellhead pressure of 849 psig. This rate was maintained for almost six hours.

Table 8

Hydraulic Stimulation 3 Phase 2

| Stage	Average Injection Rate [gpm]	Injected Volume [gal]	Average Wellhead Pressure [psi]	Duration [hr:min:sec]
1	412	20,318	127	0:49:19
2	830	45,014	566	0:54:14
3	1,207	400,261	924	5:31:37
4	860	208,220	886	4:02:07
5	422	19,954	542	0:47:17
6	212	6,735	0	0:31:46
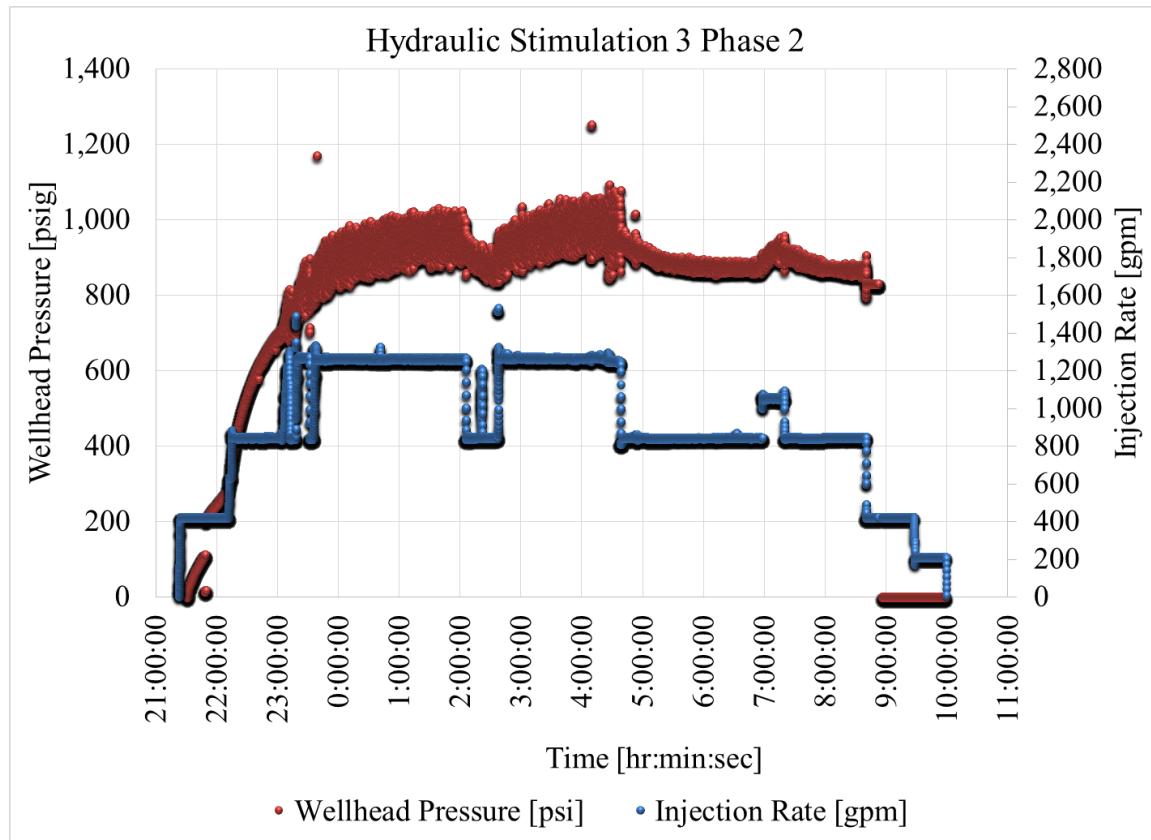
Figure 15 Hydraulic stimulation 3 phase 2. Injection rates are shown in blue, and wellhead pressures are shown in red. An injection rate of 1,207 gpm was reached at a wellhead pressure of 924 psig. Excessive vibrations in the pump at this rate required a reduction in flow rate to 860 gpm at a wellhead pressure of 866 psig.

the third pump truck. This reduced flow rate was maintained for just over four hours. 700,502 gallons were injected during phase 2. Following this third hydraulic stimulation, plant water injection was resumed through the 10-inch line. As a result of the third hydraulic stimulation, injection rates improved to 252 gpm at a wellhead pressure of 254 psig. Injection through the 10-inch line was maintained through April 27, 2015, Figure 16. Unlike the period following the second hydraulic stimulation, injection rates continued to improve after the third hydraulic stimulation, Figure 16. By April 27, 2015, injection rates had improved to 550 gpm, a rate considered successful by the DOE, at a wellhead pressure of 270 psig.
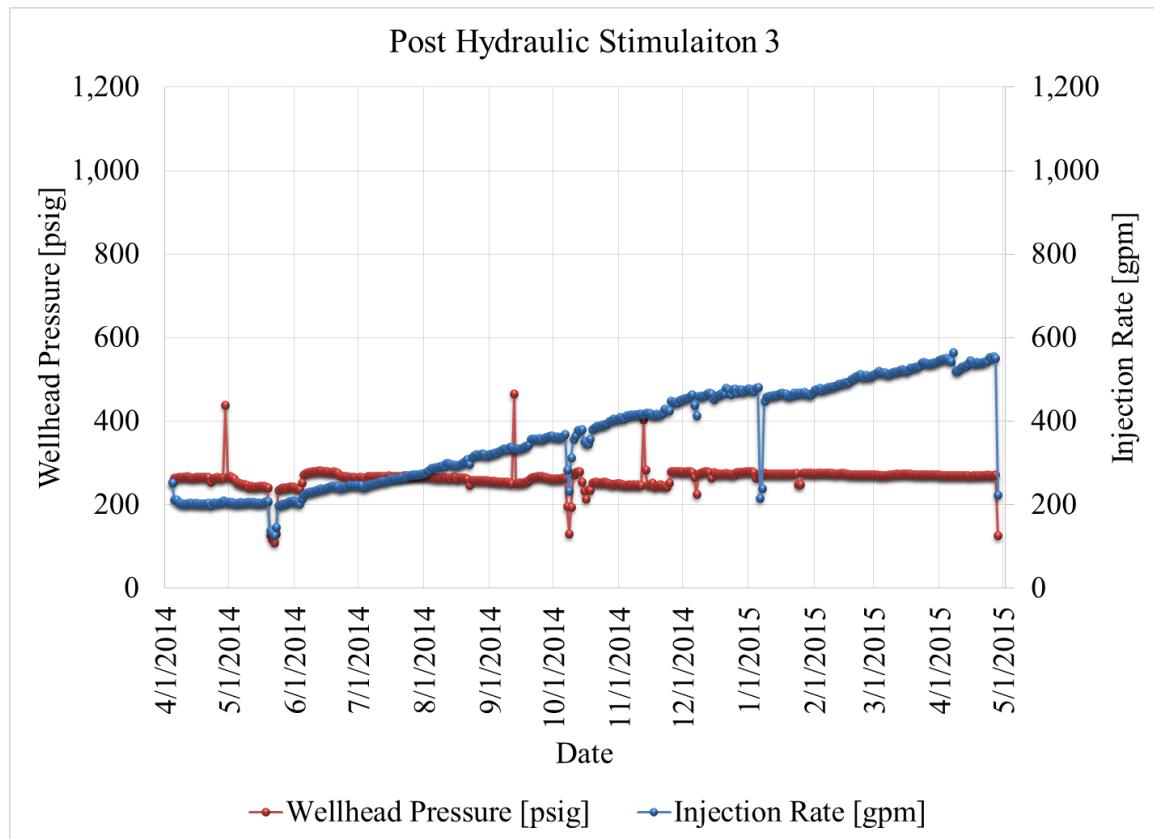
Figure 16 Post hydraulic stimulation 3. Injection rates are shown in blue and wellhead pressures are shown in red. After the third stimulation injection rates began to increase while injection pressures decreased slightly during this time period (4/4/2014 to 4/27/2015).

2.6 Shut-In and Pressure Falloff Testing

In other injection wells in the field it had been observed that shutting the wells in for a short period of time helped improve their injectivity [26]. This technique was applied to RRG-9 ST1. The well was shut in on April 28, 2015, Figure 17. During this time the plant was shut down between May 4, 2015 and May 16, 2015. The bottom-hole pressure in RRG-9 ST1 dropped further after the plant was shut down, but began to recover after several days, Figure 17. After the plant came back online the bottom-hole pressure continued to increase eventually leveling off after nearly a week, Figure 17. Injection resumed on May 27, 2015. This behavior indicates that there is some communication between RRG-9 ST and the other nearby injection wells (RRG-3, 6, and 11). Analysis of the falloff data indicates that fracture zone intersection RRG-9 ST1 is substantial [27].
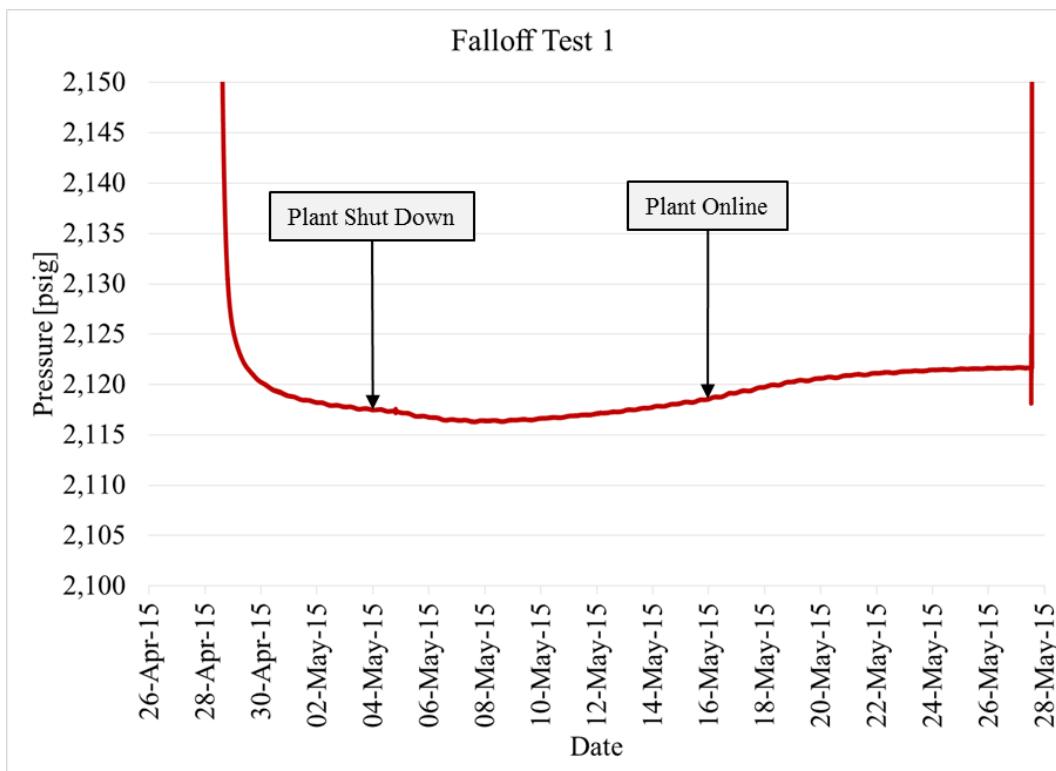
Figure 17 Falloff test 1 pressure data.

Following the shut-in, the injection rate began to improve at a faster rate than before, Figure 18. The well was shut in again from August 2 to August 18, 2015. Again, on resumption of injection, the flow rates continued to increase. By April 13, 2016, injection rates had increased to just under 970 gpm at a wellhead pressure of 190 psig. Over 605 million gallons have been injected into RRG-9 ST1 as part of the EGS stimulation program, Figure 19.

2.7 Microseismic Activity

Since 2010, 187 microseismic events related to plant activity have been recorded. The location of the microseismic monitoring stations is given in Figure 3. The recorded
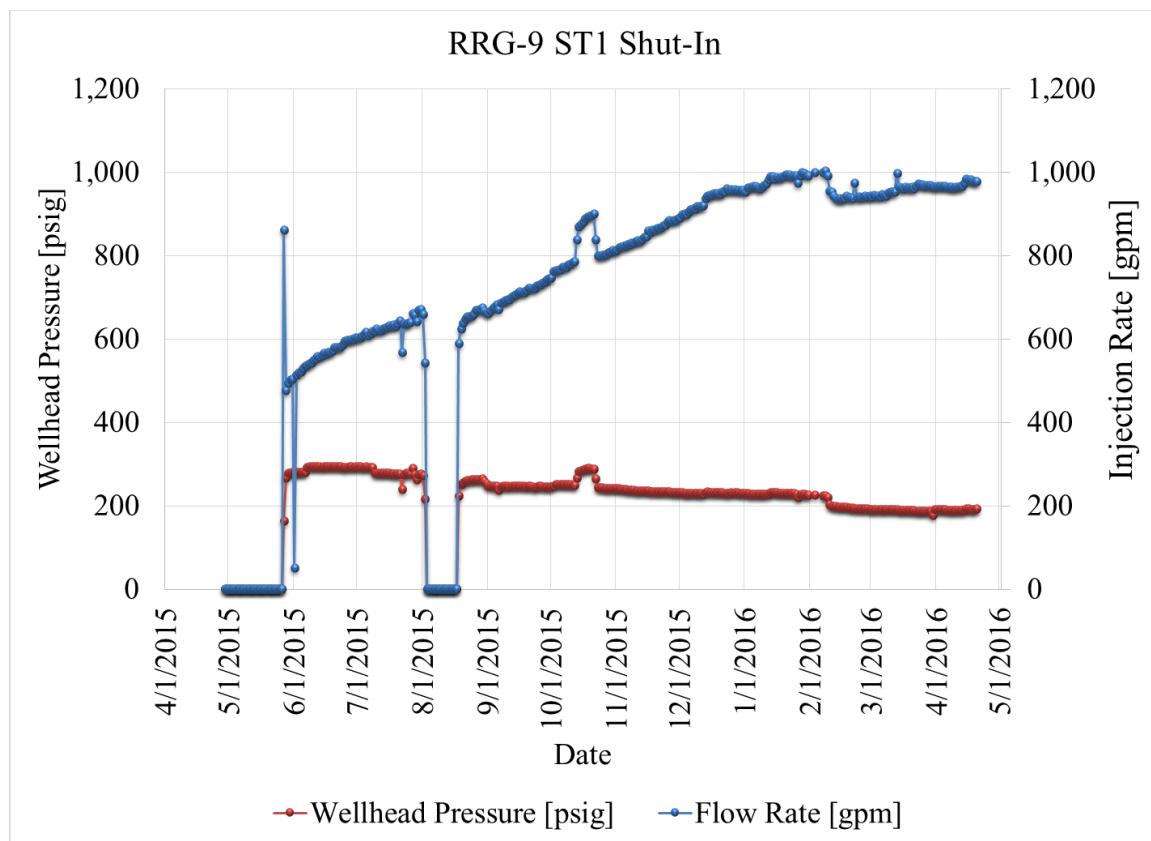
Figure 18 RRG-9 ST1 shut-in. Injection rates are shown in blue and wellhead pressures are shown in red. Injection rates increased at a greater rate than before the well was shut in. Injection pressure also decreased slightly during this time period.
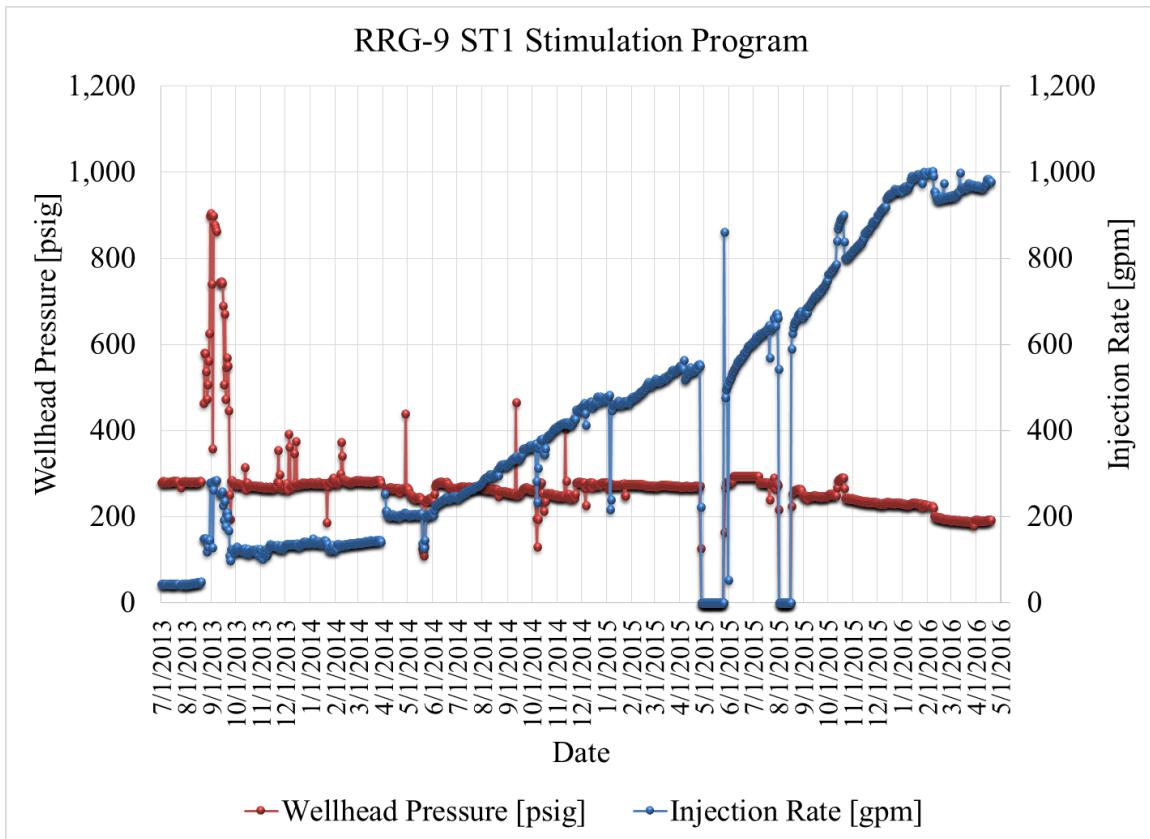
Figure 19 RRG-9 ST1 stimulaton program. Injection flow rates are shown in blue and wellhead pressures are shown in red. Injection rates increased to just under 970 gpm over the course of the stimulation program while injection pressure remained relatively stable.

events ranged in magnitude from -1.25 to 1.01. Generally, the microseismic events recorded prior to injection from the plant have a greater magnitude than those recorded after. The microseismic events recorded before June 13, 2013 have an average magnitude of 0.109. This is much larger than those recorded after June 13, 2013 which have an average magnitude of -0.46, Figure 20. The majority of microseismic activity occurred during the early part of the stimulation program through the third hydraulic stimulation, Figure 21. After the third hydraulic stimulation the number of microseismic events began to falloff rapidly, Figure 21. Microseismic events have been recorded between 1,641 ft. and 11,484 ft. in depth. Most of these events stay within the Precambrian basement.
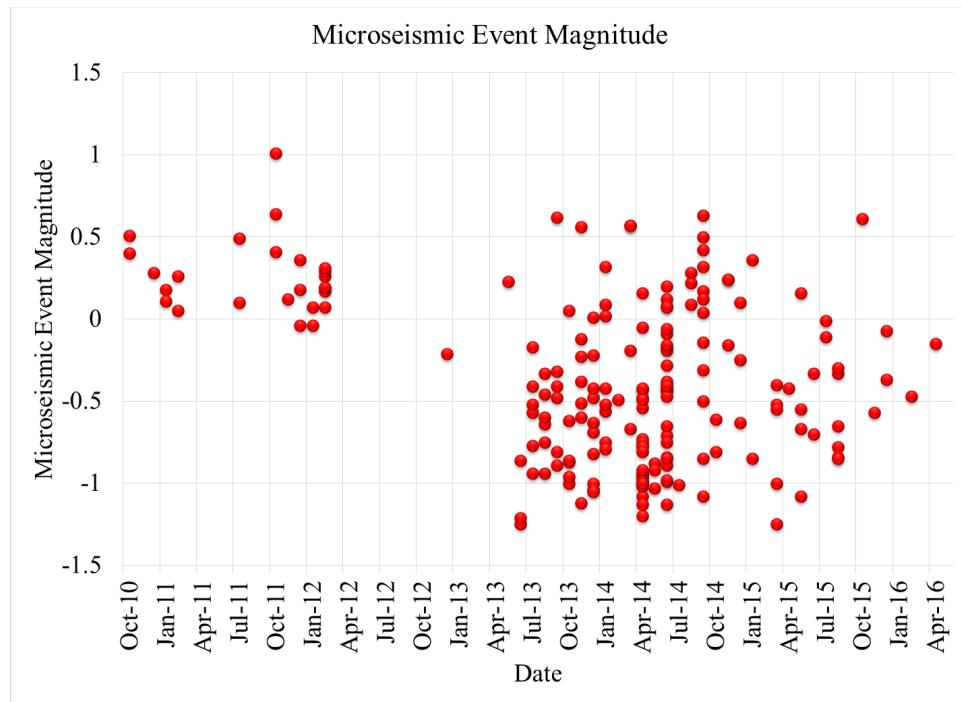
Figure 20 Microseismic event magnitudes. The events prior to injection from the plant have on average a greater magnitude than events recorded after injection from the plant.
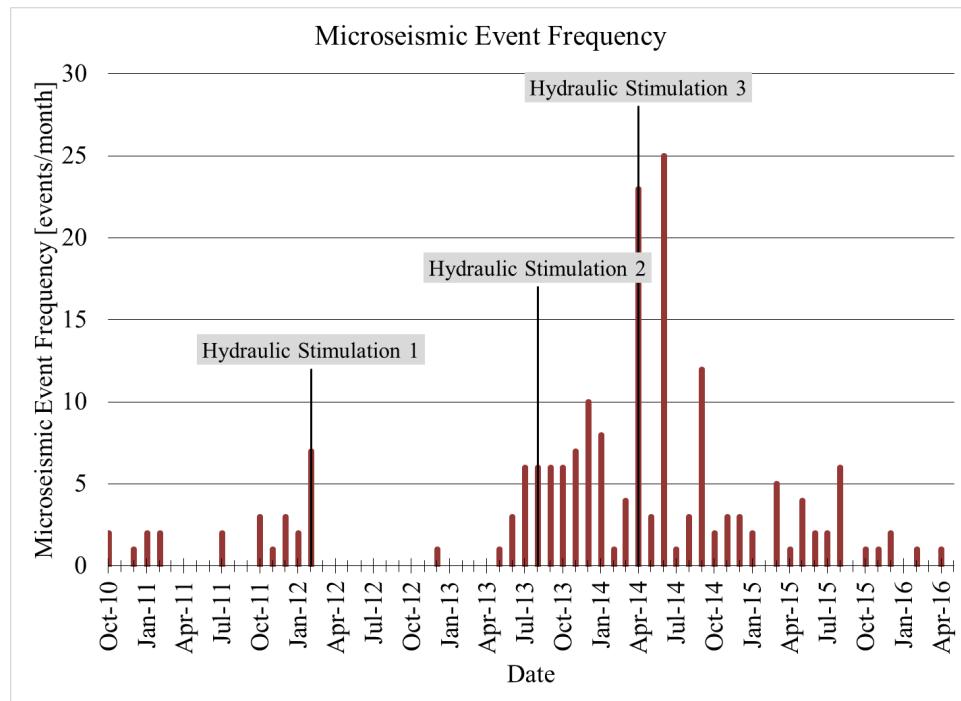
Figure 21 Microseismic event frequency. The majority of microseismic events occur between the start of injection from the plant and the third hydraulic stimulation. Following the third hydraulic stimulation the number of microseismic events decrease.

Consider a cross-section of the field centered on RRG-9 ST1 and cutting across the field from west to east, Figure 22. This cross-section shows two distinct populations of microseismic events. The first population is located between RRG-9 ST and RRG-3 and the sources are gradually deeper to the east. A second population is centered between RRG-11 and RRG-6. These events are deeper as they move to the west and to a lesser extent as they move east from the cluster center. The majority of events cluster at the
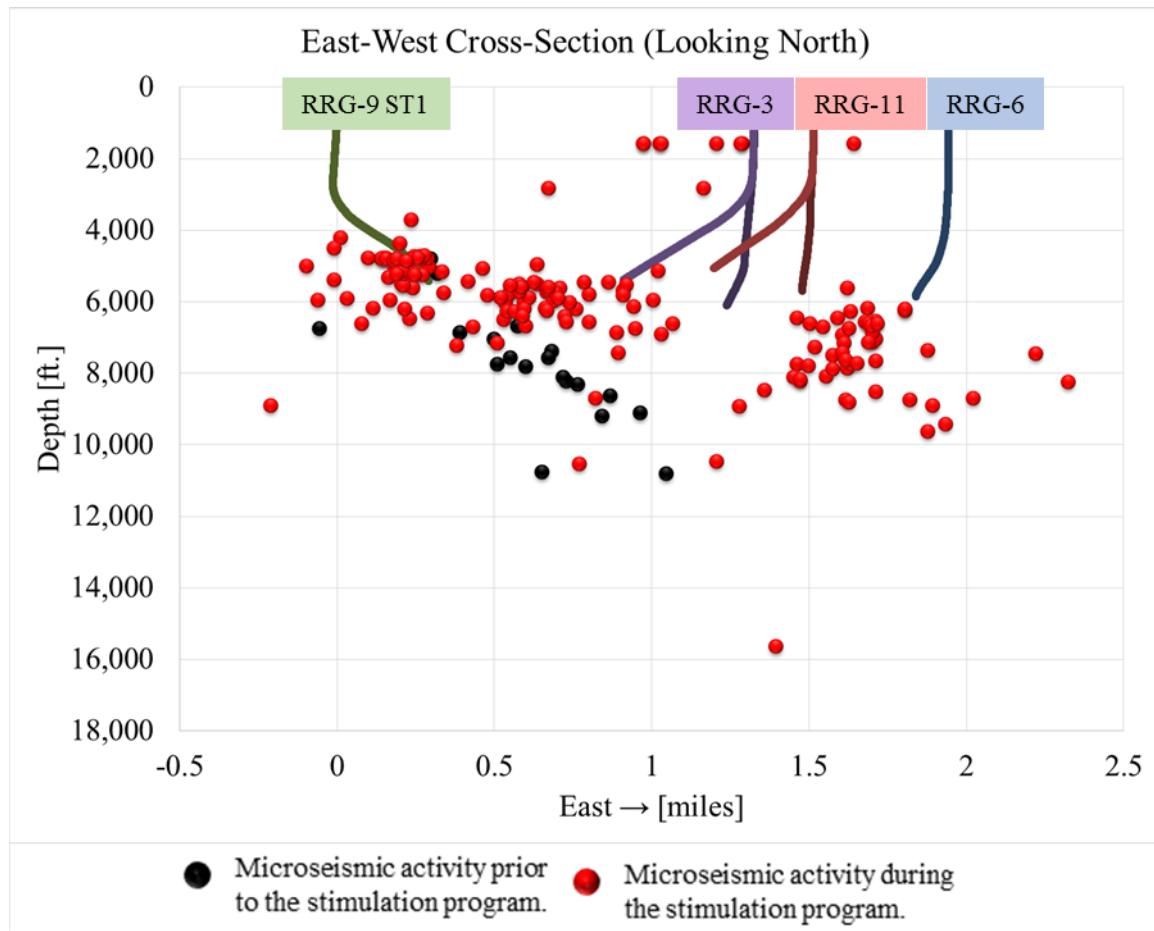
Figure 22 microseismic event depths east-west cross-section. Well trajectories include RRG-3C (dark purple), RRG-3D (light purple), RRG-6 (blue), RRG-9 ST1 (green), RRG-11A (dark red), and RRG-11B (light red). Microseismic events recorded prior to the RRG-9 ST1 stimulation program are shown as black dots. Microseismic events occurring during the stimulation program are shown as red dots. The majority of microseismic events occur at the base of the injection wells.

base of the injection wells. A second cross-section of the field centered on centered RRG-9 ST1 wellhead and bisecting the field from south to north shows that microseismic events tend to occur deeper further to the north, Figure 23. A further six east-west cross-sections provide increased resolution on the spatial distribution of these microseismic events. Each cross-section covers a zone that is a little over 1,000 ft. in width and is four miles in length, Figure 24. Zones 1 and 2 show that microseismic activity is clustered around the base
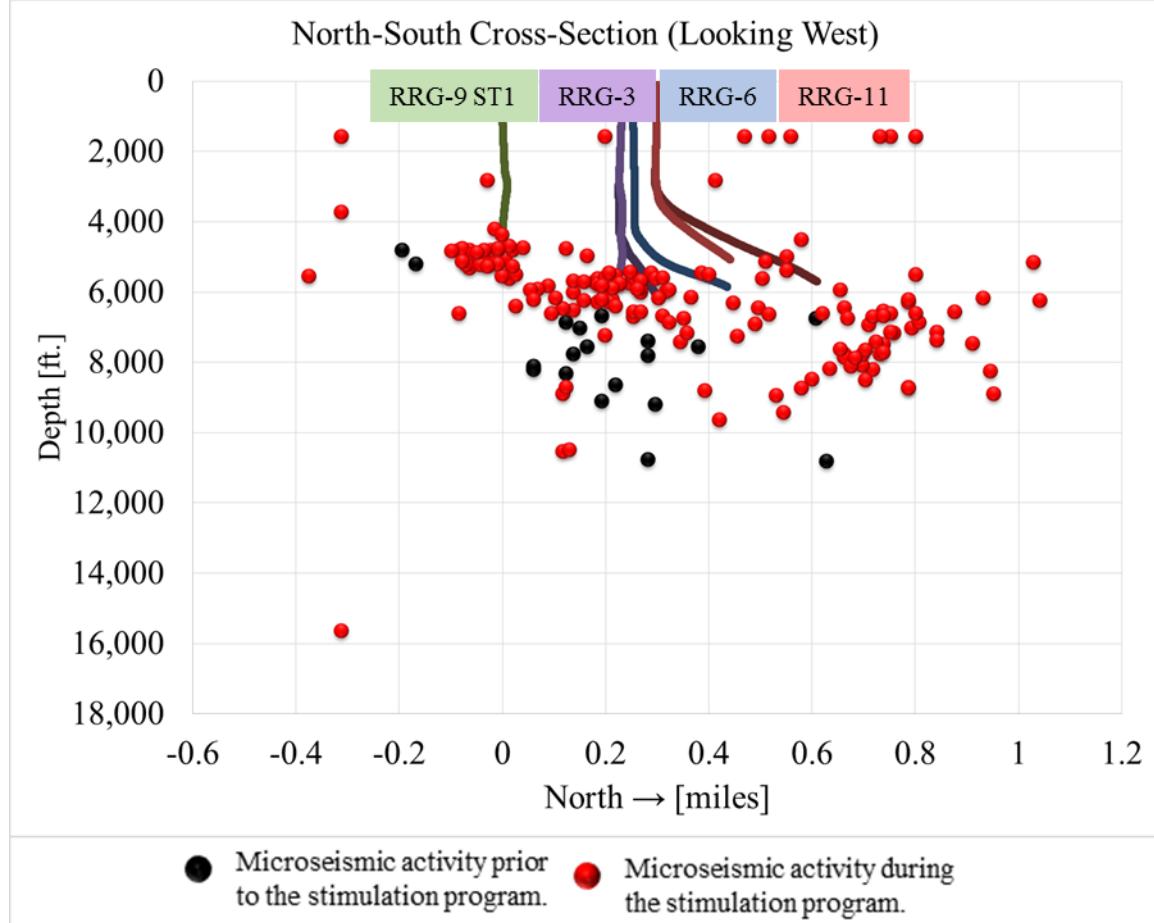
Figure 23 microseismic event depths north-south cross-section. Well trajectories include RRG-3C (dark purple), RRG-3D (light purple), RRG-6 (blue), RRG-9 ST1 (green), RRG-11A (dark red), and RRG-11B (light red). Microseismic events prior to the RRG-9 ST1 stimulation program are shown as black dots. Microseismic events during the stimulation program are shown as red dots. Events tend to occur deeper further to the north.
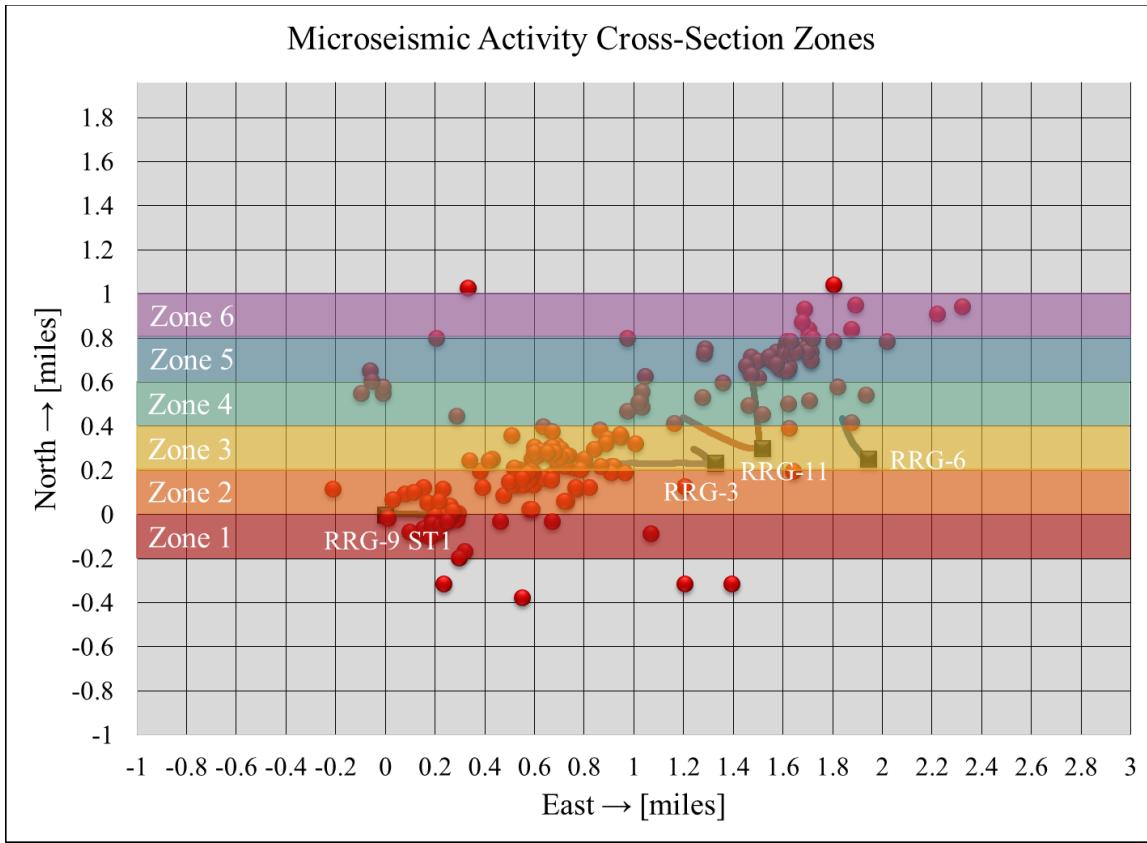
Figure 24 Microseismic activity cross-section zones. Well trajectories include RRG-3C (dark purple), RRG-3D (light purple), RRG-6 (blue), RRG-9 ST1 (green), RRG-11A (dark red), and RRG-11B (light red). Microseismic are shown as red dots. Each zone is four miles long nearly 1,000 ft. in width.

of RRG-9 ST1 Figure 25. Another cluster of events is shown at the base of RRG-3 in zone 3, Figure 26. These events are slightly deeper than those at the base of RRG-9 ST1. Event clusters occur near the bases of RRG-6 and 11A as n in zones 4 and 5, Figure 26 and Figure 27. However it is doubtful these events are related to activity at either RRG-6 or RRG-11 since these wells inject into shallower tertiary rocks. Additionally no microseismic activity was detected in this location prior to injection into RRG-9 ST1. A cluster of events north of RRG-6 and 11 are shown in zone 6, Figure 27.

Existing fluid pathways can be inferred during fluid injection by observing the location and timing of induced seismic events. This has been applied at various locations
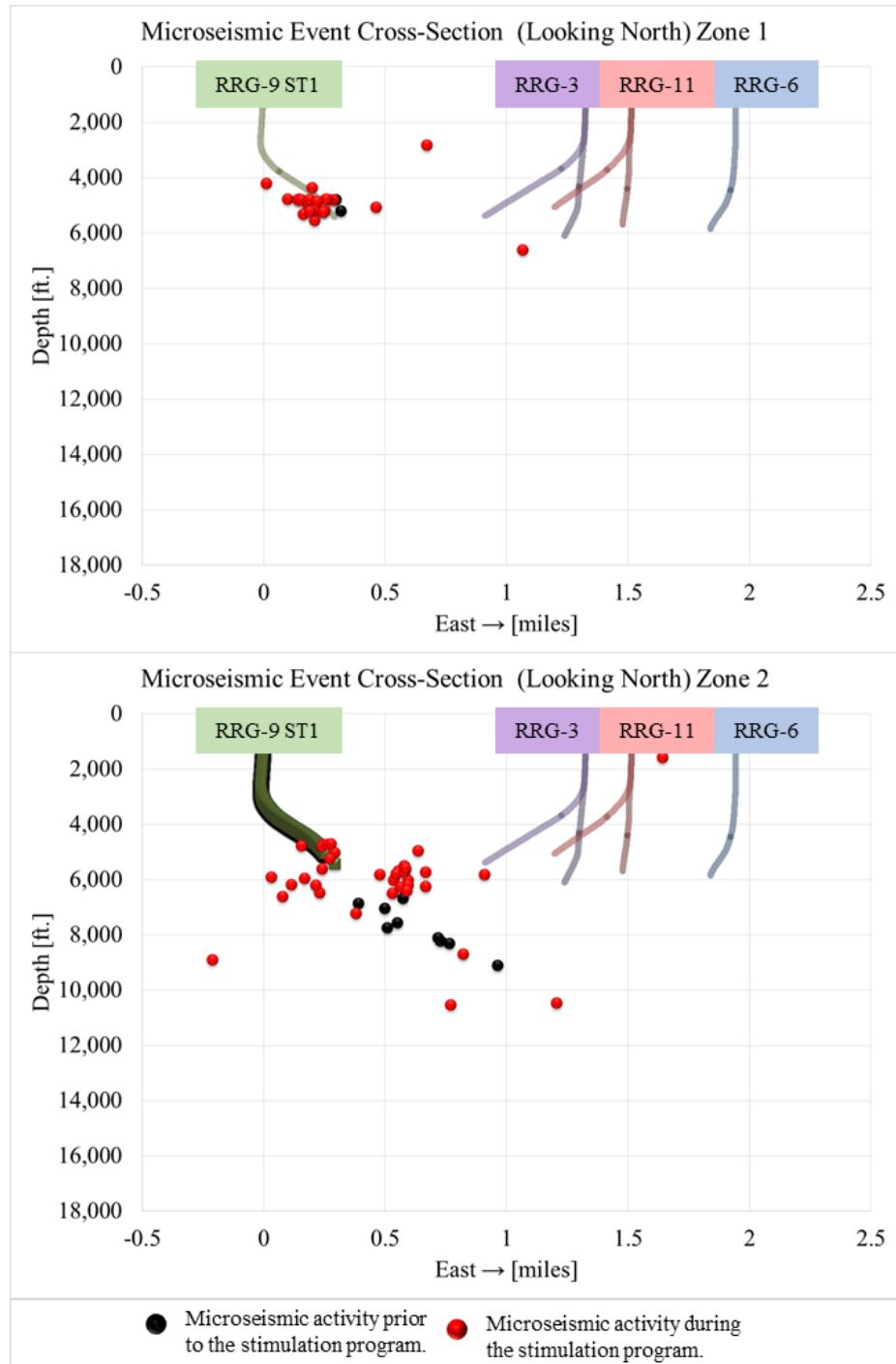
Figure 25 Microseismic event cross-section zones 1 and 2. Well trajectories include RRG-3C (dark purple), RRG-3D (light purple), RRG-6 (blue), RRG-9 ST1 (green), RRG-11A (dark red), and RRG-11B (light red). Well trajectories that are faded are displayed for reference purposes and are not located within the zone. The portions of each well located in the zone are denoted by appropriately colored squares. Microseismic events prior to the RRG-9 ST1 stimulation program are shown as black dots. Microseismic events during the stimulation program are shown as red dots.
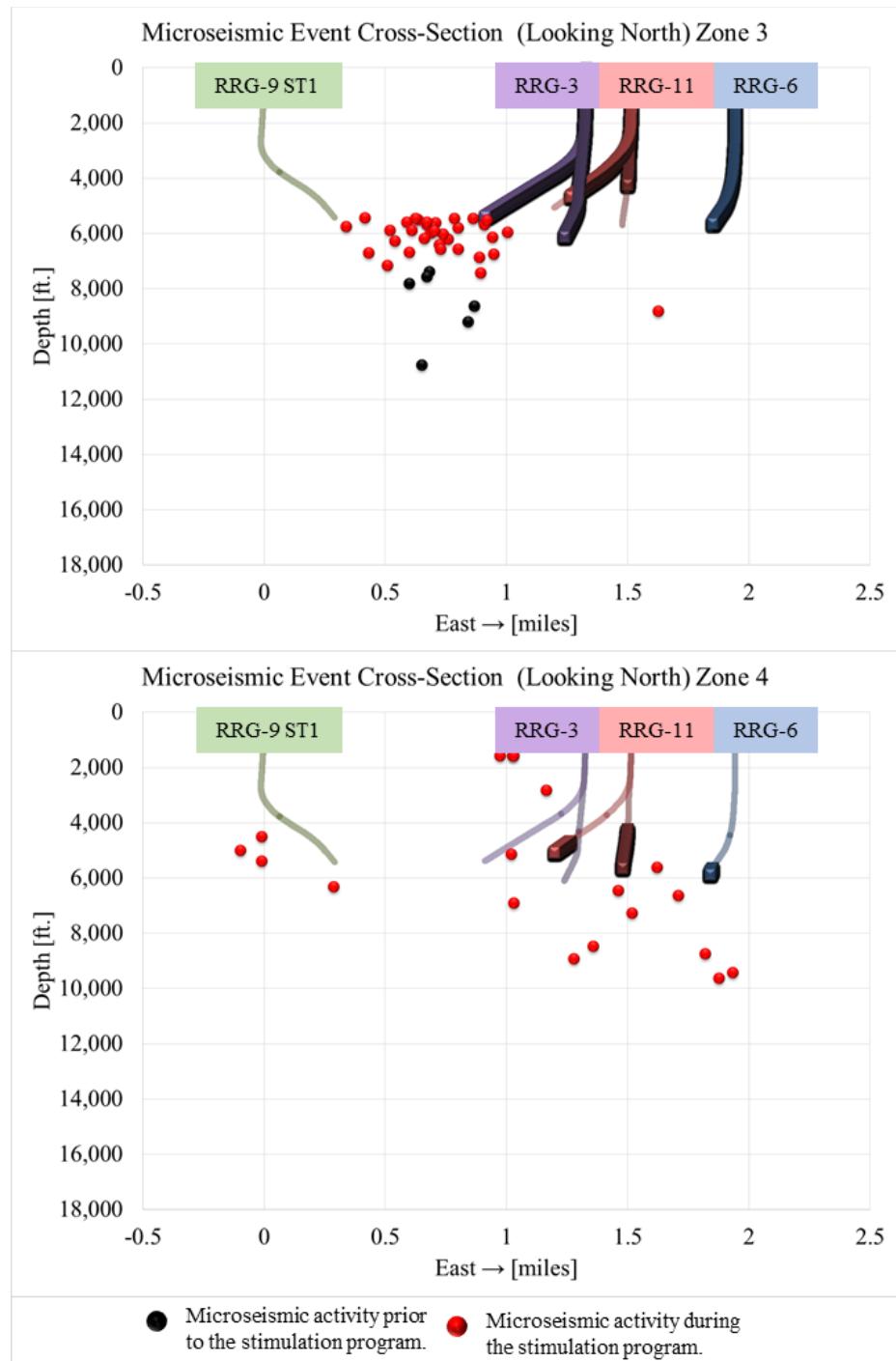
Figure 26 Microseismic event cross-section zone 3 and 4. Well trajectories include RRG-3C (dark purple), RRG-3D (light purple), RRG-6 (blue), RRG-9 ST1 (green), RRG-11A (dark red), and RRG-11B (light red).Well trajectories that are faded are displayed for reference purposes and are not located within the zone. The portions of each well located in the zone are denoted by appropriately colored squares. Microseismic events prior to the RRG-9 ST1 stimulation program are shown as black dots. Microseismic events during the stimulation program are shown as red dots.
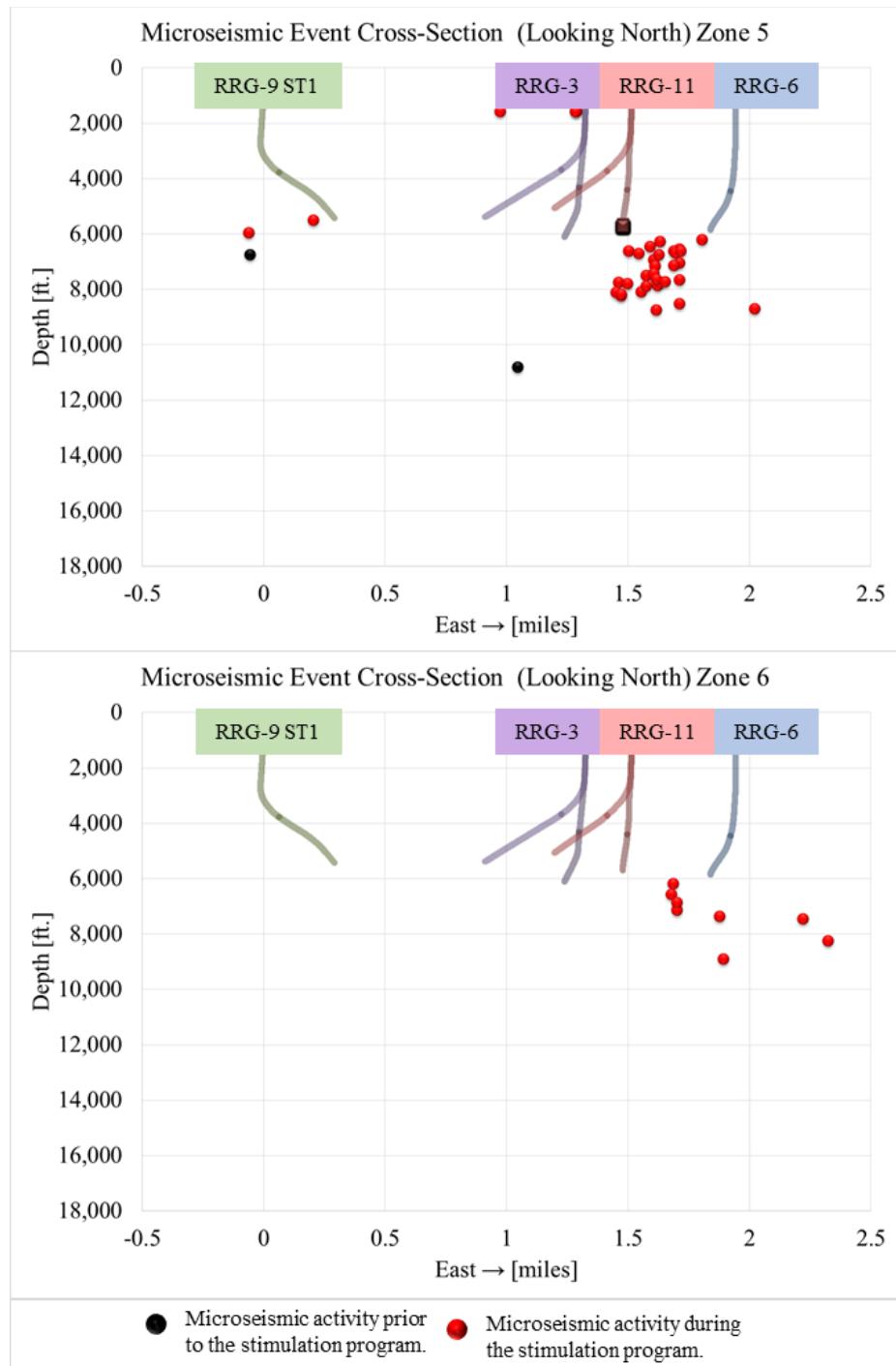
Figure 27 Microseismic event cross-section zones 5 and 6. Well trajectories include RRG-3C (dark purple), RRG-3D (light purple), RRG-6 (blue), RRG-9 ST1 (green), RRG-11A (dark red), and RRG-11B (light red).Well trajectories that are faded are displayed for reference purposes and are not located within the zone. The portions of each well located in the zone are denoted by appropriately colored squares. Microseismic events prior to the RRG-9 ST1 stimulation program are shown as black dots. Microseismic events during the stimulation program are shown as red dots.

including Los Alamos's Hot Dry Rock Reservoir located at Fenton Hill, New Mexico [28] and [29], and in the Barnett shale [30]. The general length and height of hydraulic fractures can also be estimated using microseismic activity [31]. Analysis of microseismic activity throughout the course of the stimulation program has provided insights into these possible fluid pathways and fracture dimensions. Between 2010 and the first hydraulic stimulation, February 2012, 19 local microseismic events were recorded at the field, Figure 28. Most of these occurred in a linear trend between RRG-9 ST1 and RRG-3. The events occur in two distinct groups. The first group of events occurs from October 2010 to February 2010 and the second grouping from June 2011 through February 2012. The microseismic events generated by the first stimulation occur just north of the RRG-9 ST 1 wellbore, Figure 28. Relatively few events were recorded between stimulation 1 and the start of injection from the plant, Figure 29. The general lack of events at the base of wells RRG-6 and 11 during this timeframe indicate that the events recorded in this area after injection of plant water into RRG-9 ST1 are primarily due to the stimulation program. After injection began from the plant several events were recorded between RRG-3 and RRG-9 ST1, Figure 29. During the second hydraulic stimulation, a cluster of events was recorded near the RRG-9 ST1 wellbore, Figure 30. As the second hydraulic stimulation continued with cold well water injection, another pulse of events was recorded along the Narrows Zone. Following the second hydraulic stimulation, the frequency of microseismic events increased along the Narrows Zone, Figure 30. Microseismic events were also detected in areas that had previously exhibited no discernable activity. Of these, the most significant was a large cluster of events recorded between RRG-6 and 11. Since these wells inject into the tertiary formations above the Precambrian basement these events likely occurred as a result of
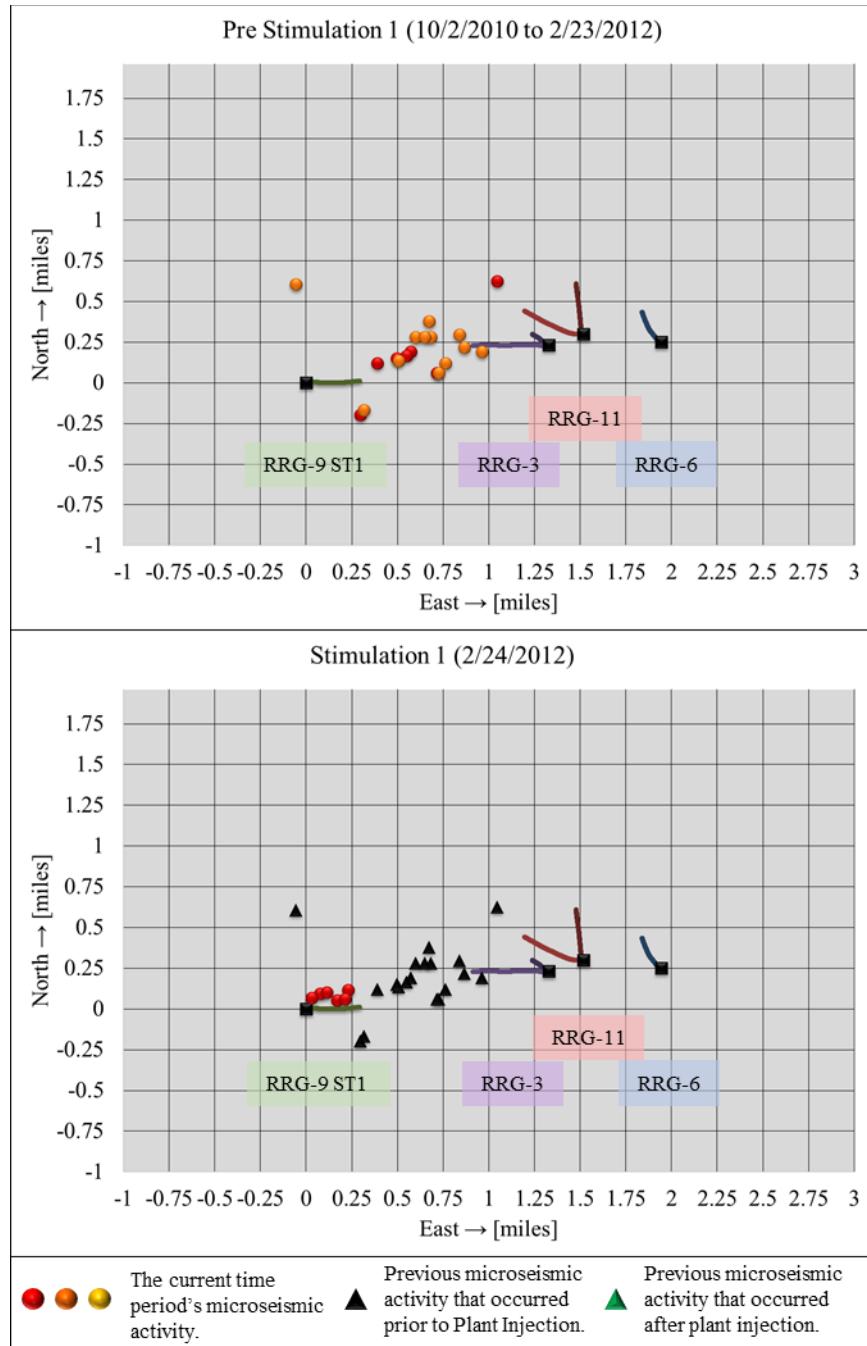
Figure 28 Pre stimulation 1 and stimulation 1 microseismic activity. Well trajectories are indicated as follows: RRG-9 ST1 (green), RRG-3D (light purple), RRG-3C (dark purple), RRG-11B (light red), RRG-11A (dark red), and RRG-6 (blue). Wellhead locations are shown as black squares. Pre Stimulation 1: red dots denote the location of microseismic events that occurred between October 2010 and February 2011, and orange dots are the locations of microseismic events that occurred between June 2011 and the first hydraulic stimulation in February 2012. Stimulation 1: red dots denote the location of microseismic activity that occurred as a result of the first hydraulic stimulation.
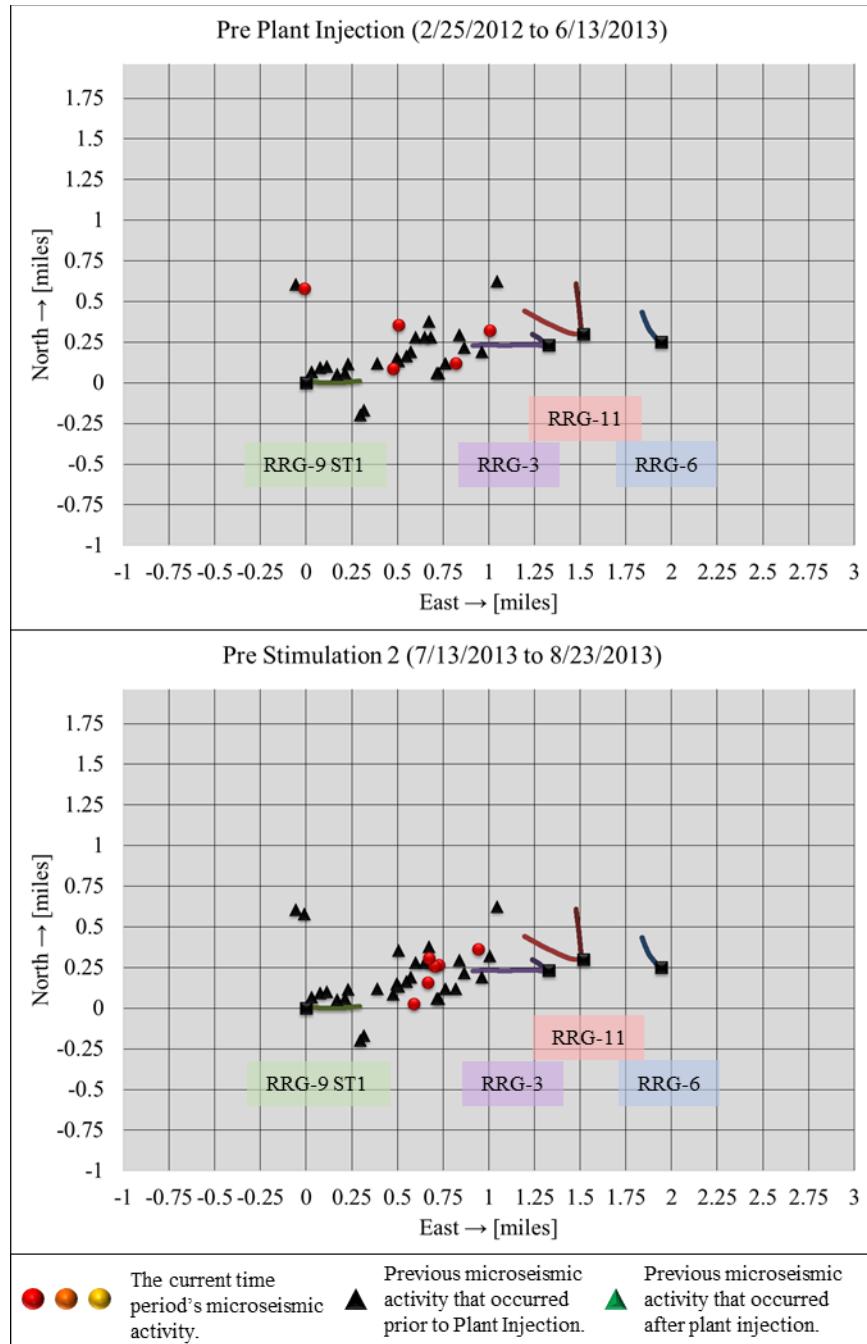
Figure 29 Pre plant injection and pre stimulation 2 microseismic activity. Well trajectories are indicated as follows: RRG-9 ST1 (green), RRG-3D (light purple), RRG-3C (dark purple), RRG-11B (light red), RRG-11A (dark red), and RRG-6 (blue). Wellhead locations are shown as black squares. Pre Plant Injection: red dots show microseismic events occurring between the first hydraulic stimulation an injection through the 10-inch line in June 2013. Pre Stimulation 2: red dots show microseismic activity after injection from the plant started, June 2013.
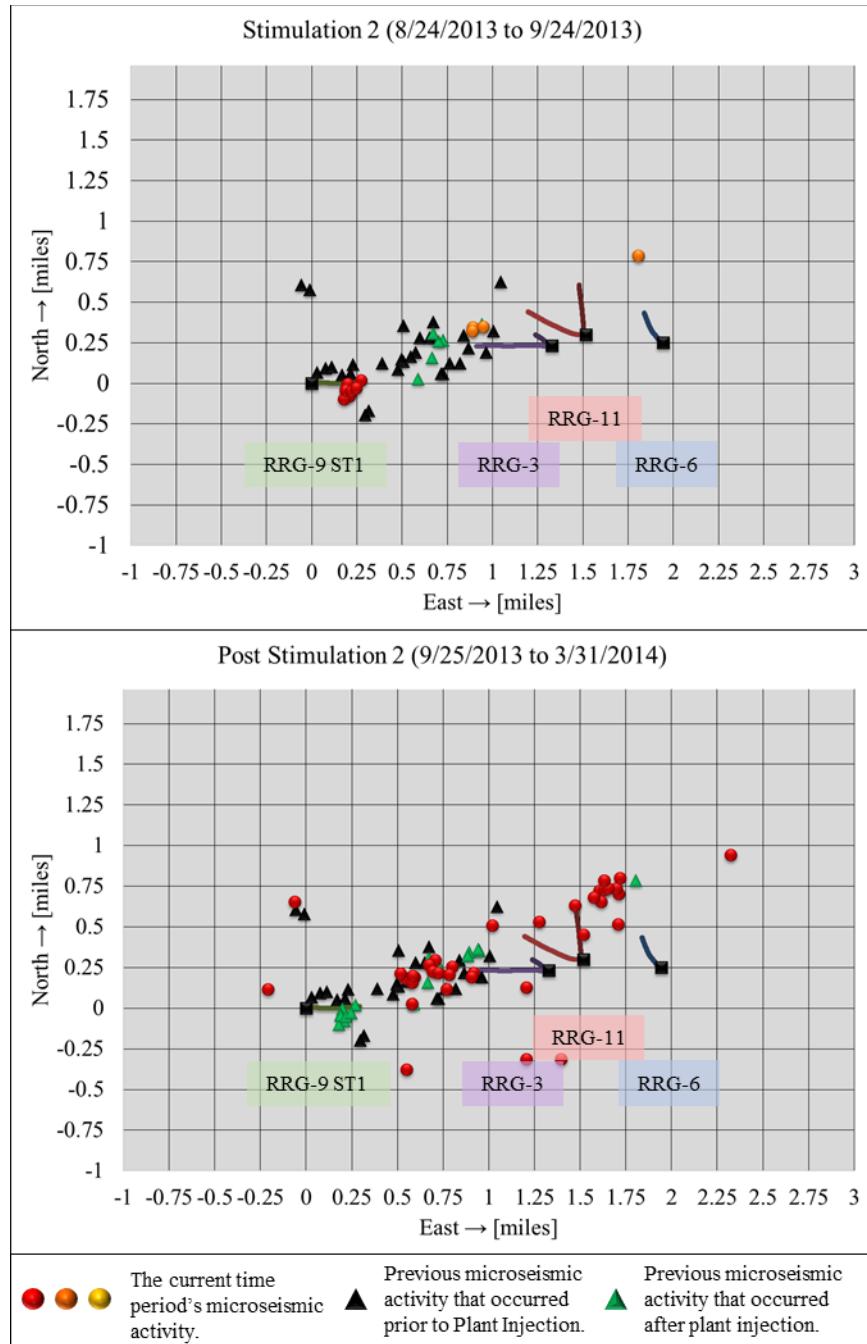
Figure 30 Stimulation 2 and post stimulation 2 microseismic activity. Well trajectories are indicated as follows: RRG-9 ST1 (green), RRG-3D (light purple), RRG-3C (dark purple), RRG-11B (light red), RRG-11A (dark red), and RRG-6 (blue). Wellhead locations are shown as black squares. Stimulation 2: red dots shown microseismic activity between August 31, 2013 and September 2, 2013, and orange dots denote microseismic activity between September 16, 2013 and September 18, 2013. Post Stimulation 2: red dots show microseismic activity after stimulation 2.

stimulation program activity at RRG-9 ST1. During stimulation 3 a cluster of events was again detected near the base of RRG-9 ST1, Figure 31. These events were in the same location as those observed during the second hydraulic stimulation. Following stimulation 3 microseismic activity continued northeast along the Narrows Zone, Figure 32. Two major periods of enhanced microseismic activity were observed following the April 2014 stimulation, Figure 32. The first of these occurred between June 5, 2014 and June 8, 2014. The second period of enhanced microseismic activity occurred between September 20, 2014 and September 21, 2015. Microseismic events during the second period moved further along the Narrows Zone than had previously been observed. The frequency of events began to gradually decrease following the third hydraulic stimulation. Relatively
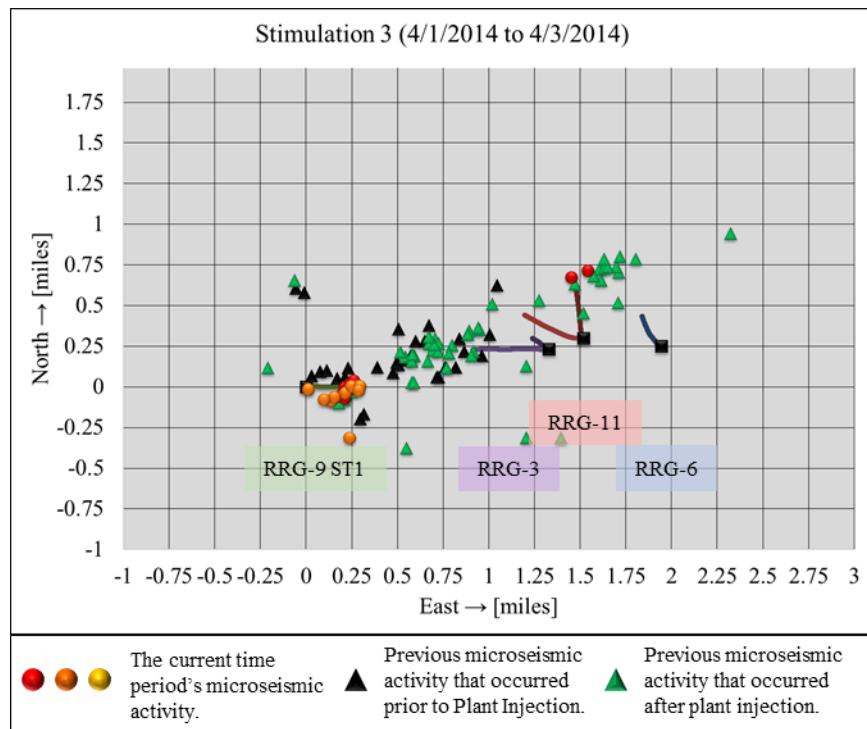
Figure 31 Stimulation 3 microseismic activity. Well trajectories are indicated as follows: RRG-9 ST1 (green), RRG-3D (light purple), RRG-3C (dark purple), RRG-11B (light red), RRG-11A (dark red), and RRG-6 (blue). Wellhead locations are shown as black squares. Red dots show microseismic activity between April 1, 2014 and April 2, 2014 and orange dots denote microseismic activity that occurred on April 3, 2014.

few events have been recorded since the well was initially shut-in (since April 28, 2015), Figure 32. The last period of enhanced microseismic activity recorded was on August 8, 2015.

2.8 Tracer Tests

On three separate occasions tracers have been injected into RRG-9 ST1. The first tracer, naphthalene tri sulfonate (1,3,6-NTS), was injected on September 9, 2013. A second tracer, naphthalene sulfonate (2-NS), was injected on January 7, 2015. Finally a third tracer, naphthalene di sulfonate (1,5-NDS), was injected on February 11, 2016. The 1,3,6-NTS tracer was first detected at the production well RRG-4 on January 25, 2015, almost 503 days after injection commenced, Figure 33. The 2-NS tracer was detected at both RRG-2 and 4 on January 10, 2016, 367 days after injection, Figure 34. Since this tracer has a lower detection limit than the 1,3,6-NTS tracer the disparity in detection times between the two might not be as large as would superficially seem to be the case. The 1,5-NDS tracer has yet to be detected. The tracer returns indicate that a connection exists between RRG-9 ST1 and the production wells to the north and northeast. The simultaneous return of the 2-NS tracer in both RRG-2 and RRG-4, which are significant distance from each other, implies that the Narrows zone provides a relatively effective conduit for fluid passage to the production wells.

2.9 Stimulation Program Timeline

RRG-9 ST1 has been hydraulically stimulated three times in addition to nearly continuous injection of plant water since June 2013. Injection rate, pressure, and temperature have been monitored throughout the stimulation program. Microseismic
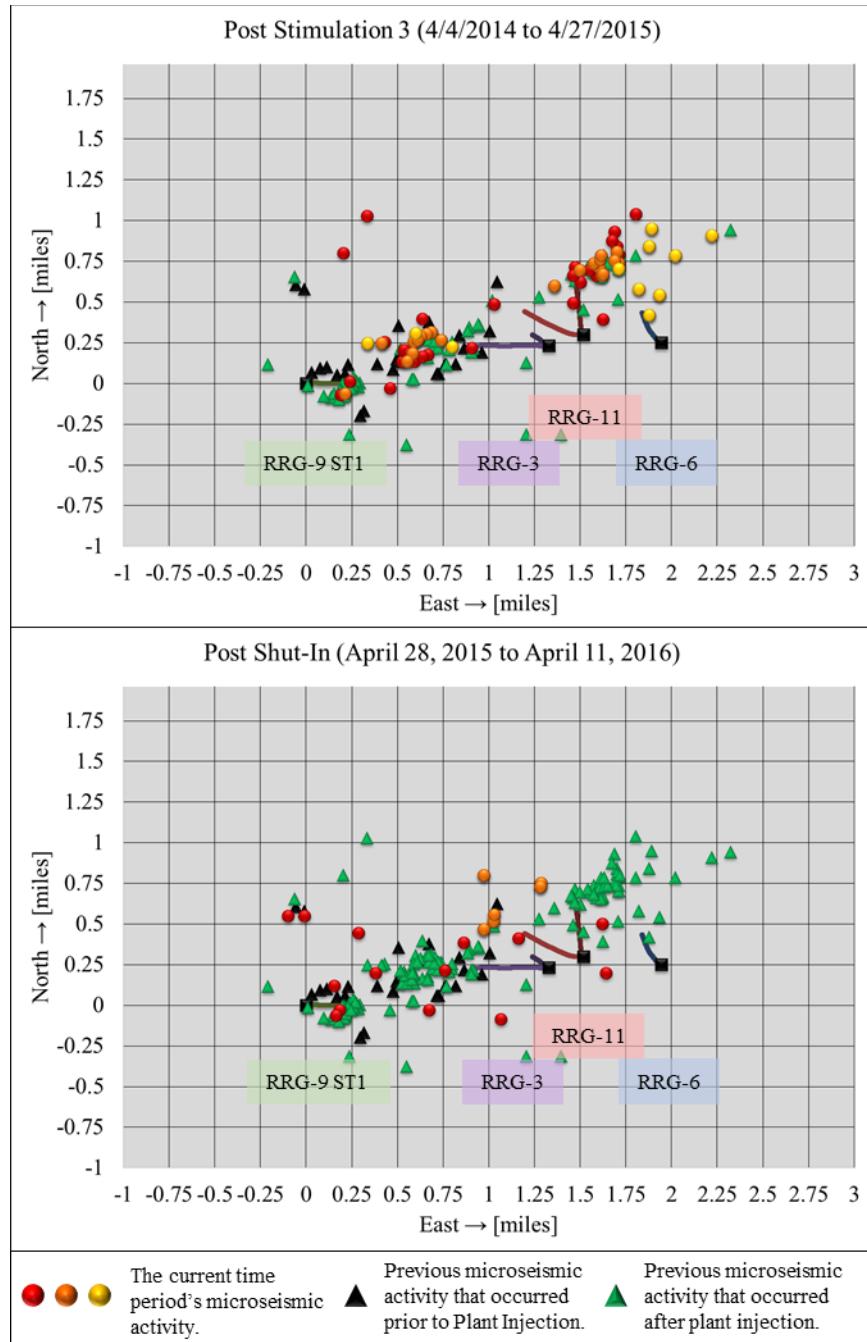
Figure 32 Post stimulation 3 microseismic activity and post shut-in microseismic activity. Post Stimulation 3: red dots show microseismic activity between April 4, 2014 and April 27, 2015; orange dots denote a period of enhanced microseismic activity that occurred on June 5, 2014 and June 8, 2014; yellow dots denote another period of enhanced microseismic activity that occurred between September 20, 2014 and September 21, 2014. Post Shut-In: red dots show microseismic activity between April 28, 2015 and April 11, 2016; orange dots denote a period of enhanced microseismic activity that occurred on August 8, 2015.
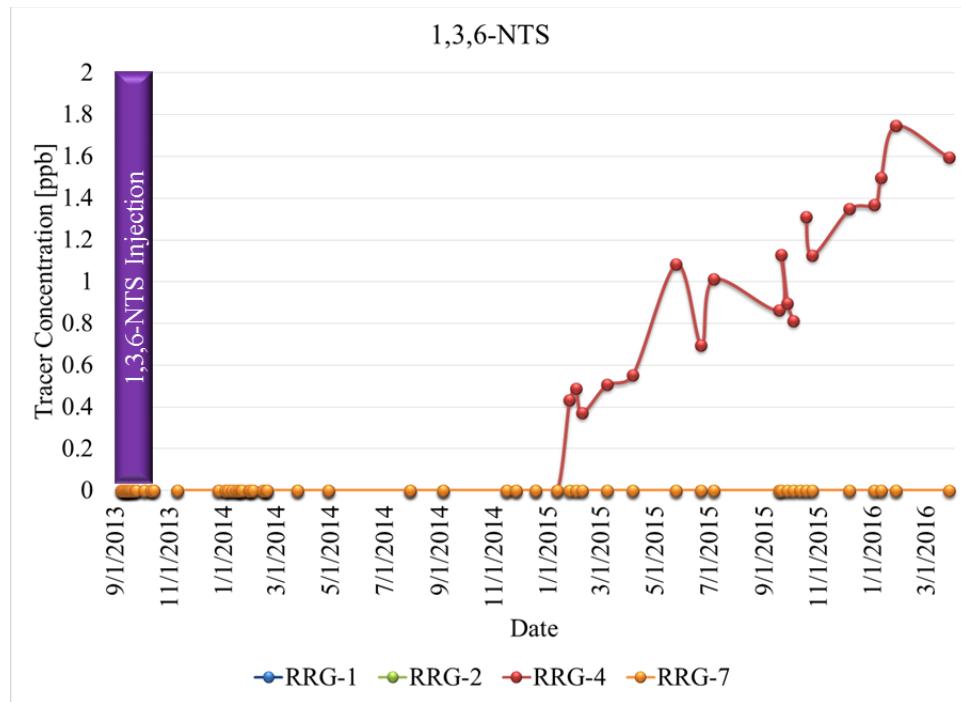
Figure 33 1,3,6-NTS tracer results.
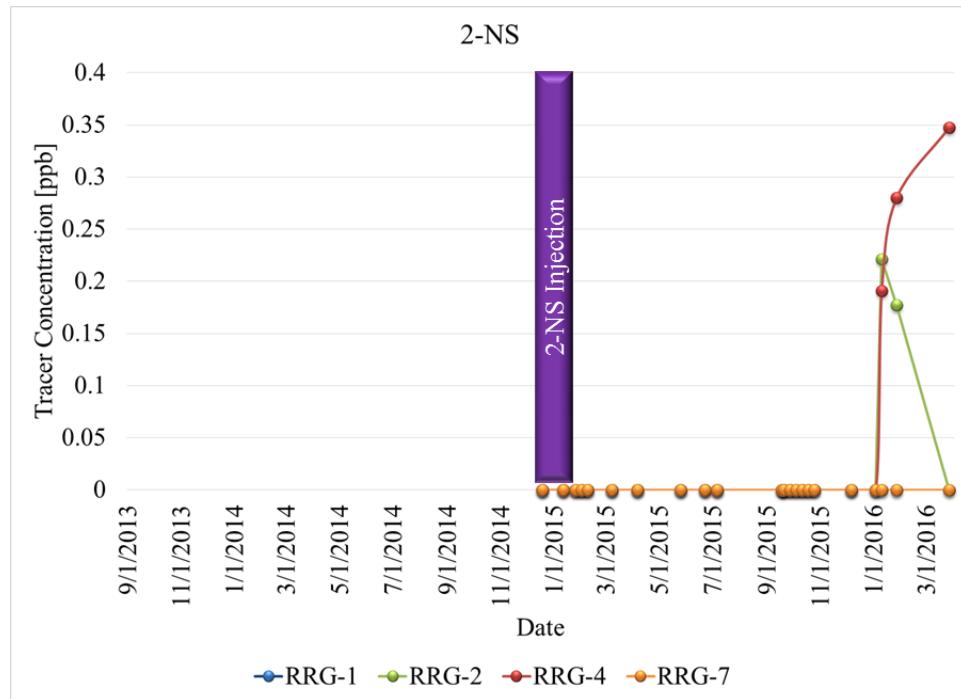
Figure 34 2-NS tracer results.

activity related to plant activity have been recorded through an eight station microseismic array. Three different tracers have been injected into RRG-9 ST1. Two of these have been detected in other production wells. A timeline of this events as well as other stimulation program activity at Raft River is summarized in Figure 35 and Figure 36.
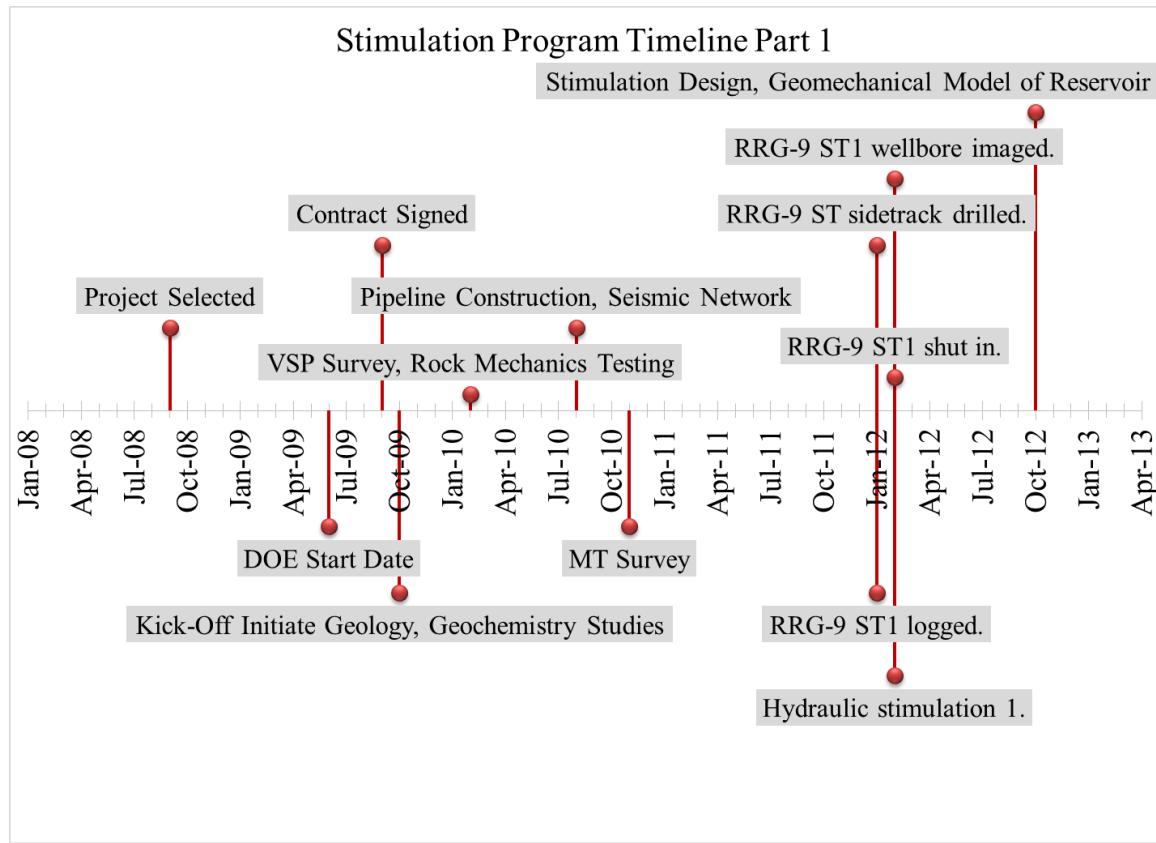
Figure 35 Stimulation program timeline part 1.

Figure 36 Stimulation program timeline part 2.

DISSCUSION

Injection rates, wellhead pressures, injection temperatures, and microseismic activity have been continuously monitored throughout the stimulation program. A Modified Hall's analysis of these data provides insights into changing reservoir properties. The timing and location of microseismic activity along with tracer mapping have been used to track fluid movement through the Raft River geothermal system. This information has been used to develop a conceptual model describing the effects of the stimulation program on RRG-9 ST1.

3.1 Modified Hall and Injectivity Plot Analysis

A modified Hall plot is constructed by plotting the cumulative bottomhole flowing pressure versus the cumulative volume of fluid injected, Equation 3-1 [32]

$$\int_0^t p_{tf}\,dt - (p_e - \Delta p_{tw})t = \frac{\mu(p_D + s)}{2\pi kh}\int_0^t q\,dt \qquad [\,3\text{-}1\,]$$

The term p_{tf} is the wellhead pressure, p_e is the reservoir pressure at the external boundary, Δp_{tw} is the hydrostatic pressure in the well, t is time, μ is the fluid viscosity, p_D is the dimensionless pressure (the natural log of the external reservoir radius r_e divided by the

effective wellbore radius r_w), s is the skin factor, k is the absolute permeability, h is the formation height, and q is volumetric flow rate. The slope of Equation 3-1 is given by Equation 3-2. The term m_H is the slope of Equation 3-1.

$$m_H = \frac{\mu(p_D + s)}{2\pi kh} \qquad\qquad [\text{ 3-2 }]$$

Assuming the reservoir properties and geometry remain constant plotting the cumulative bottomhole flowing pressure versus the cumulative volume injected produces a straight line. However, this is rarely the case and changes in the plotted slope can be used to infer reservoir properties. The slope of this line is proportional to the skin factor around the well and inversely proportional to reservoir permeability, Equation 3-2. Increases or decreases in the slope are used to infer reservoir properties. For example a decreasing slope indicates an increase in the permeability and/or a decrease in the skin factor around the well. Equation 3-1 has been modified to account for changes in hydrostatic pressure due to changes in injection temperature as well as friction in the wellbore, Equation 3-3.

$$\sum_{0}^{t} p_{tf}\Delta t + \sum_{0}^{t} p_{tw}\Delta t - \sum_{0}^{t} p_{f}\Delta t - p_{e}t = \frac{\mu}{2\pi kh}\left(ln\left(\frac{r_e}{r_w}\right) + s\right)\sum_{0}^{t} q\Delta t \qquad [\text{ 3-3 }]$$

The term p_f is pressure loss due to friction. This term was calculated using a curve fitting relationship developed by analyzing the step down flow rate testing conducted at the end of the third hydraulic stimulation. Using injection rate, wellhead pressure, and temperature data collected at RRG-9 ST1 a modified Hall plot was prepared, Figure 37. Initially the slope of the line plotted is very steep indicating a large skin factor and/or low permeability.

Following the second hydraulic stimulation the line levels off a slightly due to an increase in the permeability and/or a reduction in the skin factor around the well. After the third hydraulic stimulation the slope begins to level off in a continuous manner, especially during the early time following the stimulation. This indicates a continuous decrease in the skin factor and/or a continuous increase in the permeability. After the well was shut-in
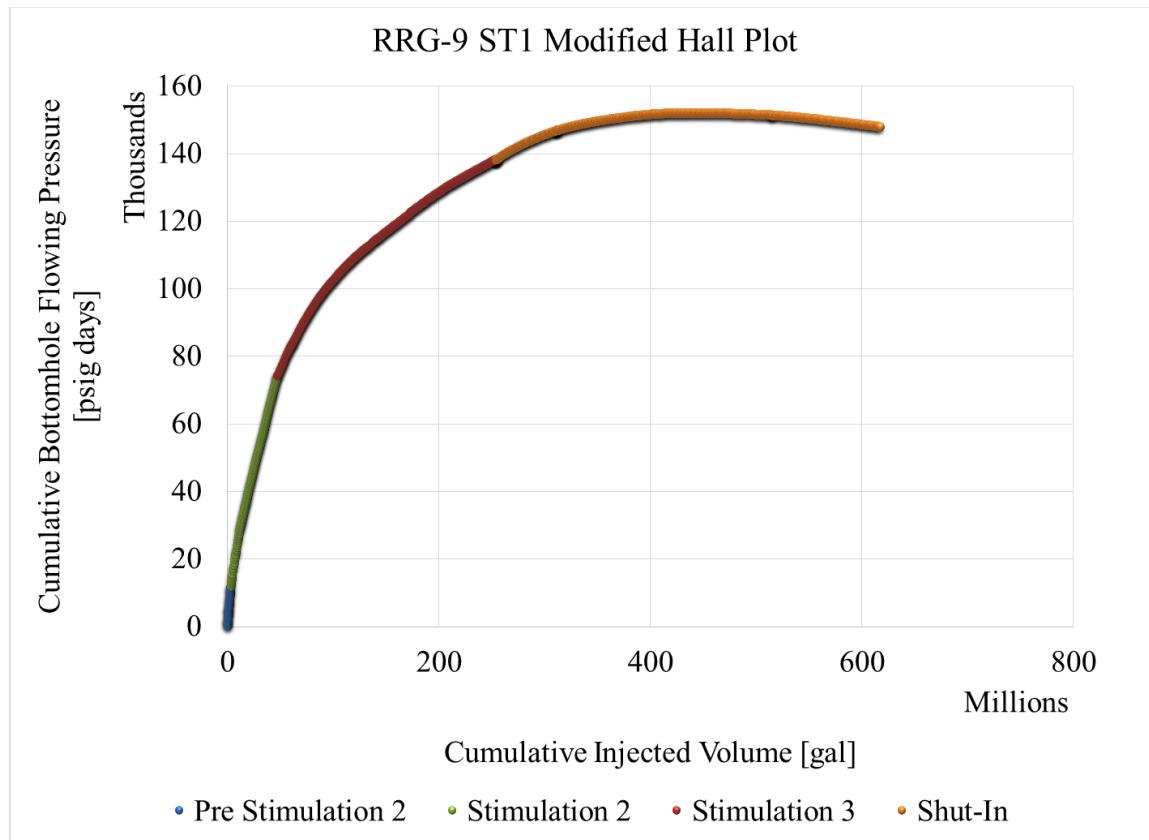
Figure 37 RRG-9 ST1 modified Hall plot. Blue is injection prior to hydraulic stimulation 2. Green is injection during and after hydraulic stimulation 2. Red is injection after hydraulic stimulation 3. Orange is injection after the well was shut-in.

(between April 28, 2015 and May 26, 2015 and again between August 2, 2015 and August 17, 2015) the slope decreased at a greater rate than before, again most noticeably in the early time following the two shut-ins. During this time period, the permeability increased at a greater rate than before and/or the skin factor was reduced more rapidly than before

the shut-in. Overall there have been significant reductions in the skin factor and/or increases in permeability in the well as a result of the stimulation program.

A similar analysis has been applied to the other injection wells at Raft River, Figure 38. Flow rates have been measured at the wellheads and line pressure data have been collected since 2008. The hydrostatic pressure term has been calculated using the depths of fluid loss zones in the injection wells and an average surface injection temperature. The friction term for the other injection wells has not been calculated due to lack of friction data for the other wells. In Figure 38 the slope for well RRG-5 remains relatively steep compared to the other injection wells. Well RRG-3's slope slightly decreases with time while the slopes of Wells RRG-6 and 11generally increase slowly over time. None of these wells show the rapid change in slope that occurred in RRG-9 ST1. The modified Hall plot analysis shows that the stimulation program has improved the injection capability of RRG-9 ST1 relatively quickly compared to the other wells.

In addition to the modified Hall's analysis an injectivity index has been calculated daily for RRG-9 ST1, Figure 39. A chronological injectivity index plot represents the
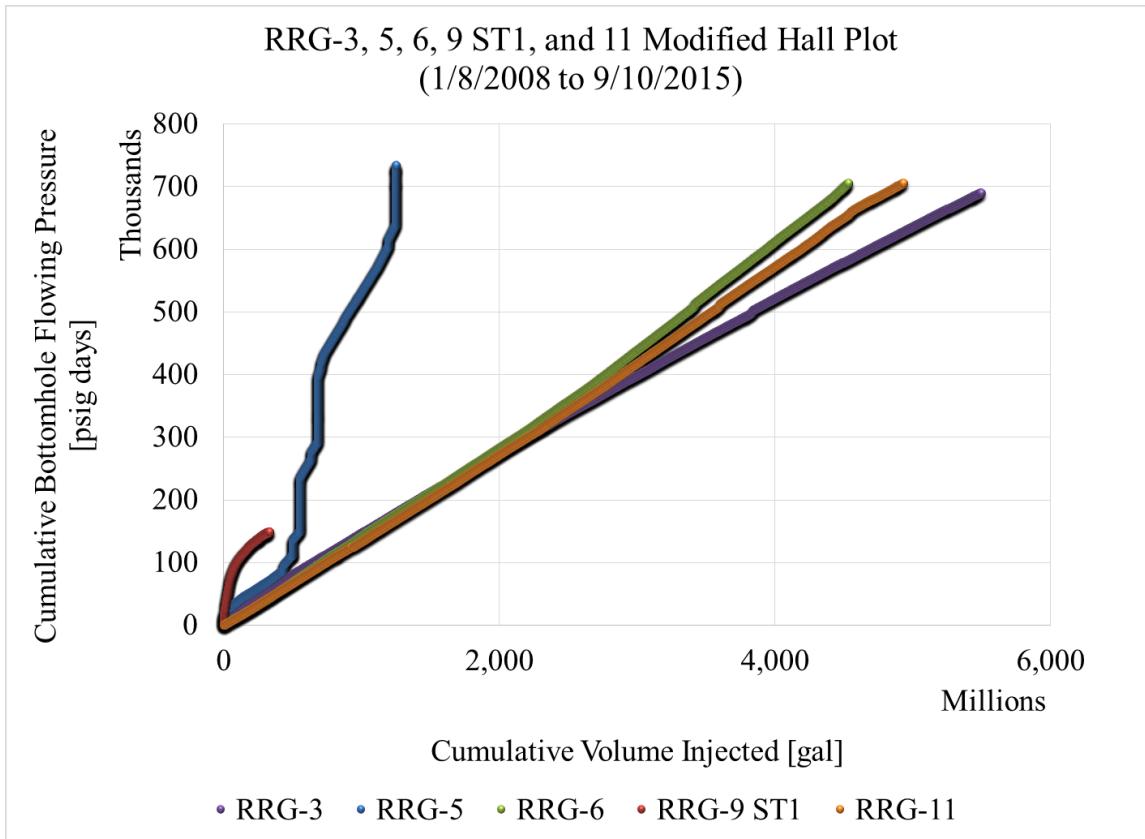
Figure 38 RRG-3, 5, 6, 9 ST1, and 11 modified Hall plot 1/8/2008 to 9/10/2015. RRG-3, 5, 6, 9 ST1, and 11 are shown as purple, blue, green, red, and orange lines respectively.
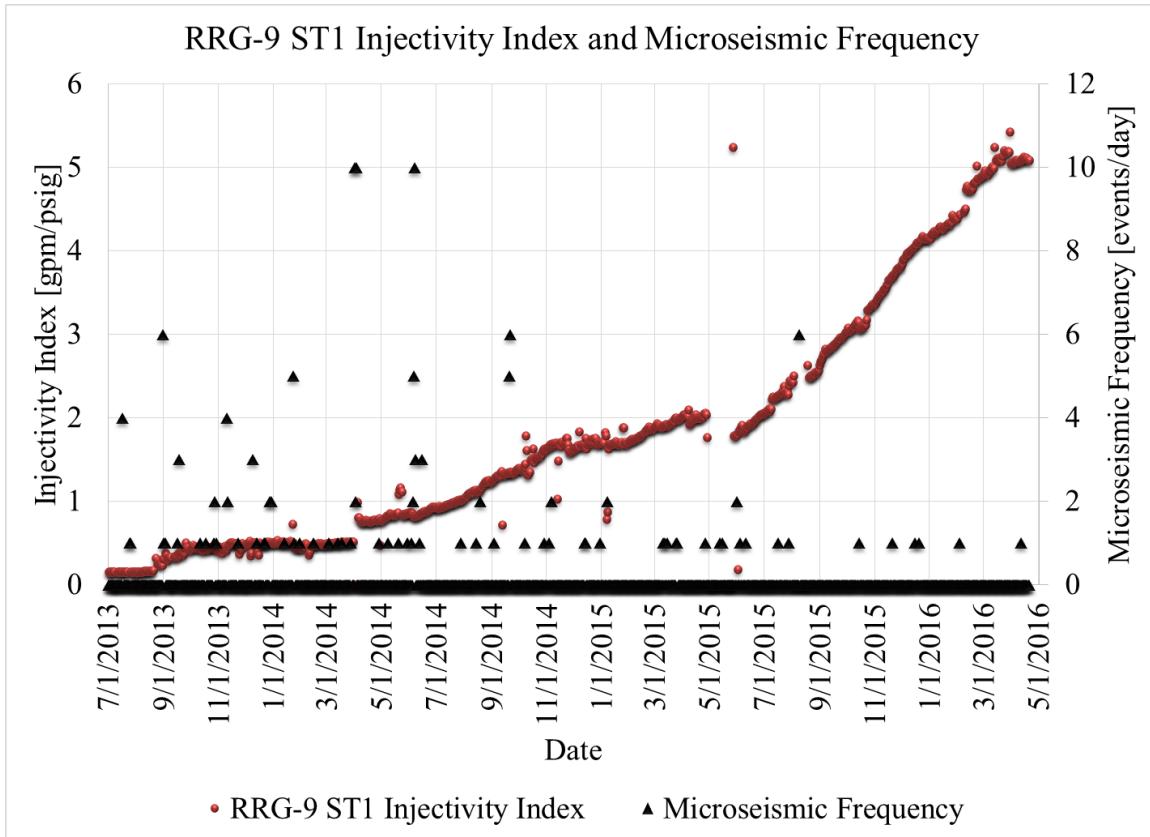
Figure 39 RRG-9 ST1 injectivity index. The injectivity index is shown as red circles and the microseismic frequency (events/day) is shown as black triangles.

injection rate divided by the injection pressure as a function of time. Prior to the second hydraulic stimulation the injectivity index was fairly low; around 0.15 gpm/psig. During the second stimulation the injectivity index rose to 0.5 gpm/psig. Following the second stimulation, the injectivity index remained relatively stable; rising slightly up to 0.51 gpm/psig by March 31, 2013. After the third hydraulic stimulation the injectivity index increased to 0.77 gpm/psig. The injectivity index continued to rise to 2.1 gpm/psig by April 28, 2014. Following the shut-in of RRG-9 ST1, from April 28, 215 to May 26, 2015 and again from August 2, 2015 to August 17, 2015, the rate of improvement in the injectivity increased substantially. By April 4, 2016 the injectivity index had reached 5.1 gpm/psig.

Since the beginning of the stimulation program the injectivity index has increased by 3,300%.

Plotted alongside the injectivity index in Figure 39 is the frequency (events per day) of microseismic events that were detected during the stimulation program. There appears to be a correlation between enhanced microseismic activity and increases in the injectivity index. Notable examples are the second and third hydraulic stimulations as well as the when the well was shut-in, during April 28, 2015 to May 26, 2015 and during August 2, 2015 to August 17, 2015. Additionally after the third hydraulic stimulation more microseismic events were detected prior to significant increases in the injectivity, see the frequency of events during June and September 2014 in Figure 39.

Injectivity indexes were prepared for the other injection wells, Figure 40. RRG-5 has been used periodically as an injection well. This accounts for the volatility in its injectivity index. RRG-3 shows gradual improvement in injectivity with time while both RRG-6 and 11 exhibit decreasing injectivity with time. These trends precede the stimulation program. By comparison the increase in injectivity at RRG-9 ST1 is relatively rapid.

3.2 Conceptual Model

Geologic, water chemistry, microseismic activity, borehole imaging, and tracer data have been used to construct a conceptual model of the Raft River geothermal system surrounding RRG-9 ST1, Figure 41. This model consists of the Narrows Zone and the fracture zone that intersects the RRG-9 ST1 wellbore between 5,640 and 5,660 ft. MD. Fluid injected into the well passes through the fracture zone until it connects into the Narrows Zone. The fluid then moves along the Narrows Zone to the northeast. Preexisting

RRG-3, 5, 6, 9 ST1, and 11 Injectivity Indexs
1/1/2008 to 9/10/2015
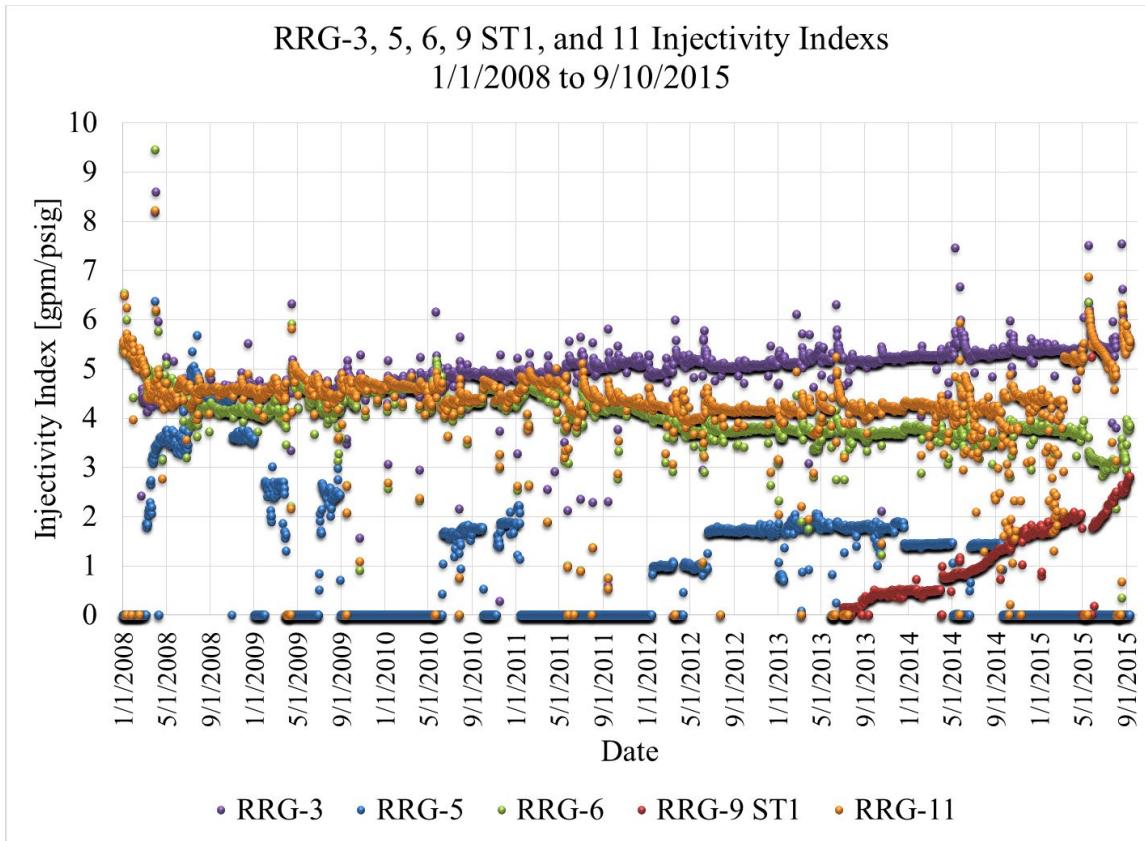
Figure 40 RRG-3, 5, 6, 9 ST1, 11 injectivity indexes. RRG-3, 5, 6, 9 ST1, and 11 are displayed as purple, blue, green, red, and orange dots respectively.

and/or generated fluid pathways reopened/opened during the stimulation program perpendicular to the Narrows Zone convey the fluid to the production wells to the north and northeast.

3.3 Numerical Model

FALCON is one of Idaho National Laboratories' reservoir simulation codes. It has been chosen as a platform for numerically modeling the stimulation program at RRG-9 ST1. The traditional mass and momentum balance for porous media conditions is given by Equation 3-4 [33]. In Equation 3-4 ϕ is the formation porosity, p is the pressure, $\mathbf{g}$ is the gravitational acceleration vector, and $\acute{q}$ is the mass injected/removed per second per unit

volume. In
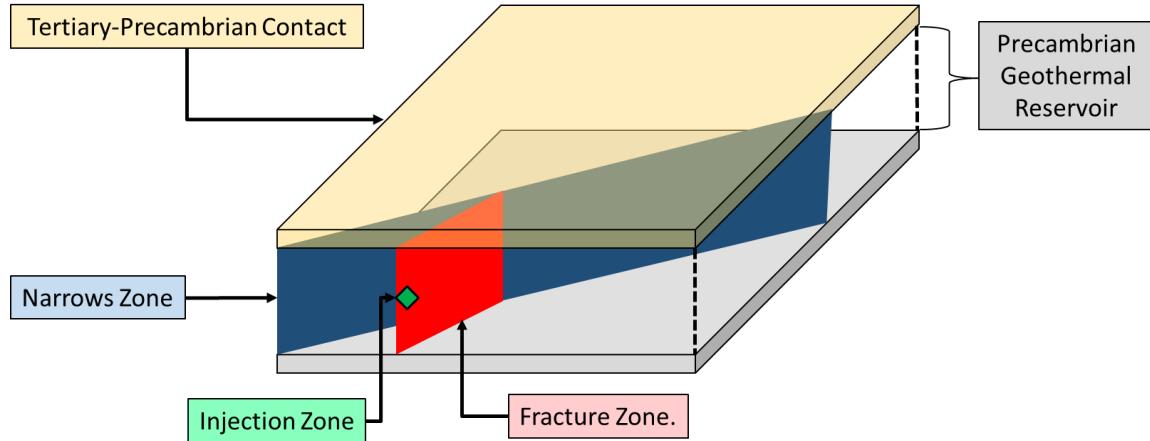
Figure 41 RRG-9 ST1 conceptual model. The tan plane is the contact between the Tertiary and Precambrian rocks while the blue and red plane are the Narrows Zone and intersecting fracture zone respectively.

$$\frac{\partial \phi \rho}{\partial t} = \left(\nabla \cdot \rho \left(\frac{k}{\mu} (\nabla p - \rho \boldsymbol{g}) \right) \right) + \acute{q} \qquad [\,3\text{-}4\,]$$

order to use Equation 3-4 in FALCON it must be arranged in terms of pressure. The left hand side of Equation 3-4 is expanded in Equation 3-5.

$$\rho \frac{\partial \phi}{\partial t} + \phi \frac{\partial \rho}{\partial t} = \left(\nabla \cdot \rho \left(\frac{k}{\mu} (\nabla p - \rho \boldsymbol{g}) \right) \right) + \acute{q} \qquad [\,3\text{-}5\,]$$

In Equation 3-5 terms on the left hand side are gathered and the left hand side is multiplied by $\partial p / \partial p$ to give Equation 3-6.

$$\left(\rho \frac{\partial \phi}{\partial p} + \phi \frac{\partial \rho}{\partial p} \right) \frac{\partial p}{\partial t} = \left(\nabla \cdot \rho \left(\frac{k}{\mu} (\nabla p - \rho \boldsymbol{g}) \right) \right) + \acute{q} \qquad [\,3\text{-}6\,]$$

The compressibility of water C_w is given by Equation 3-7 [34].

$$C_w = \frac{1}{\rho} \frac{\partial \rho}{\partial p} \qquad [\,3\text{-}7\,]$$

The compressibility of the formation C_f is given by Equation 3-8 [32].

$$C_f = \frac{1}{\phi}\frac{\partial \phi}{\partial p}$$

[3-8]

Applying Equation 5-4 and 5-5 to Equation 5-3 results in Equation 3-9.

$$\left(\rho\phi C_f + \rho\phi C_w\right)\frac{\partial p}{\partial t} = \left(\nabla \cdot \rho\left(\frac{k}{\mu}(\nabla p - \rho\boldsymbol{g})\right)\right) + \acute{q}$$

[3-9]

The total compressibility C_t of the system is equal to the sum of the formation compressibility and the water compressibility resulting in Equation 3-10.

$$\rho\phi C_t\frac{\partial p}{\partial t} = \nabla \cdot \frac{\rho k}{\mu}(\nabla p - \rho\boldsymbol{g}) + \acute{q}$$

[3-10]

The energy balance is given by Equation 3-11 [33].

$$\frac{\partial\left[\phi\rho\hat{C}_w + \left((1-\phi)\rho_r\hat{C}_r\right)\right]T}{\partial t} = \nabla \cdot (K_m\nabla T) + \rho\hat{C}_w\frac{k}{\mu}(\nabla p - \rho\boldsymbol{g}) + \acute{Q}$$

[3-11]

FALCON uses the Galerkin finite element method to approximate the solution of the given partial differential equations [35]. The solution to the resulting system of coupled nonlinear equations is obtained using the Jacobian Free Newton Krylov method [35] and [36].

3.4 Model Validation

Each component of the mass and energy balances, Equations 3-10 and 3-11 are broken up into small sections of code called kernels. For example the convection and conduction terms in the energy balance are assigned to separate kernels. These kernels are individually tested against known solutions to insure that simulated results reflect reality. Groups of kernels can be combined together to solve engineering problems. These can also

be tested against known solutions to insure simulation accuracy as was done for 1 dimensional flow and heat transport [35].

3.5 The RRG-9 ST1 FALCON Model

The conceptual model developed earlier provides the basis for modeling the stimulation program. A 6 mile by 6 mile section 837 ft. thick was meshed into FALCON. The model centers on the RRG-9 ST1 wellhead and covers an 837 ft. section starting from the top of the Tertiary-Precambrian contact and ending in quartz monzonite basement rock, Figure 42. A constant pressure boundary condition, equal to the reservoir pressure, is applied to the sides of the model. Both the Narrows Zone and the intersecting fracture zone where meshed into the model using a custom-built module for FALCON. This module, FracManMapAux, allows for discrete fracture networks generated using Golder Associates' software program FracMan® to be meshed in FALCON. The mesh is adaptively refined around the fractures to provide greater solution resolution in these areas of interest. A continuum approach is used to model these fractured elements. Elements containing fractures are assigned a larger permeability than the surrounding rock matrix to simulate the presence of fractures. The Narrows zone was further subdivided into three laterally adjacent but contiguous zones. The purpose of this delineation is to represent the inferred decrease in the number of fractures, and thus the decreasing permeability, as one moves away from the Narrows Zone fault core to the southeast. Fault zones sometimes contain an impermeable core that is surrounded by permeable fractures, the number of which rapidly decrease as one moves away from the core [37]. Reservoir properties are representative of Elba quartzite which is the primary reservoir rock, Table 9. The source/sink terms in both Equation 3-10 and 3-11 provide point source injection into the
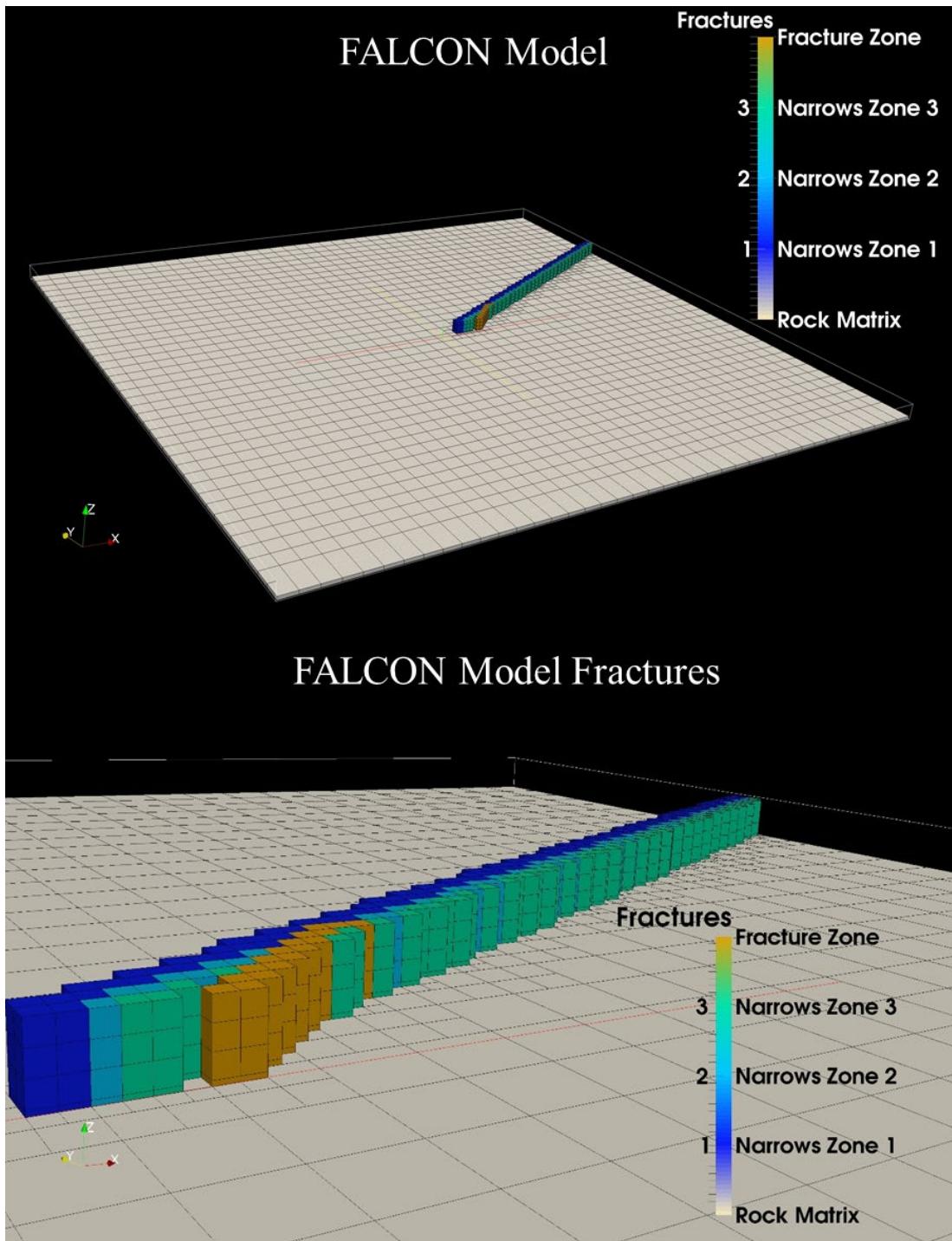
Figure 42 FALCON model. The model consists of a 6 mile by 6 mile section of the reservoir centered on the RRG-9 ST1 1 wellhead. An 837 ft. section below the Tertiary-Precambrian contact is considered. The rock matrix is shown as grey elements while Narrows Zones 1, 2, and 3 are dark blue, light blue, and aqua blue respectively. The fracture zone intersecting the RRG-9 ST1 wellbore is depicted as orange elements. In this image the rock matrix elements are transparent around the fracture allowing the viewer to see the imbedded fractures.

Table 9

Model Properties

Model Property	Value
Fracture Porosity	0.3
Reservoir Pressure [lb/in^2]	2,233
Reservoir Temperature [°F]	302
Rock Density [lb/ft^3]	165
Rock Permeability [mD]	5.07×10^{-3}
Rock Porosity	0.01
Water Density [lb/ft^3]	57.2
Water Viscosity [cP]	0.181
Total Compressibility [1/psi]	6.89×10^{-6}

reservoir. The same daily average flow rates used to create the modified Hall and injectivity index plots were used as inputs into the point injection source/sink terms. The permeability along the entire length of the fractures was adjusted in a step wise fashion based on the timing and location of microseismic activity, hydraulic stimulations, and well shut in. The value of these adjustments were iteratively adjusted to match the calculated bottomhole pressure. The final set of permeability results is shown, Table 10. The stimulation program was simulated from June 30, 2013 to January, 18, 2016.

3.6 Pressure History Match

Using the FALCON model a pressure history match was obtained for the stimulation program. During the first part of the stimulation program (from the star of injection through the 10-inch line through the second stimulation) the FALCON model tracked the overall shape of the calculated bottomhole pressure curve fairly well with a small amount of departure during the second stimulation, Figure 43. The FALCON model also tracks the post second stimulation quite well up to the third stimulation, Figure 44. After the third stimulation it becomes much more difficult to obtain a pressure history

Table 10

Model Permeability Adjustments

| Date	Fracture Zone Permeability [mD]	Narrows Zone 1 Permeability [mD]	Narrows Zone 2 Permeability [mD]	Narrows Zone 3 Permeability [mD]
6/30/2013	2	1,013	101	10
8/21/2013	3	1,013	101	10
8/31/2013	4	1,013	101	10
9/25/2013	7	1,013	101	10
1/23/2014	7	1,013	101	10
4/1/2014	15	1,013	101	10
4/3/2014	15	1,013	101	10
6/7/2014	15	4,053	405	41
9/21/2014	15	8,106	811	81
10/8/2014	20	8,106	811	81
1/6/2015	25	8,106	811	81
4/29/2015	30	8,106	811	81
8/9/2015	41	13,173	1,317	132
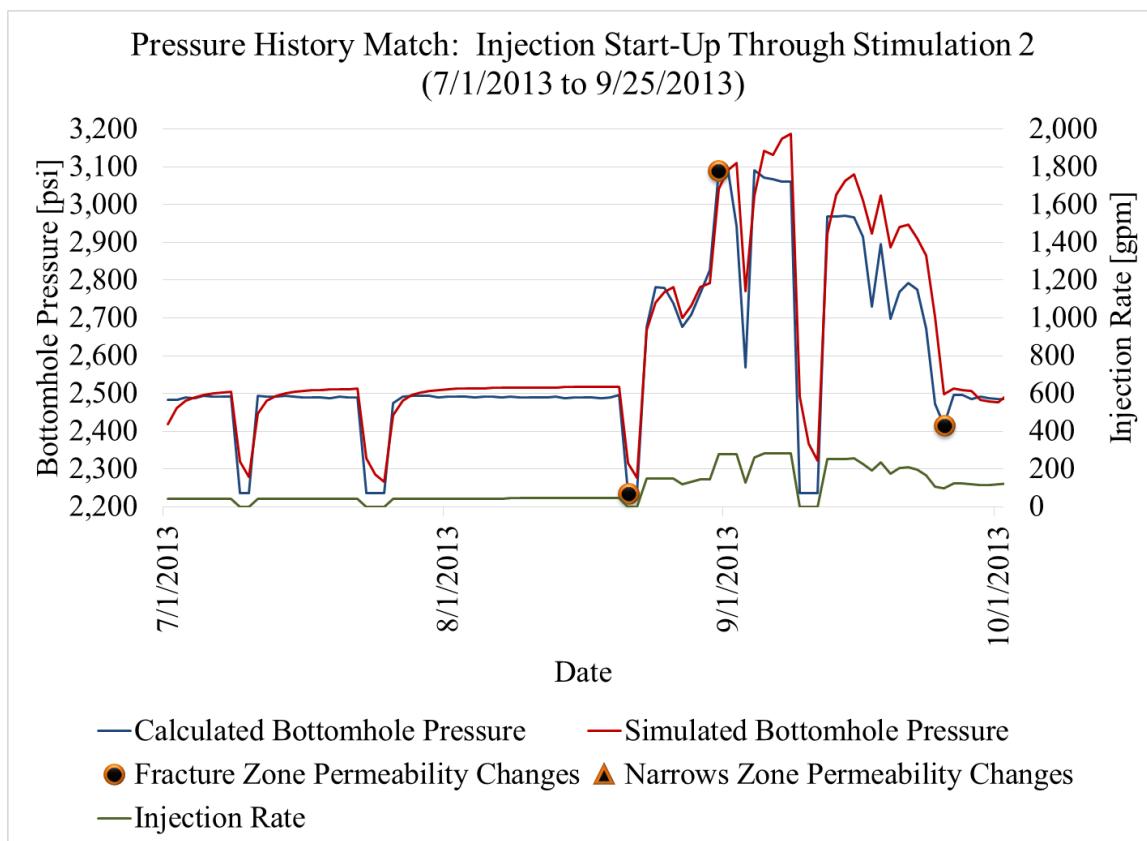
Figure 43 Pressure history match: injection start-up through stimulation 2.
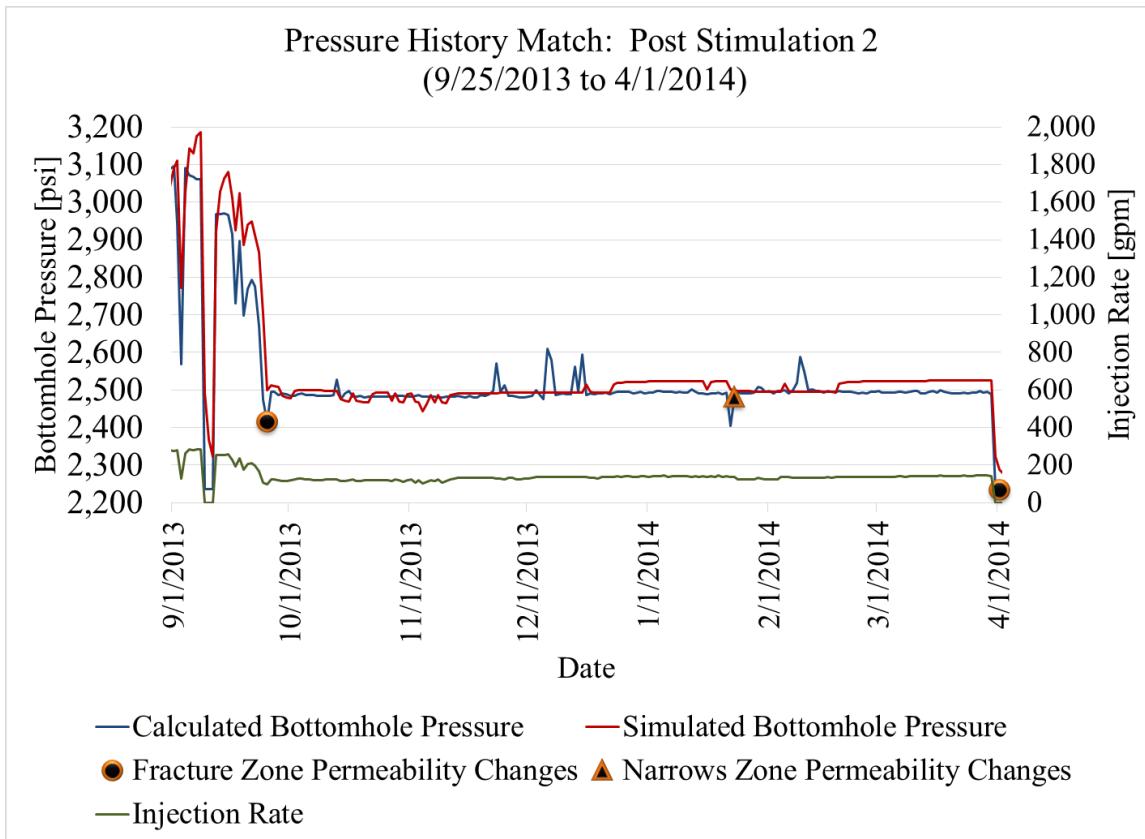
Figure 44 Pressure history match: post stimulation 2.

match by only changing the fracture permeability based on enhanced levels of microseismic events. The lack of relatively high levels of microseismic activity coupled with ever increasing flow rates at nearly constant pressures leads to difficulty tracking the bottom-hole pressure. Despite this the simulation solution result kept reasonably close to the RRG-9 ST1 bottom-hole pressure between April 1, 2013 and April 28, 2014, Figure 45. Following the shut in of RRG-9 ST1 the simulated bottom-hole pressure begins to significantly depart from the calculated bottom-hole pressure, Figure 46. This occurs for the same reasons previously mentioned. It is theorized that the mechanism behind this is the thermal contraction of the surrounding rock matrix opening up existing fractures and improving their permeability. Despite this the simulation solution kept relatively close to
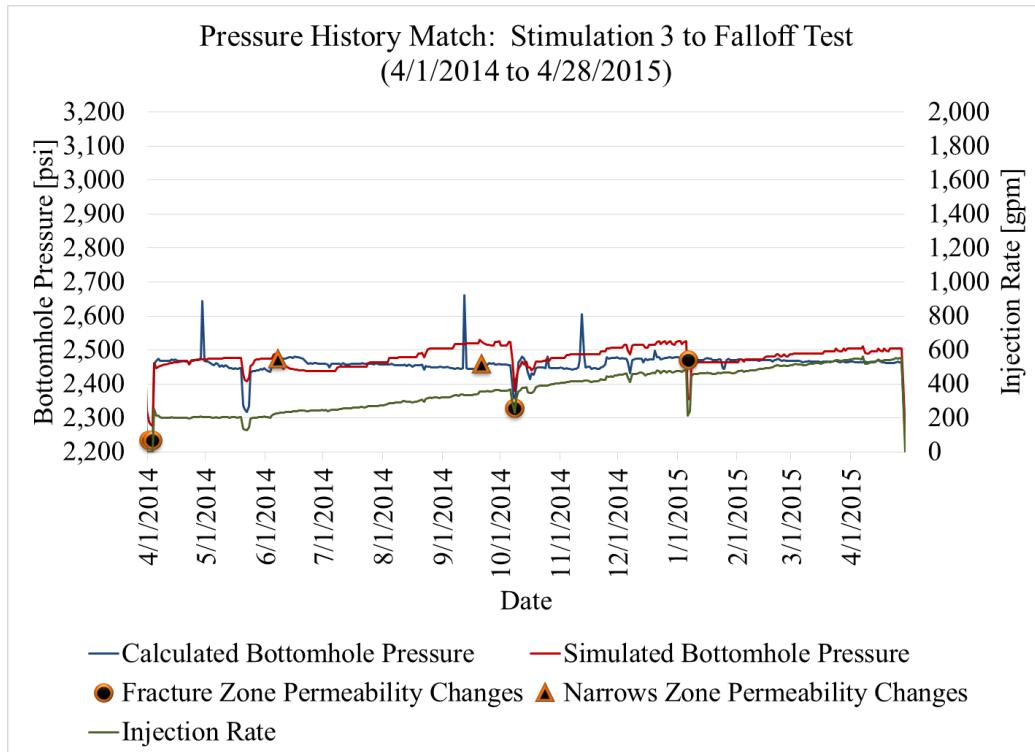
Figure 45 Pressure history match: stimulation 3 to falloff test.
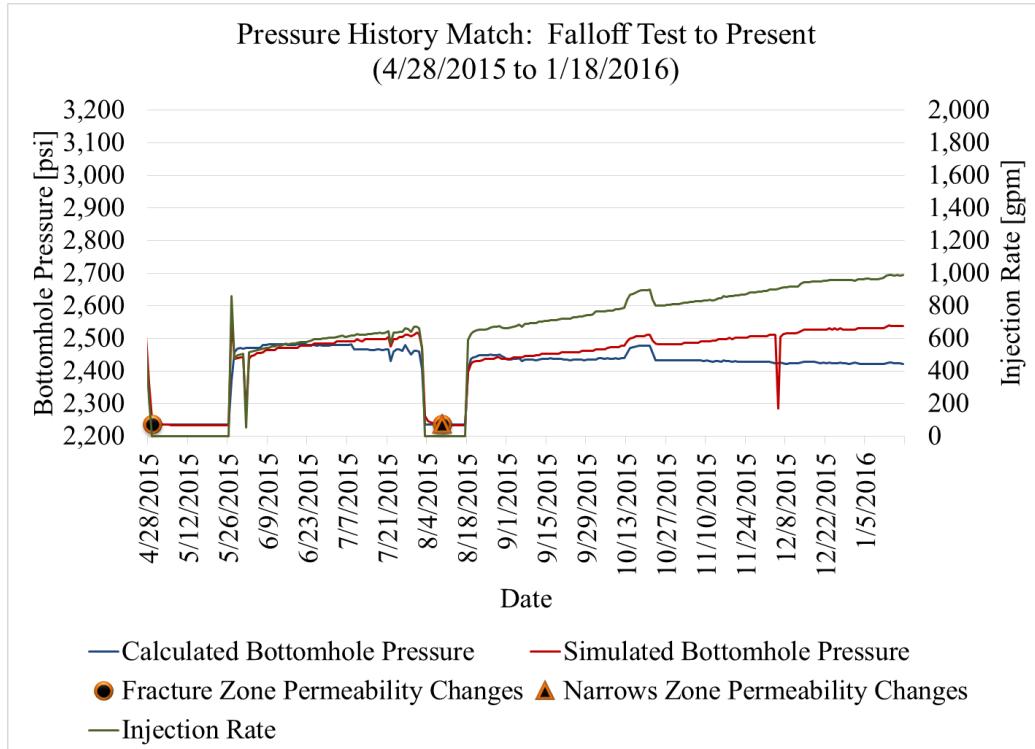

Figure 46 Pressure history match: falloff test to January 18, 2016.

the bottom-hole pressure, Figure 47. The simulated solution stayed within 10% of the calculated bottom-hole pressure value, Figure 48.

During the first part of the stimulation program (July, 2013 to April, 2014) the second hydraulic stimulation resulted in a step change in injection rate while the injection pressure remained nearly constant. The model was able to simulate this behavior with three step changes in the permeability of the intersecting fracture zone. The conclusions from the model for this time period is that the increase in injectivity is primarily due to the second hydraulic stimulation. Following the third hydraulic stimulation the injection rate behaves very differently from the first part of the stimulation program. The third hydraulic stimulation resulted in a positive step change in the injection rate, which remained relatively constant for almost two months. However, following this time period the injection rate begins to steadily increase at constant or decreasing pressures. As stated previously the model had a very difficult time tracking the calculated bottom-hole pressure for this part of the stimulation program. The conclusion based on the model for this part of the stimulation program is that an additional mechanism besides hydraulic fracturing is needed to explain the nearly continuous increase in injectivity. The most likely candidate is expansion of fracture apertures due to thermal contraction of the surrounding rock matrix. Since heat transfer in a fracture dominated system is primarily through convection larger flow rates result in a higher rate of cooling of the surrounding rock matrix. This leads to increasing growth in the fracture's aperture, increasing the fracture's permeability. The primary conclusion of the numerical model is that both hydraulic and thermal stimulation techniques resulted in the large increase in the injectivity of RRG-9 ST1.
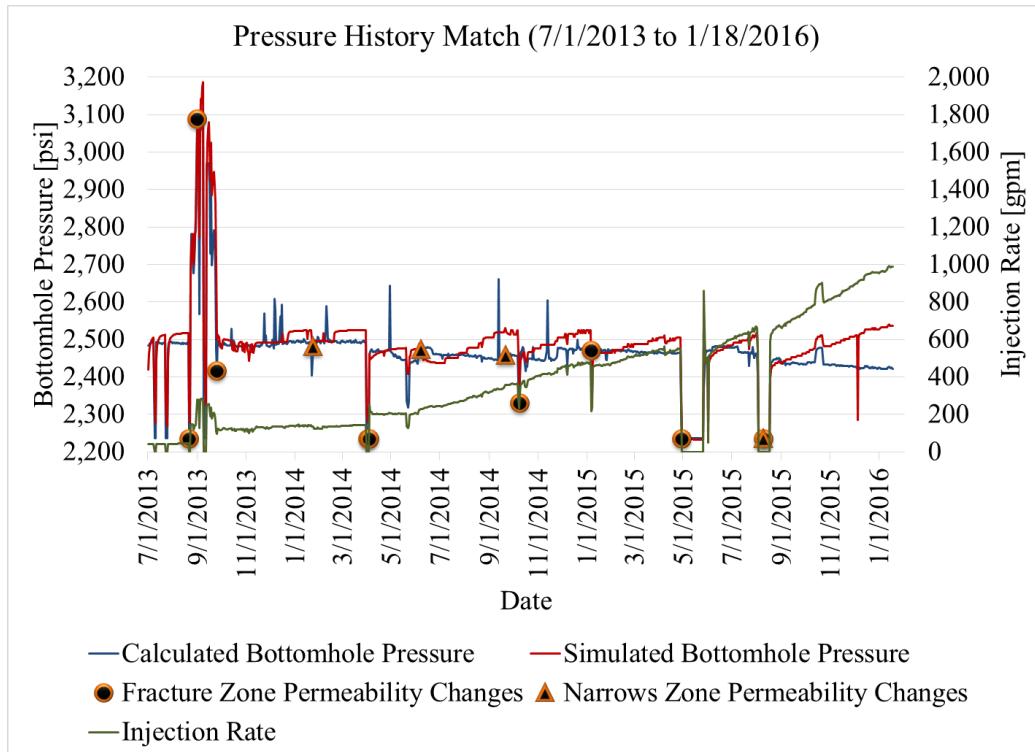
Figure 47 Pressure history match.
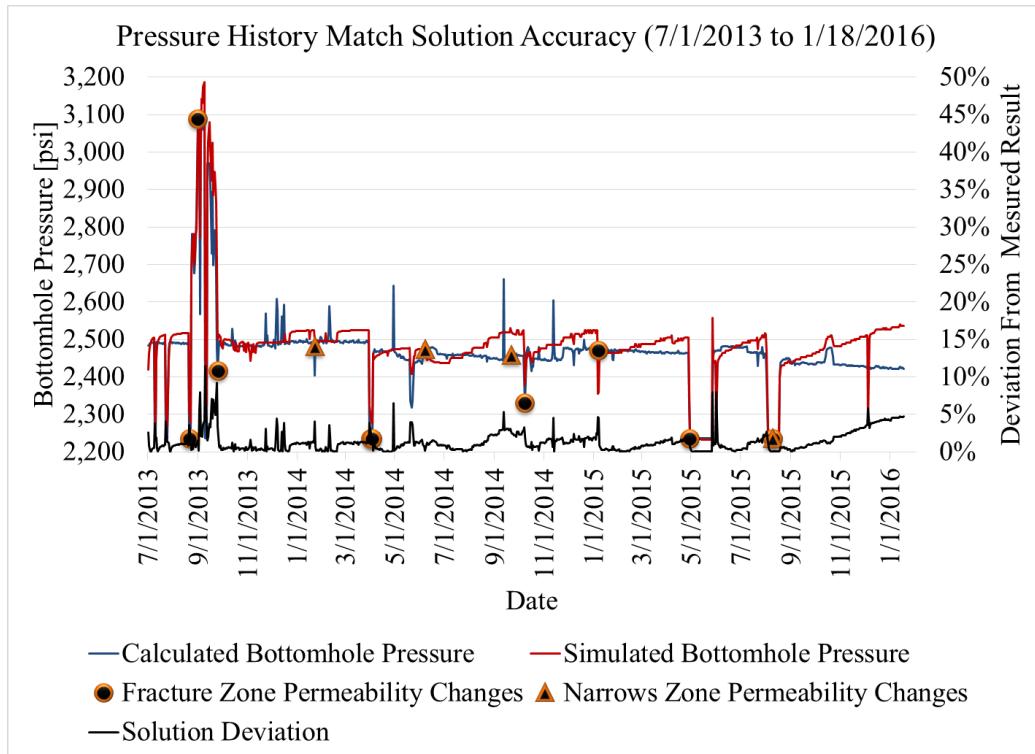
Figure 48 Pressure history match solution accuracy.

CONCLUSIONS

The Raft River EGS project has been very successful at demonstrating the viability of EGS techniques. The important conclusions drawn from this project are as follows.

- The Raft River stimulation program improved injection rates from less than 20 gpm to almost a 1,000 gpm. The injectivity index has risen form 0.15 gpm/psig to nearly 5.1 gpm/psig, an improvement of nearly 3,300%. Both hydraulic and thermal stimulation techniques contributed to this success.

- 187 microseismic events related to plant activity were recorded since 2010. Clusters of enhanced levels of microseismic activity, occurring near the RRG-9 ST1 wellbore and in the Narrows Zone, accompanied significant improvements to the injectivity index. This indicates that permeability is increasing near the wellbore and in the Narrows zone through the opening/reopening of new and/or existing fractures. Microseismic activity shows the distribution of fluid pathways in the Narrows Zone. Periods of enhanced microseismic activity.

- The Raft River stimulation program has been modeled using FALCON a finite element reservoir simulation code developed by Idaho National Laboratory. Modeling shows that positive changes in the fracture zone permeability during periods of enhanced microseismic activity produces a relatively close history match

for the first third of the stimulation program. However, after the third hydraulic stimulation injection, rates increased steadily with time and there were relatively few periods of enhanced microseismic activity. The model was unable to match this new trend solely based on permeability changes related to enhanced levels of microseismic activity. It is theorized that the consistent improvement in the injectivity index after the third hydraulic stimulation is primarily due to thermal contraction of the surrounding rock. This mechanism further opens up fracture pathways and improves injection rates at a nearly continuous rate. It is proposed that hydraulic stimulations are required to achieve a certain injection rate threshold. After this rate is achieved, the convective heat transport becomes sufficiently large to have an impact on the rate thermal contraction in the rock matrix surrounding the fractures. As the rock contracts fracture apertures grow and the fracture permeability increases. This mechanism would explain the nearly constant improvement in the injectivity of RRG-9 ST1 after the third hydraulic stimulation.

- The Raft River stimulation program also shows that existing structures play a fundamental role in EGS development. The Narrows Zone proved to be particularly valuable. This series of conductive fractures allows for fluid communication between the northern production wells and RRG-9 ST1. Once adequate communication was established between the RRG-9 ST1 wellbore and the Narrows Zone, it allowed for rapid connections to the other production wells. Tracer data

showed nearly simultaneous communication between RRG-9 ST1 and the production wells RRG-2 and 4, which are separated by just over a mile.

RRG-9 ST1 is now in commercial use as an injection well at the Raft River geothermal field.

The unique contributions this research has provided to the geothermal energy field include: an expansion of the modified Hall's technique, analysis of the correlation between increased injectivity and induced seismic activity, and the construction of a three dimensional reservoir model that incorporates changes in permeability based on enhanced levels of microseismic activity. The modified Hall's technique was expanded to include changing hydrostatic pressure at the base of the wellbore due to changes in injection temperature and pressure loss due to friction. A detailed analysis of the evolution of microseismic activity prior to and during the stimulation program provided an indicator of the location of the injected fluid as it traveled throughout the geothermal system. Comparing the timing and location of enhanced levels of microseismic activity allowed for a refined mechanism of permeability adjustment to be applied to the simulation model. Borehole imaging along with the locations of microseismic events allowed for the creation of a complex three dimensional model of the reservoir surrounding RRG-9 ST1. Using field data and the enhanced microseismic activity mechanism for permeability adjustment, a pressure history match for the stimulation program was obtained. These developments increase the understanding of how geothermal systems behave when hydraulically and thermally stimulated as well as providing a base of knowledge for further investigation into the development of enhanced geothermal systems.

APPENDIX

IMPORTING A DISCRETE FRACTURE NETWORK INTO FALCON

In FALCON fractures are defined as infinite planes consisting of a least three points. These points are imported into FALCON using a custom auxiliary kernel. This auxiliary kernel takes the imported fracture data and generates an infinite plane for each fracture. FALCON then proceeds to go through each element in a user created mesh to determine if it contains the imported fracture. This process contains the following steps. First the nearest point of the fracture to the center of the element is determined. Next the distance between this point and the center of the element is calculated. Finally if this distance is less than a defined tolerance and the element resides within the boundaries set by the user the element is assigned the fractures identification number. This number is used to assign the element the material properties of the corresponding fracture.

The iterative process of changing permeability to generate a pressure history match makes lowering the simulation speed a high priority. This must be balanced with a sufficiently refined mesh to improve solution accuracy. A two-step process was used create a mesh to simulate the RRG-9 ST1 stimulation program. First a very fine mesh was applied to the model and the fractures were mapped in. Elements that did not contain fractures were coarsened, Figure 49. Following this step the elements containing fractures were then

refined, Figure 50. The result is a mesh that has high resolution around the fracture zones while not wasting computational resources on areas that are not of interest. A mesh created using this process allowed for the entire stimulation program to be simulated on a standard desktop computer.
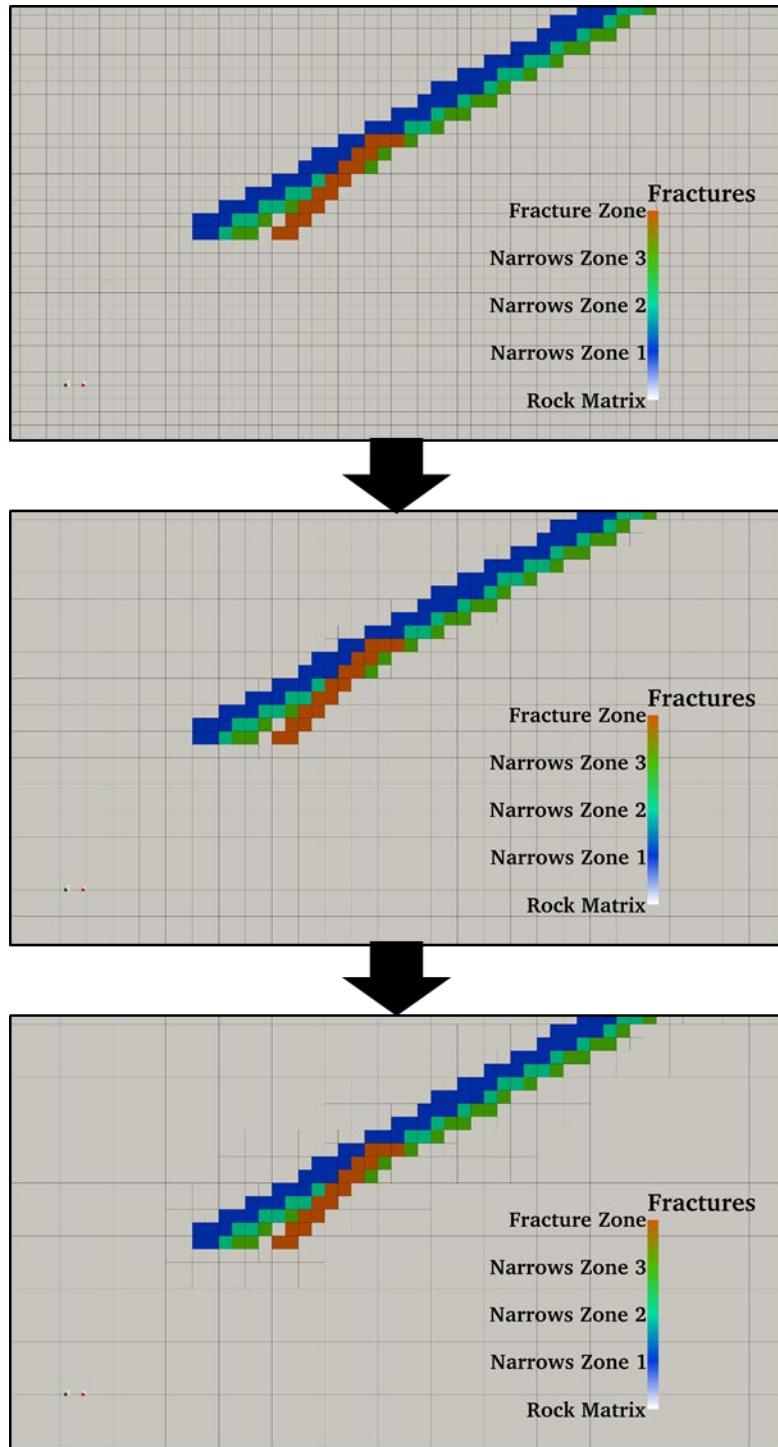
Figure 49 Mesh creation step 1: coarsen mesh around fractures.
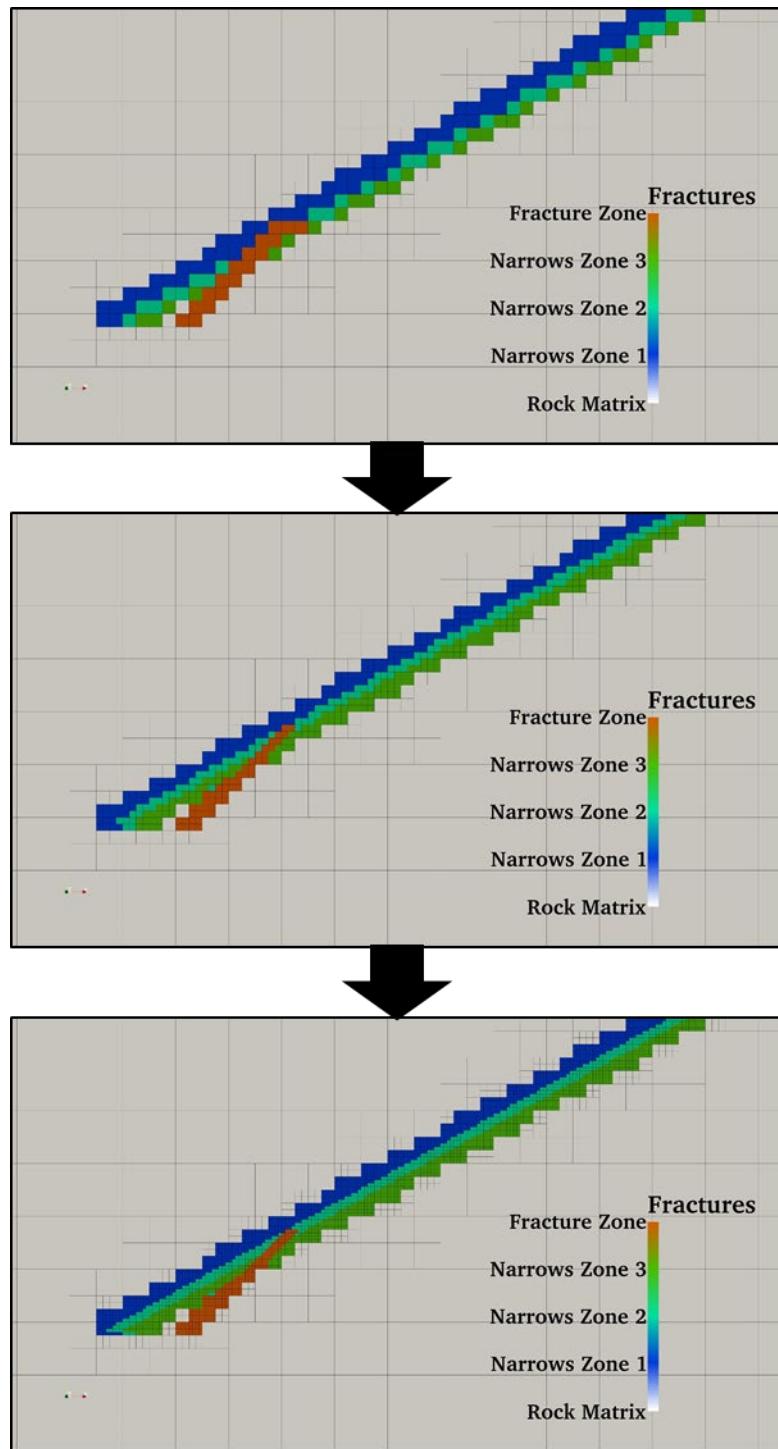
Figure 50 Mesh creation step 2: refine mesh in the fractured elements.

REFERENCES

[1] C. T. Montgomery and M. B. Smith, "Hydraulic Fracturing: History Of An Enduring Technology," *Journal of Petroleum Technology,* vol. 62, no. 12, pp. 26-40, 2010.

[2] M. K. Hubbert and D. G. Willis, "Mechanics of Hydraulic Fracturing," in *M 18: Underground Waste Management and Environmental Implications*, American Association of Petroleum Geologists, 1972, pp. 239-257.

[3] S. L. Craig, K. S. Udell, J. McLennan and J. Moore, "An Experimental Study of Thermal and Hydraulic Geothermal Reservoir Stimulation of Brittle Impermeable Material," in *Thirty-Ninth Workshop on Geothermal Reservoir Engineering*, Stanford, CA, 2014.

[4] T. K. Perkins and J. A. Gonzalez, "Changes in Earth Stresses Around a Wellbore Caused by Radially Stymmetrical Pressure and Temperature Gradients," *Society of Petroleum Engineers,* pp. 129-140, 1984.

[5] T. K. Perkins and J. A. Gonzalez, "The Effect of Thermoelastic Stresses on Injection Well Fracturing," *Society of Petroleum Engineers,* pp. 78-88, 1985.

[6] J. L. Detienne, M. Creusot, N. Kessler, B. Sahuquet and J. L. Bergerot, "Thermally Induced Fractures: A Field-Proven Analytical Model," *SPE Reservoir Evaluation & Engineering,* pp. 30-35, 1998.

[7] A. Ghassemi, "Stress and Pore Pressure Distribution Around A Pressurized, Cooled Crack In Low Permeability Rock," in *Thirty-Second Workshop on Geothermal Reservoir Engineering*, Stanford, California, 2007.

[8] D. D. Blackwell, P. T. Negraru and M. C. Richards, "Assessment of the Enhanced Geothermal System Resource Base of the United States," *Natural Resources Research,* vol. 15, no. 4, pp. 283-308, December 2006.

[9] M. A. Grant and P. F. Bixley, Geothermal resrvoir Engineering Second Edition, Burlington, MA: Academic Press, 2011.

[10] M. W. McClure and R. N. Horne, "An investigation of stimulation mechanisms in Enhanced Geothermal Systems," *International Journal of Rock Mechanics & Mining Sciences,* vol. 72, pp. 242-260, 2014.

[11] W. E. Glassley, Geothermal Energy Renewable Energy and the Evironment, Boca Raton, FL: CRC Press Taylor & Francis Group, 2010.

[12] P. P. Williams, H. R. Covington and K. L. Pierce, "Cenozoic stratigraphy and tectonic evolution of the Raft River basin, Idaho, in Cenozoic Geology of Idaho," *Idaho Bureau of Mines and Geology Bulletin,* vol. 26, pp. 491-504, 1982.

[13] H. R. Covington, "Subsurface geology of the Raft River geothermal area, Idaho," *Transactions - Geothermal Resources Council,* vol. 4, pp. 113-115, 1980.

[14] B. Ayling and J. N. Moore, "Fluid geochemistry at the Raft River geothermal field, Idaho, USA: New data and hydrogeological implications," *Geothermics,* pp. 116-126, 2013.

[15] GeothermEx Inc., "Technical Report on the Raft River Geothermal Resource, Cassia County, Idaho," GeothermEx Inc., Richmond, CA, 2002.

[16] Republic Geothermal, Inc., "Geothermal-Reservoir Well-Stimulation Program," Republic Geothermal, Inc., Santa Fe Springs, CA, 1982.

[17] D. A. Campbell, R. J. Hanold, A. R. Sinclair and O. J. Vetter, "A Review of the Geothermal Reservoir WEll Stimulation Program," in *International Geothermal Drilling and Completion Technology Conference*, Albuquerque, NM, 1978.

[18] W. S. Keys, "The Application of the Acoustic Televiewer to the Characterization of Hydraulic Fractures in Geothermal Wells," in *Proceedings of the Geothermal Reservoir Well Stimulation Symposium*, San Francisco, CA, 1980.

[19] U.S. Geothermal Inc., "Raft River," 2013. [Online]. Available: www.usgeothermal.com/projects/1/Raft%20River. [Accessed 16 March 2016].

[20] H. R. Covington, "Structural evolution of the Raft River Basin, Idaho," *Geological Society of America,* pp. 229-237, 1983.

[21] J. Moore, "Enhanced Geothermal Systems - Concept Testing and Development at the Raft River Geothermal Field, Idaho," Salt Lake City, 2012.

[22] J. Castell, S. Pullammanappallil and R. J. Mellors, "Estimating Subsurface Permeability with 3d Seismic Attributes: A Neural net Approach," in *41st Workshop on Geothermal Reservoir Engineering*, Stanford, CA, 2016.

[23] J. Bradford, J. Moore, M. Ohren, J. McLennan, W. L. Osborn, E. Majer, G. Nash, R. Podgorney and B. Freifeld, "Recent Thermal and Hydraulic Stimulation Results at Raft River, ID EGS Site," in *Proceedings, Fourtieth Workshop on Geothermal Reservoir Engineering*, Stanford, CA, 2015.

[24] J. Bradford, J. McLennan, J. Moore, D. Glasby, D. Waters, R. Kruwell, A. Baily, W. Rickard, K. Bloomfield and D. King, "Recent Developments At The Raft River Geothermal Field," in *Proceedings, Thirty-Eighth Workshop on Geothermal Reservoir Engineering*, Stanford, CA, 2013.

[25] R. W. Veatch Jr. and Z. A. Moschovidis, "An Overview of Recent Advances in Hydraulic Fracturing Technology," in *International Meeting on Petroleum Engineering*, Beijing, 1986.

[26] J. Bradford, J. McLennan, J. Moore, R. Podgorney, G. Nash, M. Mann, W. Rickard and D. Glaspey, "Numerical Modeling of the Stimulation Program at RRG-9 ST1, a DOE EGS," in *Proceedings, 41st Workshop on Geothermal Reservoir Engineering*, Stanford, CA, 2016.

[27] J. Bradford, J. McLennan, J. Moore, R. Podgorney and S. Tiwari, "Hydraulic and Thermal Stimulation Program at Raft River Idaho, A DOE EGS," in *GRC Transactions, Volume 39*, Reno, NV, 2015.

[28] L. House, "Locating Microearthquakes Induced by Hydraulic Fracturing in Crystalline Rock," *Geophysical Research Letters,* vol. 14, no. 9, pp. 919-921, 1987.

[29] L. V. Block, C. H. Cheng, M. C. Fehler and W. S. Phillips, "Seismic imaging using microearthquakes induced by hydraulic fracturing," *Geophysics,* vol. 59, no. 1, pp. 102-112, 1994.

[30] J. P. Vermylen and M. D. Zoback, "Hydraulic Fracturing, Microseismic Magnitudes, and Stress Evolution in the Barnett Shale, Texas, USA," in *SPE Hydraulic Fracturing Technology Conference and Exhibition*, Woodlands, Texas, 2011.

[31] N. R. Warpinski, S. L. Wolhart and C. A. Wright, "Analysis and Prediction of Microseismicity Induced by Hydraulic Fracturing," *SPE Journal,* vol. 9, no. 01, pp. 24-33, 2004.

[32] R. C. Earlougher, JR., Advances In Well Test Analysis, Dallas: American Institute of Mining, Metallurgical, and Petroleum Engineers, Inc., 1977.

[33] R. B. Bird, W. E. Stewart and E. N. Lightfoot, Transport Phenomena Second Edition, Phoenix: John Wiley & Sons, Inc., 2007.

[34] R. A. Freeze and J. A. Cherry, Ground Water, Englewood Cliffs, N.J.: Prentice-Hall, 1979.

[35] R. Podgorney, H. Huang and D. Gaston, "Massively Parallel Fully Coupled Implicit Modeling of Coupled Thermal-Hydrological-Mechanical Processes For Enhanced Geothermal System Reservoirs," in *Thirty-Fifth Workshop on Geothermal Reservoir Engineering*, Stanford, California, 2010.

[36] K. Smith, M. Plummer, J. Bradford and R. Podgroney, "Adaptive Mesh Refinement and Time Stepping Strategies for Incorporating Discrete Fracture Networks Into a High Performance Computing Framework for Geothermal Reservoir Simulation," in *GRC Transactions*, 2013.

[37] A. Brogi, "Fault zone architecture and permeability features in silicious sedimentary rocks: Insights from the Rapolano geothermal area (Northern Apennines, Italy)," *Journal of Structural Geology,* pp. 237-256, 2008.

[38] R. Nersesian, Energy for the 21st Century, Armonk, New York: M.E. Sharpe, Inc., 2014.

ADDENDUM

Final Results

June 2019

Microseismic data and analyses, updated Modified Hall plot and injection rates and tracer monitoring during the no-cost extension after project completion (June 2019).

1) Seismic monitoring has been discontinued at the beginning of 2019. Until then, there have been 369 locally generated seismic events through March 2019, ranging in magnitude from -1.29 to 1.75. A plot of seismic activity and injectivity shows a correlation between large numbers of seismic events and improvements in the injectivity of the well. The correlation is especially noticeable after the April 2014 stimulation.

This map shows locally generated seismic activity at Raft River since August 2010 through March 2019. Data was acquired and analyzed by LBL.
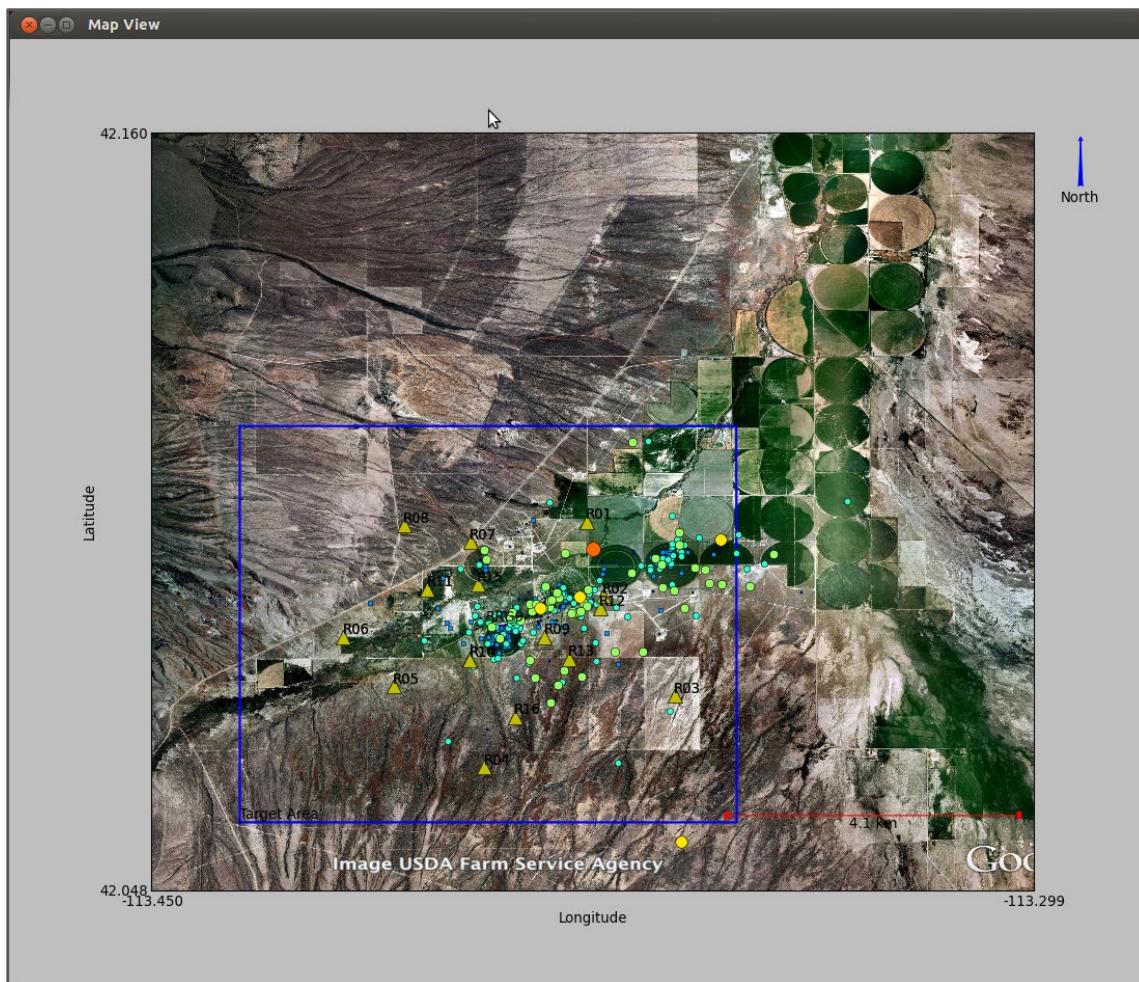
2) This is the injectivity index through June 2019. The multicolored dots represent injectivity data while black triangles show the daily frequency of seismic events.
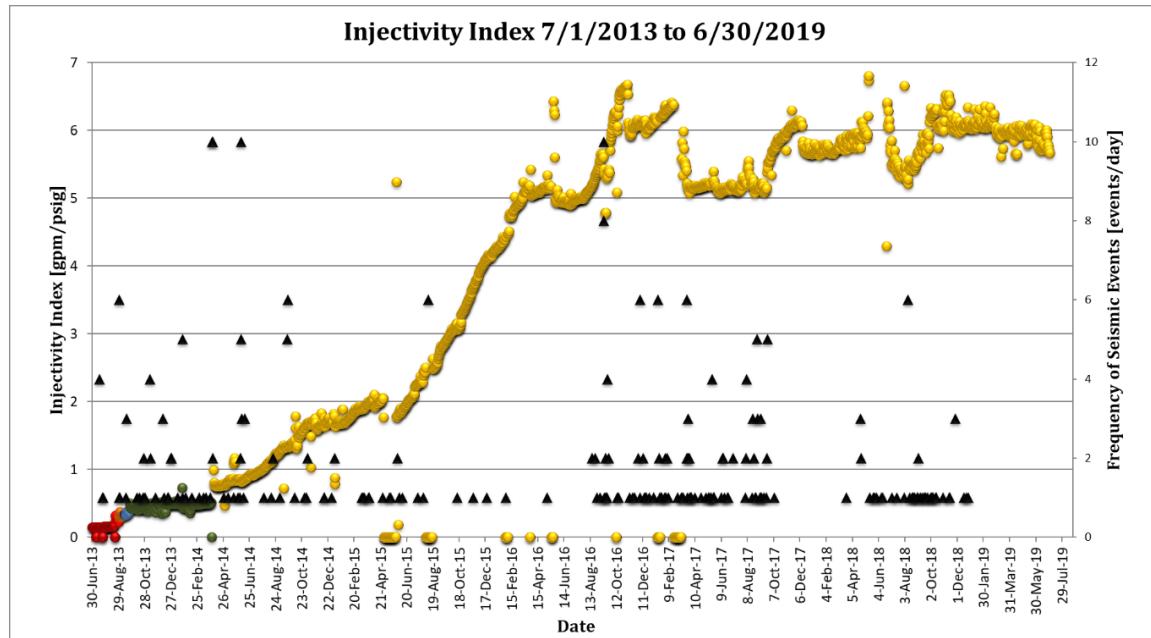

3) Monitoring of flow rates, well head and line pressures, and line temperature continued. The figure below summarizes the data since injection began in June of 2013. Flow and injection pressure rates were provided by the plant as daily averages after telemetered data was discontinued.
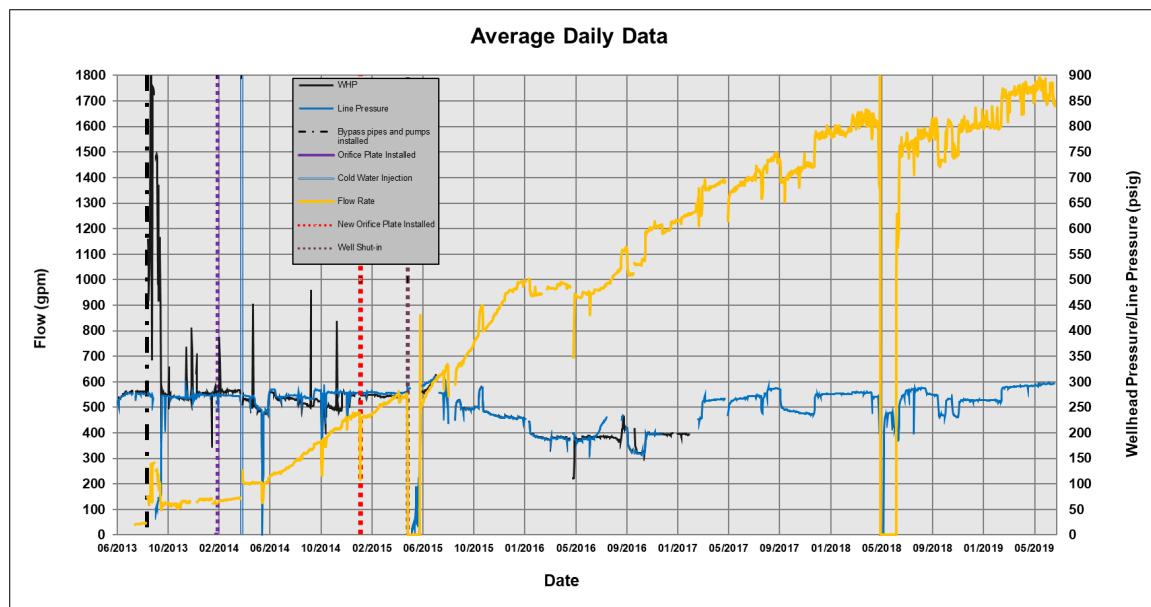
4) This modified Hall plot below shows a decreasing slope as the stimulation program moved forward. This decreasing slope indicates an increase in the permeability and/or a reduced skin factor around the well.
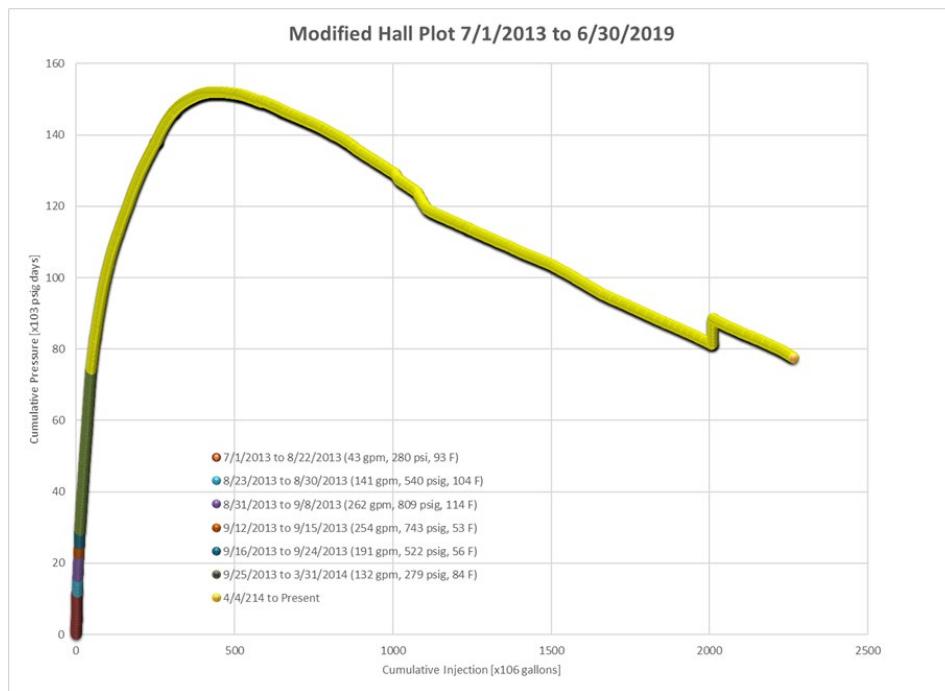
5) The injectivity of the well has also improved. After the third stimulation in April of 2014 and the falloff test conducted in April of 2015 the injectivity has increased rapidly, see figure below.
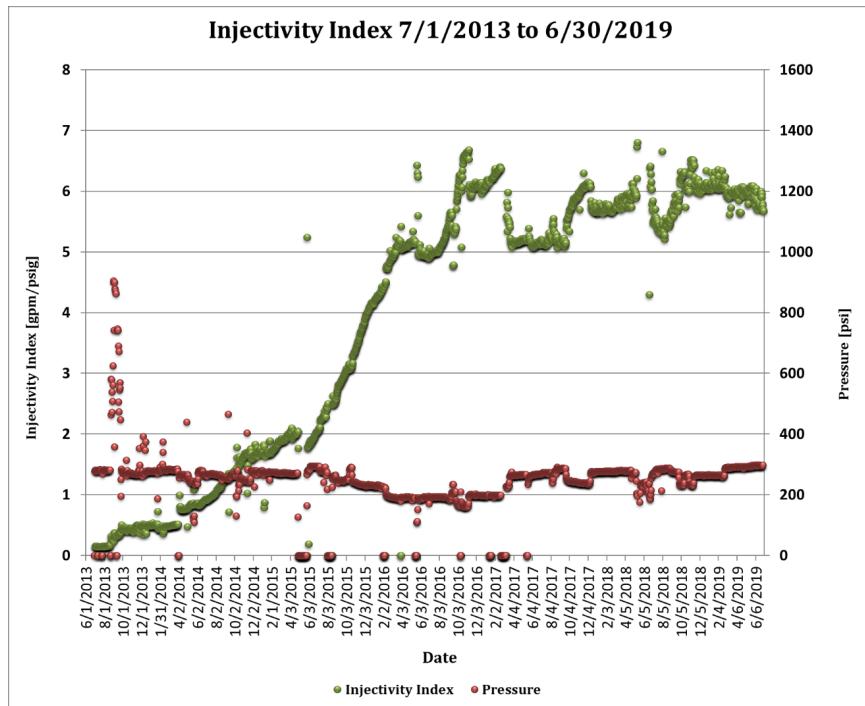
6) Tracer monitoring continued through the no-cost extension period until July 2019. Below are the final tracer results for wells" RRG1, RRG2, RRG4, and RRG7.

RRG 1

RRG 1

RRG 2

RRG 2

RRG 4

RRG 4